NAT'L INST. OF STAND & TECH
A11106 368391
NIST
PUBLICATIONS
REFERENCE

NIST

MSEL

FY 2001 PROGRAMS
AND ACCOMPLISHMENTS

NIST CENTER FOR NEUTRON RESEARCH

QC
100
.U56
#6798
2001

On the cover

A view of instruments in the cold neutron guide hall at the NCNR looking back towards the neutron source. The blue biological shielding covering cold neutron guide NG-6 runs down the middle of the picture. In the foreground are two instruments exemplifying important types of measurements on materials made with cold neutrons: on static atomic structures (SANS, red tank on the left), and on atomic dynamics (FCS, below the yellow structure on the right).

National Institute of Standards and Technology
Karen H. Brown,
Acting Director

Technology Administration

U.S. Department of Commerce
Donald L. Evans,
Secretary

MATERIALS SCIENCE AND ENGINEERING LABORATORY

FY 2001 PROGRAMS AND ACCOMPLISHMENTS

NIST
CENTER FOR
NEUTRON
RESEARCH

J. Michael Rowe, Director

NISTIR 6798

September 2001

DISCLAIMER

Certain commercial equipment, instruments, or materials are identified in this report to foster understanding. Such identification does not imply recommendation or endorsement by the National Institute of Standards and Technology, nor does it imply that the materials or equipment identified are necessarily the best available for the purpose.

Contents

Foreword iv
Introduction 1
NCNR Layout 2
NCNR Images 2001 4
Research Highlights
Measurement of the Free Neutron Lifetime 6
ETS-4: Maxwell's Zeolite 8
Stresses in Electron Beam Weld Joints of Superalloys 10
EXPGUI: Smoothing the Path to Powder Crystallography 12
Neutron Diffraction Contributes to Improving the Fatigue Life of Bridges 14
Neutron Imaging and Prompt Gamma Activation Analysis Using a Monolithic Capillary Neutron Lens 16
Giant Anharmonicity and Theory of Surprising BCS Superconductivity In MgB_2 At 40 K 18
Polaron Formation and Colossal Magnetoresistance in Manganites 20
Ferromagnetism and Spontaneous Vortex Formation in Superconducting $ErNi_2B_2C$ 22
Structure of a Local Spin Resonance in a Geometrically Frustrated Antiferromagnet 24
Pressure-Induced Phase Transition of $C_{12}E_5$ Micelles 26
Probing the Structure of Aerosol Nanodroplets 28
Nanoporous Ultra-Low Dielectric Constant Materials 30
Neutron Reflectivity Studies of Surfactants at Electrode Surfaces 32
Magnetic Semiconductor Superlattices 34
Pinpointing Chiral Structures With Front/Back Polarized Neutron Reflectometry 36
The Nature of Vibrational Softening in α-Uranium 38
Dynamics of Native and Partially Unfolded Proteins by Inelastic Neutron Scattering and Molecular Dynamics Simulations 40
Dynamics in Confined Polymer Films 42
Intimate Relationship Between Structural Deformation and Properties of Carbon Nanotubes 44
Serving the Scientific and Technological Communities 46
The NCNR User Program 46
The Center for High Resolution Neutron Scattering 46
Seventh Annual Summer School 47
Collaborations 47
Independent Programs 48
Reactor Operation and Engineering 51
Instrumentation Developments 52
Publications 57
Instruments and Contacts 68
Contacts ..... Inside Back Cover

Foreword

As this is being written, we have just begun a three-month shutdown during which we will, among other changes, install a next generation liquid hydrogen cold source, which will increase cold neutron intensities by almost a factor of two. This is an excellent example of the necessary operating philosophy for any facility – improvement and change are the only constants. During the past year, we have had many changes in reactor systems, in instrumentation, in staff, and in science, all of which are aimed at continuing the development of the NIST Center for Neutron Research as a first rate neutron facility.

A new cooling tower, which is specially designed to reduce the visible vapor plume during winter months, as well as to provide full cooling ability for the next twenty years, has been constructed. It will be connected into the reactor secondary systems during the shutdown that has just started. A new analysis of major reactor systems has been initiated using the most modern tools as part of preparing the application for a license extension through 2024. Many other improvements, ranging from instrumentation renewal to better provision for maintenance to improved electrical distribution, are under way as part of the preparation for re-licensing. In spite of the shutdown that just started, the reactor has once again performed admirably, operating for 240 days during the fiscal year, meeting our scheduled operating time.

The three new inelastic scattering instruments, which were just coming on line last year, are now being fully incorporated into the user program, with encouraging user demand. The joint National Science Foundation (NSF)/NIST Center for High Resolution Neutron Scattering is being expanded to include operation of these instruments in addition to the prior SANS and triple axis instruments. The thermal neutron upgrade program, which includes two new triple axis spectrometers, an improved filter analyzer spectrometer, and other instruments, is advancing well, with characterization of monochromator crystals now complete, and contracts awarded for the manufacture of monochromator drums and focusing devices. A new cold neutron triple axis spectrometer is currently entering detailed design phase as a joint construction project with Johns Hopkins University (partially funded by the NSF). In order to create more research space in the guide hall, a new building for our technical support activities is nearing completion. In response to many recommendations, we have significantly strengthened our sample environment support and our data acquisition and analysis computing effort, adding additional staff and refocusing efforts. The number of research participants continues to grow, surpassing all of our expectations. Overall, we are moving forward on many fronts to strengthen our research facility operations efforts, in order to better serve our customers.

And, as always, the scientific results are the true measure of success, and the highlights that form the largest portion of this report comprise an excellent set of examples of the exciting outputs of the facility. I hope that you enjoy reading them as much as I did.

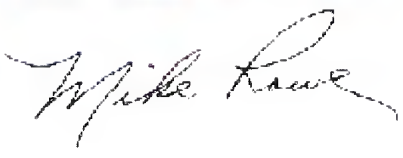

Introduction to the NIST Center for Neutron Research (NCNR)

Modern technological society is dependent upon increasingly sophisticated use of materials with attributes dictated by their sub-microscopic structural and dynamical properties. A wide range of techniques provides knowledge of these properties. Scattering probes (for example: x-rays, light, electrons, neutrons) are arguably the most important. Of these probes, neutrons are perhaps least familiar, but they provide important advantages for many types of measurements.

Modern sources provide neutrons moving at speeds comparable to those of atoms at room temperature, thus providing the ability to probe dynamical behavior. Neutrons are also well matched to probe lengths ranging from the distances between atoms to the size of biological or polymer macromolecules. Neutrons are sensitive to the magnetic properties of atoms and molecules, allowing study of the underlying magnetic properties of materials. They also scatter differently from normal hydrogen atoms than they do from heavy hydrogen (deuterium), allowing selective study of individual regions of molecular systems. Finally, neutrons interact weakly with materials, providing the opportunity to study samples in different environments more easily (at high pressures, in shear, in reaction vessels, etc.), and making them a non-destructive probe. These favorable properties are offset by the weakness of the best neutron sources compared to x-ray or electron sources, and by the large facilities required to produce neutrons. As a result, major neutron sources are operated as national user facilities to which researchers come from all over the United States and abroad to perform small-scale science using the special measurement capabilities provided.

In addition to scattering, neutrons can be captured by nuclei to probe the atomic composition of materials. The subsequent characteristic radioactive decays provide "fingerprints" for many atomic nuclei, allowing studies of environmental samples for pollutants (e.g. heavy metals), characterization of Standard Reference Materials, and other measurements. There are important areas in physics that can be explored by measuring fundamental neutron behavior. Examples include the lifetime of the free neutron, important for the theory of astrophysics; the neutron beta decay process, that provides a stringent test of nuclear theory; and the effects of various external influences such as gravity or magnetic fields on neutrons.

The NCNR's 20 MW NIST Research Reactor provides a national user community with facilities, including the nation's only internationally competitive cold neutron facility, for all of the above types of measurements. There are about 35 stations in the reactor and its associated beams that can provide neutrons for experiments. At the present time 28 of these are in active use, of which 6 provide high neutron flux positions in the reactor for irradiation, and 22 are beam facilities. The following pages show a schematic layout of the facility. More complete descriptions of instruments can be found at http://www.ncnr.nist.gov.

These facilities are operated both to serve NIST mission needs and as a national facility, with many different modes of access. Some instrumentation was built years ago, and is not suited to general user access; however, time is available for collaborative research. NIST has recently built new instrumentation, and reserves 1/3 of available time for mission needs with the balance available to general users. In other cases, instrumentation was built and is operated by Participating Research Teams (PRT); PRT members have access to 75 % of available time, with the balance available to general users. Additionally, NIST and the National Science Foundation operate the Center for High Resolution Neutron Scattering at the NCNR, with one thermal and five cold neutron instruments. For these facilities, most time is available for general users. While most access is for research, with results that are freely available to the general public, proprietary research can be performed under full cost recovery. Each year, about 1600 researchers (persons who participated in experiments at the facility, but did not necessarily come here) from all areas of the country, from industry, academia, and government use the facility for measurements not otherwise possible. The research covers a broad spectrum of disciplines, including chemistry, physics, biology, materials science, and engineering.

NIST Center for Neutron Research Layout

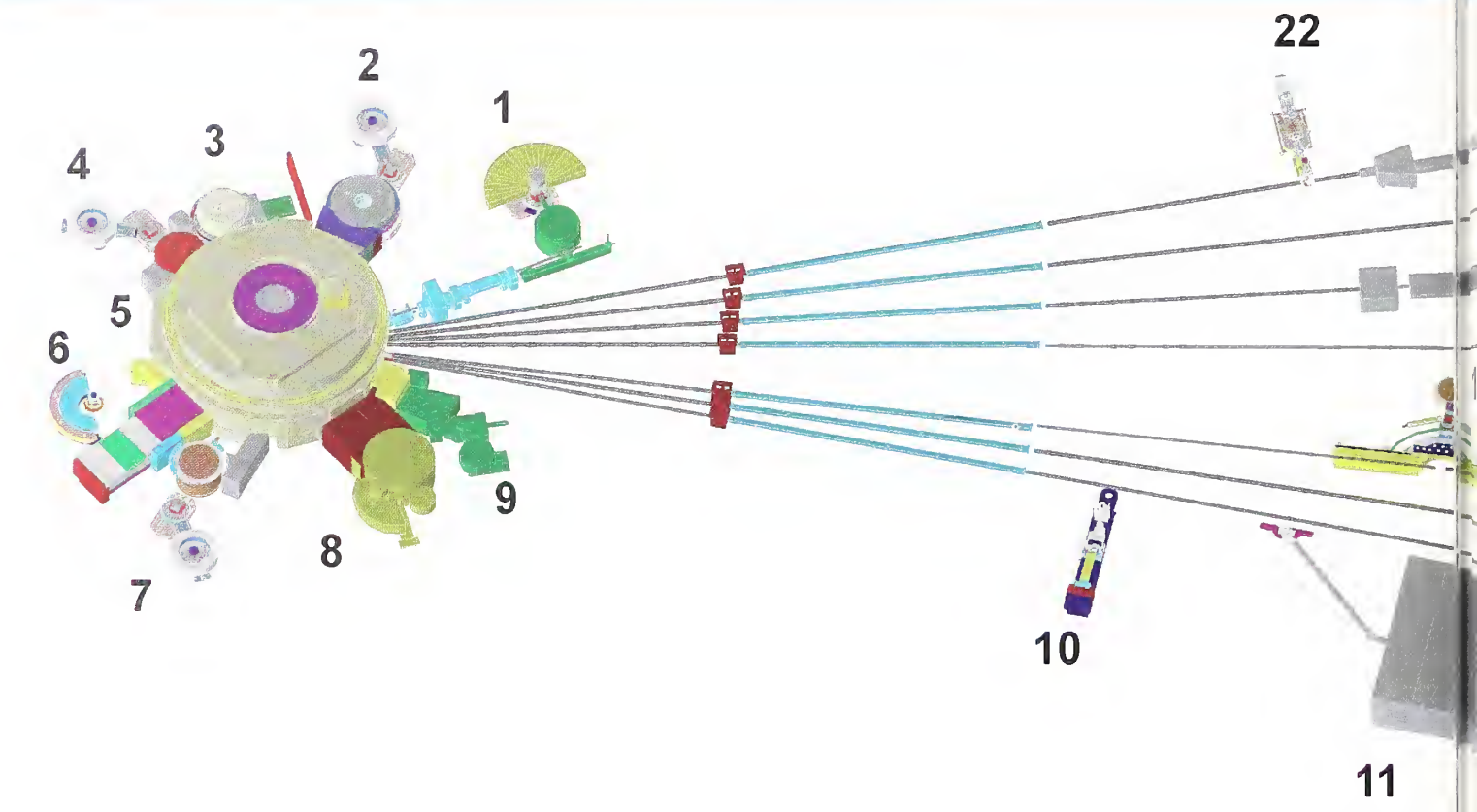

1. **A Cold Neutron Depth Profiling** instrument (not shown) for quantitative profiling of subsurface impurities currently at this site will be moved to another position. Shown is a proposed **Triple Axis Cold Neutron Crystal Spectrometer** with double focusing monochromator and multiple crystal analyzer/detectors that can be flexibly configured for several energies simultaneously or for high throughput at one energy.
2. **BT-7 Triple Axis Spectrometer** with fixed incident energy for measurements of excitations and structure.
3. **BT-8 Residual Stress Diffractometer** optimized for depth profiling of residual stress in large components.
4. **BT-9 Triple Axis Crystal Spectrometer** for measurements of excitations and structure.
5. **Thermal Column** A very well-thermalized beam of neutrons used for radiography, tomography, dosimetry and other experiments.
6. **BT-1 Powder Diffractometer** with 32 detectors; incident wavelengths of 0.208 nm, 0.154 nm, and 0.159 nm, with highest resolution of $\delta d/d = 8 \times 10^{-4}$.
7. **BT-2 Triple Axis Crystal Spectrometer** with polarized beam capability for measurement of magnetic dynamics and structure.
8. **BT-4 Filter Analyzer Neutron Spectrometer** with cooled Be/Graphite filter analyzer for chemical spectroscopy.
9. **BT-5 Perfect Crystal Diffractometer SANS** small angle neutron scattering instrument for microstructure on the 10^4 nm length scale sponsored by the National Science Foundation and NIST, part of the Center for High Resolution Neutron Scattering (CHRNS).
10. **NG-7 Horizontal Sample Reflectometer** allows reflectivity measurements of free surfaces, liquid vapor interfaces, as well as polymer coatings.
11. **Neutron Interferometry and Optics Station** with perfect silicon interferometer; vibration isolation system provides exceptional phase stability and fringe visibility.
12. **Spin Polarized Triple Axis Spectrometer (SPINS)** using cold neutrons with position sensitive detector capability for high resolution studies — part of CHRNS.

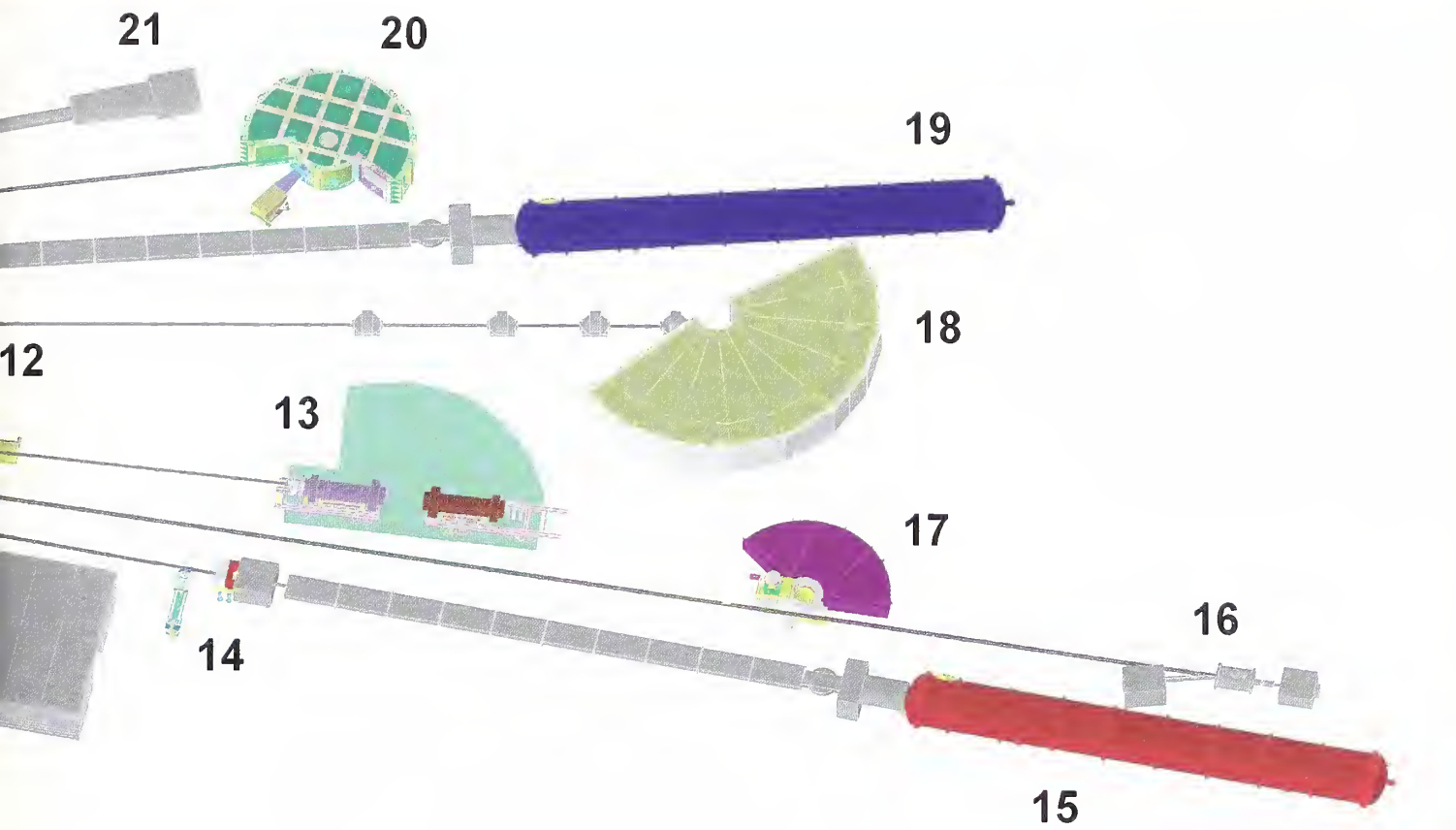

13. **Spin Echo Spectrometer** offering neV energy resolution, based upon Jülich design, sponsored by NIST, Jülich and ExxonMobil — part of CHRNS.
14. **Prompt Gamma Activation Analysis** cold neutron fluxes allow detection limit for H of 1 μg to 10 μg. Focused beams are available for profiling.
15. **NG-7 30 m SANS** for microstructure measurements sponsored by NIST, ExxonMobil, and the University of Minnesota.
16. **Neutron Physics Station** a cold neutron beam 150 mm x 60 mm, available for fundamental neutron physics experiments.
17. **Fermi Chopper TOF Spectrometer** a hybrid time-of-flight spectrometer for inelastic scattering with incident wavelengths between 0.23 nm and 0.61 nm chosen by focusing pyrolytic graphite crystals. A simple Fermi chopper pulses the beam.
18. **Disk Chopper TOF Spectrometer** versatile time-of-flight spectrometer, with beam pulsing and monochro-matization effected by 7 disk choppers. Used for studies of dynamics in condensed matter, including macromolecular systems — part of CHRNS.
19. **NG-3 30 m SANS** for microstructure measurements sponsored by the National Science Foundation and NIST — part of CHRNS.
20. **Backscattering Spectrometer:** high intensity inelastic scattering instrument with energy resolution < 1 μeV, for studies of motion in molecular and biological systems — part of CHRNS.
21. **8 m SANS** for polymer characterization, sponsored by NIST Polymers Division.
22. **Vertical Sample Reflectometer** instrument for measuring reflectivities down to 10^{-8} to determine subsurface structure, with polarization analysis capability.

NCNR Images 2001

NCNR reactor operators Chris Grant and Steve Pierce at the control panel.

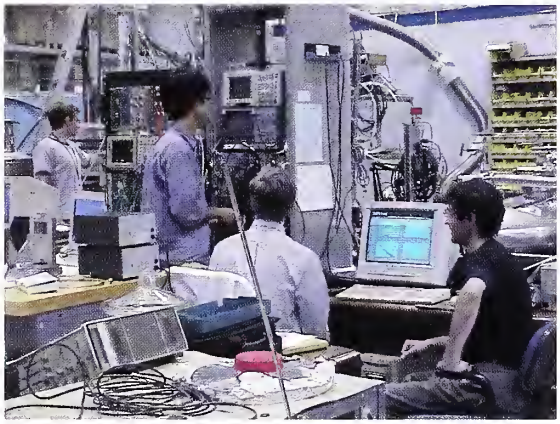

Jeff Nico (center, Ionizing Radiation Div.) with NRC and Harvard researchers at the ultracold neutron trapping experiment to measure the neutron lifetime.

Andreas Michels (U. Saarlandes) and Raghavan Viswanath (Fz. Karlsruhe) at the NG-3 SANS display.

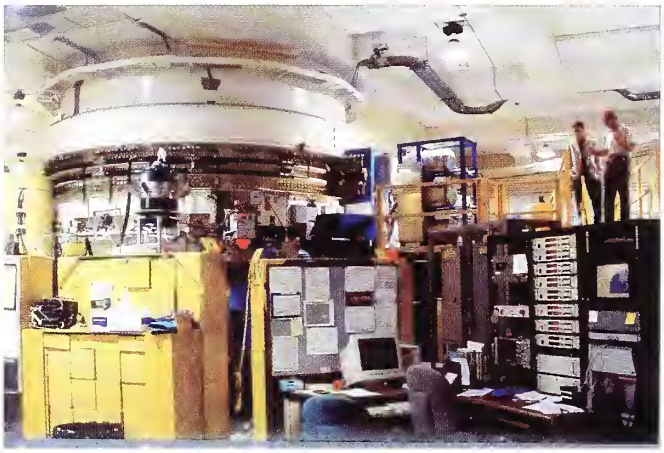

NCNR's John Copley describes the NIST reactor to a visitor.

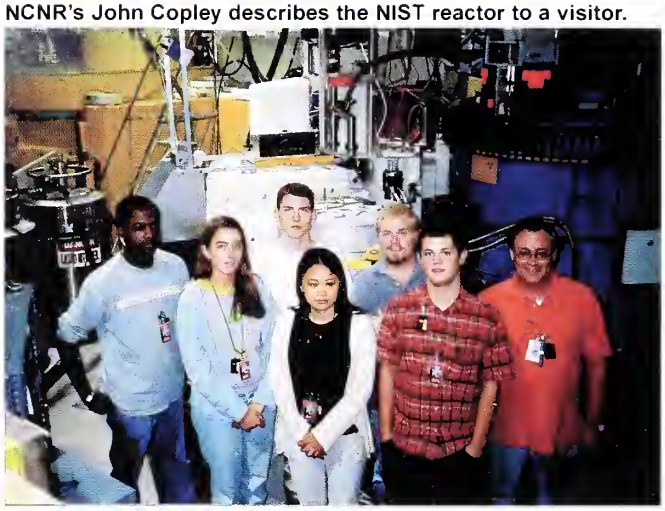

Syracuse University Professor Bruce Hudson (right) with his team at the Filter Analyzer Neutron Spectrometer.

NCNR's Steve Kline injects a sample into the SANS high pressure cell.

NCNR's Susan Krueger and Deborah Kuzmanovic (Biotechnology Div.) collect SANS data on molecules that can be used to test for diseases in humans.

Gathering of Eagles -- in search of the elusive CDW.

NCNR Support Staff enjoy a day away in Washington to visit the Dept. of Commerce and the White House.

Jamie Schulz (University of Maryland) mounts a sample on the NG-1 reflectometer.

NCNR's Paul Liposky, Dave Anderson (FDA), and Liz Mackey (Neutron Methods Group) with the new thermal neutron Prompt Gamma-ray Activation Analysis Instrument (PGAA).

NCNR's Nick Rosov instructing at the 7th annual NCNR Summer workshop.

Measurement Of The Free Neutron Lifetime

Free neutrons are unstable and decay with a lifetime of about 15 minutes into a proton, an electron, and an antineutrino. Accurate determination of this natural lifetime is important for tests of the Standard Model of Fundamental Particles and Interactions, as well for understanding certain aspects of cosmology and astrophysics. The neutron lifetime influences the predictions of the theory of Big Bang nucleosynthesis for the primordial helium abundance in the universe and the number of different types of light neutrinos. Since the dominant uncertainty for the primordial helium abundance comes from the accuracy of the neutron decay rate [1], improved neutron decay rate measurements are needed for sharpening this prediction.

The measurement of the lifetime of free neutrons in a cold neutron beam was one of the first experiments operating in the NCNR Guide Hall. The experiment occupied the NG-6 Physics Station alternatively with other fundamental physics experiments through December 2000. A statistical precision of one part per thousand was achieved in the final result. An overall standard uncertainty of about four parts per thousand has been obtained, and that uncertainty may be eventually reduced by as much as a factor of two by ongoing developments in characterization of the neutron counting for this experiment.

Figure 1 shows a schematic diagram of the apparatus. An axial 5 Tesla magnetic field provides radial containment of the decay protons, while axial containment is achieved by the positive electrostatic charge on two end electrodes, called the mirror and the gate. This combination of magnetic and electrostatic fields is called a "Penning Trap." The neutron detector consists of a well-characterized isotopic target of ^{6}Li, viewed by a set of four charged particle detectors. The charged particles from neutron reactions in the isotopic targets are counted with an accuracy of better than one part per thousand. The reaction cross sections for these standard cross sections are known to about 0.25 %.

When a neutron in the beam decays inside the trapping region, the recoil proton is trapped. Periodically, the gate electrode is lowered to ground potential to allow the

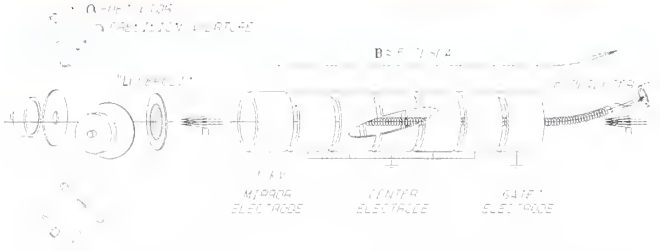

Fig. 1. Schematic drawing of the NIST Penning trap neutron lifetime experiment.

accumulated trapped proton(s) to exit the trap and be counted by the proton detector. A bend in the magnetic field makes it possible to locate the proton detector outside of the incoming neutron beam. The trapped protons have a maximum energy of less than 800 eV and are undetectable at those low energies, but by holding the proton detector at a negative high voltage of the order of −30 kV, the protons may be detected with a signal well above noise levels. The signal-to-noise ratio is further enhanced by counting for only a short time (less than 100 ms) after the trap is opened in each counting/trapping cycle. Typical trapping times are of the order of 10 ms, and typical decay event rates are of the order of a few protons per second.

Determination of the lifetime requires either an accurately known trap length or a variable trap length with accurately known differences in length. The latter is more easily realized physically and is achieved in this apparatus by the precision machining of the segmented trap structure. The hard-to-define end effects do not change significantly as the trap length is varied by applying the mirror voltage to different segments. Figure 2 shows a plot of the measured proton rate (after normalization to the neutron rate) as a function of trap length; the slope of this line is inversely proportional to the neutron lifetime.

Since the time when some of the present staff of this experiment participated in a closely related experiment [2] at the Institut Laue-Langevin, a large number of changes have been made to improve the accuracy. Perhaps the most important factor was simply having much more beam time for evaluation of significant systematic effects and accumulation of better statistical

M. S. Dewey, D. M. Gilliam, J. S. Nico, and F. E. Wietfeldt
Ionizing Radiation Division
National Institute of Standards and Technology
Gaithersburg, MD 20899-8461

W. M. Snow
Indiana University Cyclotron Facility
Indiana University
Bloomington, IN 47405-7105

G. L. Greene
Los Alamos National Laboratory
Los Alamos, NM 87545

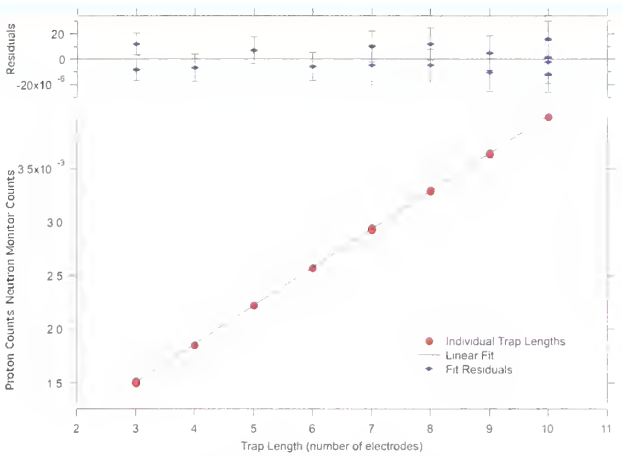

Fig. 2. A plot of the proton count rate (normalized to the neutron monitor count rate) vs. trap length. The slope of the line is inversely proportional to the measured neutron lifetime.

precision. Other factors include Monte Carlo-computed corrections due to magnetic field inhomogeneities, improved beam profiles and proton alignment, better trap voltage stability and monitoring, improved definition of the areal mass density of the isotopic targets, use of a new trap designed to minimize instabilities, and improved analysis methods.

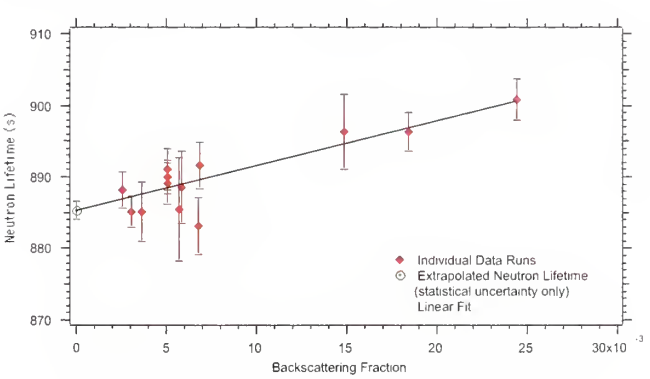

Fig. 3. A linear fit of the measured neutron lifetime at varying values of the detector backscattering fraction. The extrapolation to zero backscattering gives the free neutron lifetime.

Figure 3 shows the extrapolation of the measured lifetime as a function of the backscattering fraction for protons from the detector surface to zero backscattering. The preliminary lifetime value obtained in this experiment [3] is

$$885.3 \text{ s} \pm 4.0 \text{ s}.$$

Continuing efforts to measure the neutron count rate are underway by both calorimetric and coincidence techniques, which should reduce the final uncertainty by half. They will not only improve the results of this experiment but also provide a more accurate and direct calibration of the NIST Standard Neutron Source.

Also underway at NG-6 is a new experiment to measure the neutron lifetime by an independent method involving magnetic trapping of ultracold neutrons. This experiment is being carried out in collaboration with the Physics Department of Harvard University.

REFERENCES

[1] S. Burles, K. M. Nollett, J. W. Truran, and M. S. Turner, Phys. Rev. Lett. **82**, 4176 (1999).

[2] J. Byrne *et al.*, Phys. Rev. Lett. **65**, 289 (1990); J. Byrne *et al.*, Europhys. Lett. **33**, 187 (1996).

[3] M. S. Dewey *et al.*, manuscript in preparation.

ETS-4: Maxwell's Zeolite

Scottish physicist James Clerk Maxwell (1831-1879) discussed a mythical device that could separate molecules by temperature, a concept now known as Maxwell's demon. Maxwell used this idea to explore how sorting molecules by size would violate the second law of thermodynamics. If one did have a Maxwell's demon, a more useful task for it would likely be to separate molecules by size. This would allow mixtures to be separated into pure substances and would facilitate removal of dangerous contaminants from valuable materials. In some cases, molecular separations can be performed using zeolites and similar materials. Zeolites are composed of linked tetrahedral SiO_4 and AlO_4 species, arranged in rings to create a framework of molecule-sized cavities. Related zeolitic materials may use other tetrahedral atoms to build the framework. Molecules can access these cavities or pores, under two conditions: if they can pass through the appropriate rings in the framework and these rings are not blocked by other species in the material, such as cations. If the ring size in a material matches the needs for a particular chemical separation, the material may be appropriate. Chemical modifications, such as ion exchange or changing the framework composition can sometimes influence the

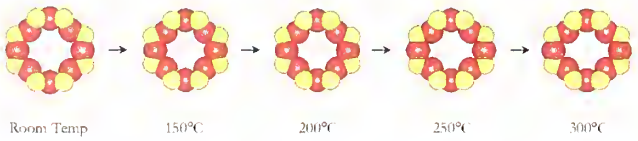

Fig. 1. Size of the eight-ring pore opening in ETS-4 as a function of dehydration temperature.

pore size. So, occasionally it is possible to modify a zeolite to a particular separation. However, this does not allow what Maxwell might envision, where the pore size can be adjusted over a wide range to suit the desired process, in effect a Maxwell's demon for size separations. This exact capability has now been demonstrated in material ETS-4 [1]. ETS-4 can be processed in such a way so that the pore sizes can be tuned for particular separations.

ETS-4 is a titanosilicate material invented by Engelhard in the 1980's [2]. ETS-4 differs from most zeolitic materials in a number of ways. Chemically, it is an oxide of Ti and Si, while the majority of zeolitic materials are oxides of Al and Si. Structurally, the material is composed of both tetrahedral TiO_4 and octahedral TiO_6 units, as well as SiO_4 units. Finally, while most zeolitic materials hydrate and dehydrate reversibly or are destroyed during dehydration, ETS-4, at least in some ion-exchanged forms, can be induced to dehydrate irreversibly and without destruction of the pores. Dehydration reduces the average pore opening size, and thus it is possible to tune the zeolite to accept molecules of a particular size by changing level of dehydration. The amount of dehydration in turn is dictated by the temperature to which the material is exposed. In 1999, the Advanced Technology Program funded Engelhard to exploit this effect, which Engelhard calls the Molecular Gate,® to develop methods for separating oxygen from air, a process with useful applications for prevention of pollution as well as medical and other industrial applications.

The mechanism behind the Molecular Gate® effect was demonstrated crystallographically using data from the BT-1 neutron powder diffractometer. Pores in ETS-4 must be accessed via a ring of eight Si and Ti atoms, each linked by oxygen atoms. This ring is commonly called an eight-ring, despite the fact that it is actually composed of

van der Waals opening (Å)	Dehydration Temperature, °C				
	RT	150	200	250	300
D_1	4.27	3.97	3.95	3.94	3.90
D_2	4.43	4.02	4.09	4.57	4.57
D_3	3.61	3.28	3.29	3.27	2.77

Table 1. Eight-ring opening as a function dehydration temperature. Distances are the separation between van der Waals radii between opposite O5 (D_1), O1 (D_2) and O2 (D_3) atom pairs (see Fig. 2).

S. M. Kuznicki, V. A. Bell and R. M. Jacubinas
Strategic Technology Group
Engelhard Corporation
Iselin, NJ 08830

S. Nair, H. W. Hillhouse, C. M. Braunbarth and M. Tsapatsis
Department of Chemical Engineering,
University of Massachusetts
Amherst, MA 01003

B. H. Toby
NIST Center for Neutron Research
National Institute of Standards and Technology
Gaithersburg, MD 20899-8562

sixteen atoms. In Fig. 1, the size of this eight-ring is shown as a function of dehydration temperature. The actual size of molecules that can be admitted via this opening are dictated by the van der Waals radii of the O atoms in the eight-ring and the van der Waals dimensions of the molecule to be admitted. Since accurate determination of oxygen atom siting is needed, and since ETS-4 does not form single crystals, neutron powder diffraction

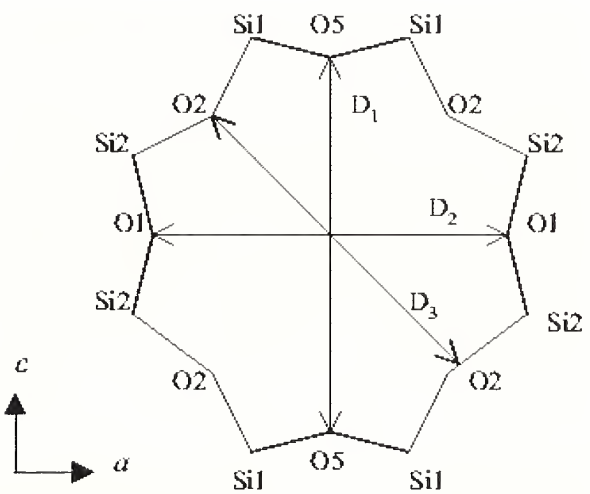

Fig. 2. Atom and pore-opening distance labeling scheme in the eight-ring opening of ETS-4.

measurements are the only way to obtain accurate measurements of the ring openings as a function of dehydration temperature. Measurements of the eight-ring opening from Rietveld refinements are shown in Table 1, relative to the distances diagrammed in Fig. 2.

The proof that dehydration indeed does change the pore access is demonstrated by adsorption isotherms, shown in Fig. 3. The separation shown in the top of this figure, between O_2 and N_2, shows how precisely the pore sizes can be adjusted. The difference in van der Waals radius between oxygen and nitrogen is only 0.1 Å.

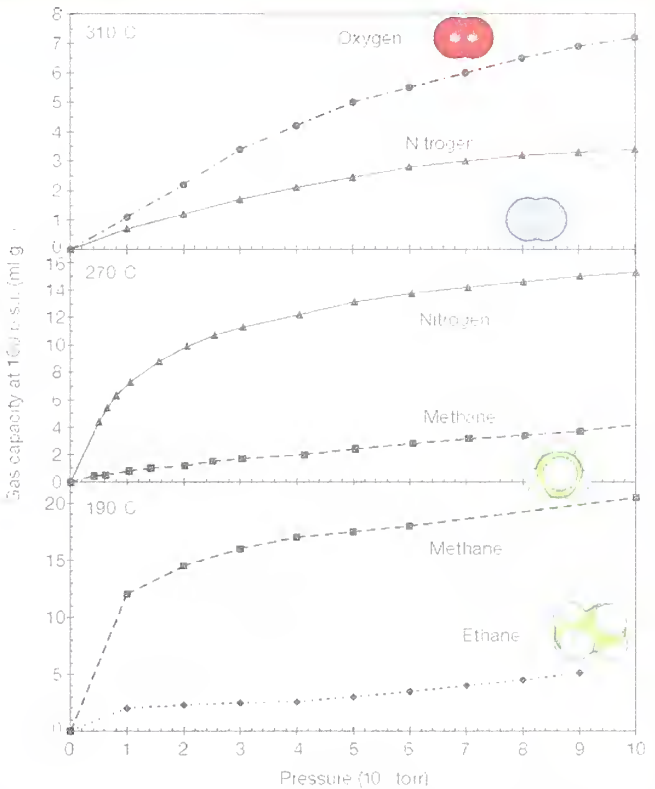

Fig. 3. Adsorption of selected molecules as a function of dehydration temperature.

REFERENCES

[1] S. M. Kuznicki, V. A. Bell, S. Nair, H. W. Hillhouse, R. M. Jacubinas, C. M. Braunbarth, B. H. Toby, and M. Tsapatsis, Nature **412**, 720 (2001).

[2] S. M. Kuznicki, US Patent 4938939 (1990).

Stresses in Electron Beam Weld Joints of Superalloys

Single-crystal turbine blades are the pinnacle of a decade-long development and refinement of nickel-based superalloys. By eliminating creep along grain boundaries as the main failure mechanism of polycrystals at high temperatures, the use of single crystal turbine blades has allowed a rise in temperature in the "hot zone" by more than 100 K, thus substantially increasing the thermodynamic efficiency. The complete turbine blade, including the mounting base and the cooling channels, is grown from the melt in a single process and represents a considerable investment. In order to protect this investment, electron beam welding (see Fig. 1) is used to repair minor structural damage of failed components.

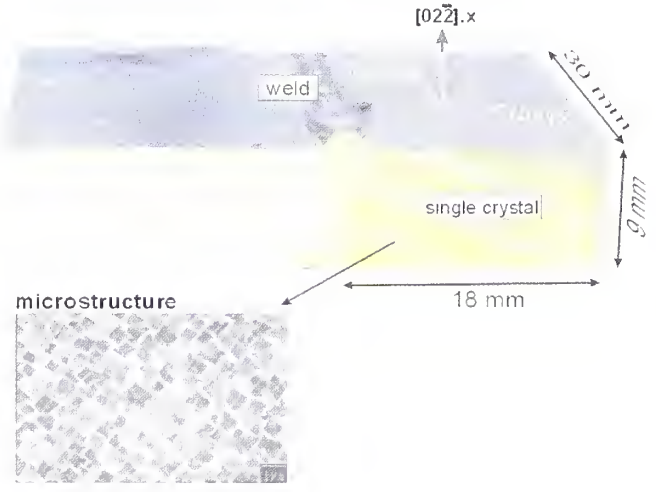

Fig. 1. Test specimen of a weld joining a Rene N5 single crystal and a polycrystal. The three different regions, polycrystal, weld, and single crystal, appear in different colors after etching which indicates a different chemical composition. The microstructure shows typical features: 60 % cuboidal γ'-precipitates and unimodal size distribution.

Usually a polycrystalline alloy of comparable composition is chosen as a replacement material. The typical grain size of the polycrystal is approximately one millimeter which is about the size of the incident neutron beam. Thus, stress measurements are not feasible for this side of the weld.

The weld process creates very high residual stresses that make the extended weld region prone to cracking. Cracks are sometimes found parallel to the weld especially in the z-direction, so that an additional heat treatment must be applied for stress relief. The standard heat treatment is 2 h at 1423 K for homogenizing (solution) and a subsequent aging treatment. In this investigation we compare the stresses before and after heat treatment in the single crystal side of the weld joint.

Compared to a measurement on a fine-grained polycrystal, the measurement procedure is rather difficult because all small angle grain boundaries (Fig. 2) have to be brought into reflection and averaged over the rocking angle ω in the data reduction.

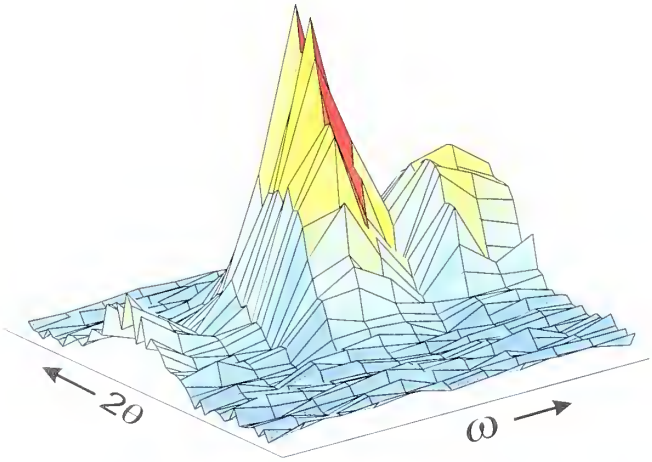

Fig. 2. Q_x-intensity map for the as-welded sample (reciprocal space) plotted vs. 2θ and the rocking angle ω. Small angle grain boundaries as indicated by the presence of several maxima are characteristic for superalloy single crystals. The existence of two maxima in 2θ (equivalent to two *d*-spacings) indicates the γ-matrix and the γ'-precipitates whose lattice parameters are close to each other.

Additionally, both the welding and the heat treatment produce position-dependent chemical gradients that affect the unstressed lattice parameters. Their measurement would have required cutting the specimen into little pieces for complete stress relief. We chose an alternative approach of applying mechanical boundary conditions at the surface. The results obtained from this procedure are shown in Fig. 3.

The effect of the heat treatment is dramatic. Both the strong tensile stresses in the heat-affected zone (5 mm from the weld center) and the strong gradients at the

T. Gnäupel-Herold and H. J. Prask
NIST Center for Neutron Research
National Institute of Standards and Technology
Gaithersburg, MD 20899-8562

interface between weld and heat affected zones are removed. Stress relief in the z-direction is especially important because it removes the driving force for crack opening parallel to the weld in the heat-affected zone.

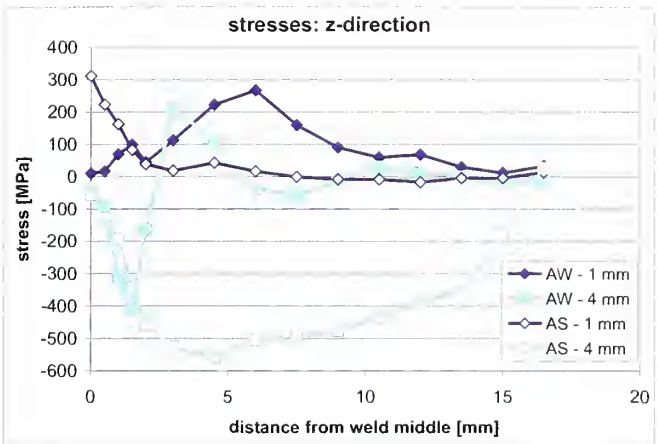

Fig. 3. Residual stresses σ_{zz} before and after the heat treatment for two different depths from the upper surface. AW stands for 'As Welded'; AS stands for 'Heat Treated'. The uncertainties are of the order of the size of the data points.

Remarkable are the strong compressive stresses after heat treatment in the middle (4 mm depth) both for the z-direction and the y-direction (Fig. 4). There is evidence that solidification partitioning can lead to a different γ/γ'-microstructure in the weld zone, thus affecting the mean lattice parameter measured by diffraction. The immediate results are apparent stresses caused by changes in the unstressed d-spacing. This effect can be removed with some confidence only for the measurements close to the surface (= 1 mm depth) by using mechanical equilibrium conditions. Further investigations are under way to clarify this effect for larger depths.

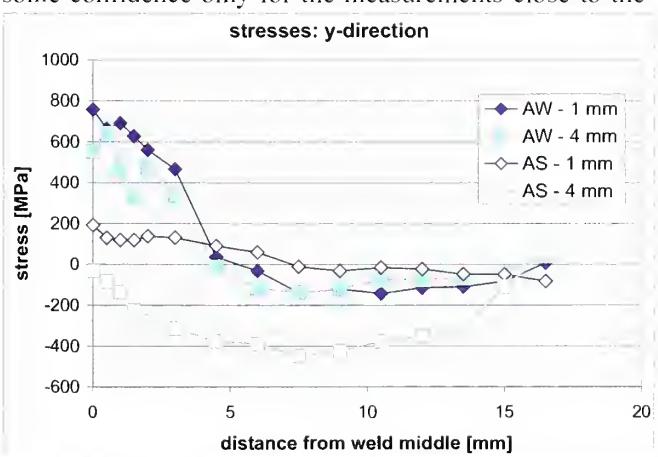

Fig. 4. Residual stresses σ_{yy} (parallel to the weld) before and after the heat treatment.

The stresses parallel to the weld (Fig. 4) are usually the highest and the most dangerous stresses because they reach the yield limit (around 600 MPa). If the weld direction is oriented such that the weld line is parallel to the main stress axis – i.e., radially for a rotating blade – then further loading would exeed the flow stress and cause a dangerous local weakening of the turbine blade. Here, the effect of the heat treatment is most beneficial because almost complete stress relief is achieved.

The stress relief effect of the heat treatment extends also to the microstresses between sub-grains by removing the dislocations created by the plastic deformation in the weld region. While direct observations of dislocations are not available, we can use the full width at half maximum (FWHM) of the measured integrated strain distributions as a measure for the dislocation density (see Fig. 5).

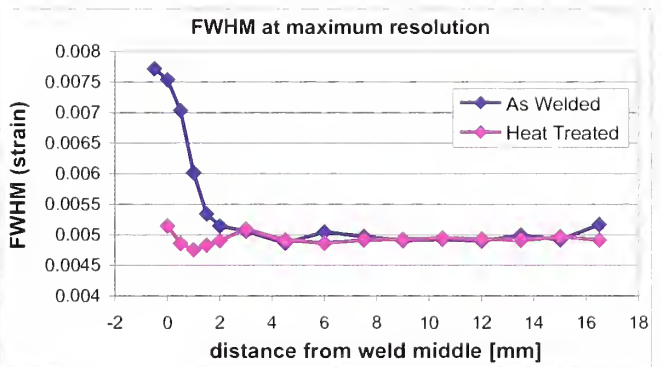

Fig. 5. FWHM at the best instrument resolution before and after heat treatment. These results are representative for all measured depths.

Figure 5 shows clearly that substantial plastic deformation exists only in the weld itself (0…1.0 mm) and within a very narrow zone of about 0.5 …1.0 mm in the base material. This effect vanishes completely after the heat treatment.

These results demonstrate that a heat treatment after welding is essential for avoiding detrimental effects to the mechanical properties of the turbine blade.

EXPGUI: Smoothing the Path to Powder Crystallography

Back in the dark ages of computational crystallography, crystallographers were expected to be able to modify their computer programs to suit the computation at hand. Most crystallographers could create programs to convert data between different formats and felt comfortable reading through a program's source code when the program documentation did not adequately explain a topic. (There is disagreement on when this ended, some say the 1950's, others say the 1980's or even the early 21st century!)

The advent of desktop computing has also introduced a new paradigm of computing — the graphical user interface (GUI). Visual analogies to physical devices (such as switches) makes operating GUI intuitive; a good GUI implementation significantly reduces learning time.

Simultaneous with the changes in computing, crystallography has evolved from a technique used exclusively by specialists to one of many tools in the arsenal of chemists, physicists and engineers. To facilitate this, the NCNR is developing GUI-based software for crystallography. There are two goals: to increase the utility of the software for the non-specialist and to improve the productivity of experts. This allows novices to concentrate on the science and techniques of neutron powder crystallography rather than devote their efforts to learning arcane details of computer software.

The Rietveld refinement technique for crystallographic analysis was adopted within the NCNR immediately after its first publication [1]. The NCNR then produced Rietveld software specifically adapted to the local instrumentation, which is still being improved [2,3]. However, the General Structure Analysis System (GSAS) package of programs from Los Alamos is also widely used [4]. GSAS has wide applicability. It can be used with virtually any type of neutron or x-ray diffraction data, including both powder and single crystal data. It supports a wide range of geometric and compositional restraints and constraints. While many new features have been added to GSAS on a continual basis, the original text-based user interface has not changed. Novice and occasional users often find the many levels of dialogs cumbersome and difficult to learn.

Work on a GUI for GSAS was begun several years ago, with the modest goal of providing a mechanism for accessing a small portion of the GSAS features. The project, now called EXPGUI, has grown in scope [5]. Most of the commonly used powder diffraction features are now implemented, allowing a complete Rietveld refinement to be performed graphically. Features not implemented in the GUI can still be accessed via the standard GSAS user interface. EXPGUI runs identically on all platforms where GSAS is supported, including both Unix and Windows. In FY2001, the Advanced Technology Program recognized the value of this effort and provided funding to accelerate development.

The GUI is designed to display information and controls in a concise and intuitive fashion. An example screen, shown in Fig. 1, manipulates structural parameters. This figure demonstrates how four atoms that share sites in this material can be selected together, so that their refinement options can be changed as a group. Another screen, shown in Fig. 2, applies constraints that link appropriate parameters in the refinement.

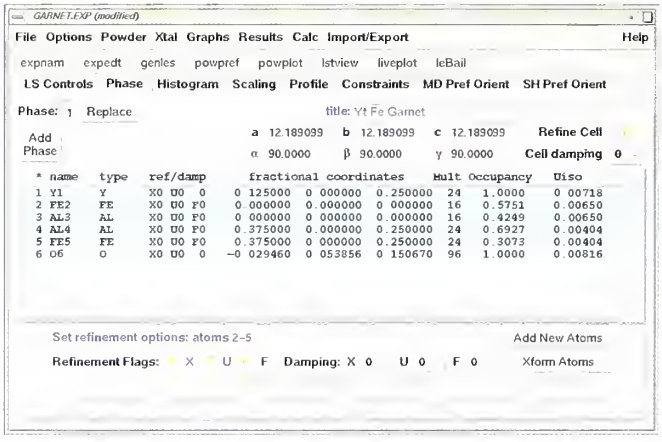

Fig. 1. Sample screen from EXPGUI, showing where atomic parameters are displayed.

Recent EXPGUI development has been aimed at extending the capabilities of the GSAS package. As an example, when EXPGUI was recently given the ability to import atomic coordinates from files, support was added for CIF, the complex standard crystallographic information file format developed by the International Union of

B. H. Toby
NIST Center for Neutron Research
National Institute of Standards and Technology
Gaithersburg, MD 20899-8562

Crystallographers. Further, the import routine was written in a general fashion, so that other formats are easy to add.

Where possible, EXPGUI takes advantage of the graphical nature of modern computers to offer scientists better access to refinement tools. Figure 3 shows a graphical display of the observed and computed diffraction pattern. Through a simple set of mouse operations, the user has "zoomed in" on a portion of the data, to better see the poor agreement between observed and computed intensity values, indicating that the structure is not well modeled.

This graphical tool also allows the user to see the fitted background and to label the reflection indices — features not previously available within GSAS. Another example is a new tool for background fitting. In most cases, background fitting is nearly automatic, but for some refinements, fitting can be quite difficult. GSAS allows a scientist to define the background either through use of a function with refinable terms or as a spline

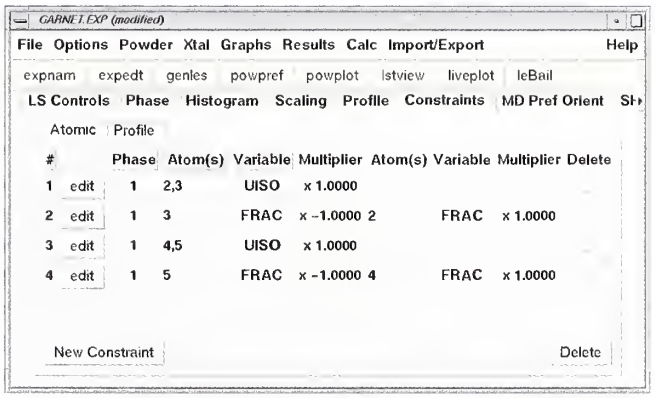

Fig. 2. EXPGUI screen for entering and display of atomic constraints. In this case, atoms sharing sites are constrained to have the same U_{iso} values and have fractional occupancies that total to unity.

drawn through a set of fixed points. A new tool in EXPGUI improves GSAS by allowing a user to define where the background curve should occur using a computer mouse. Since many experts agree that fixed background points are a poor way to treat background fitting, EXPGUI offers an augmented feature: a background function can be fit to the user's desired background curve. The terms for this function will be sufficient to obtain an initial model with good agreement to the data. At the end, the background terms can be optimized, to obtain the best possible model. This capability was not previously available in GSAS.

EXPGUI has been widely adopted by Rietveld users. It is used in most major neutron and synchrotron facilities, as well as dozens, if not hundreds, of universities, companies and research centers around the world.

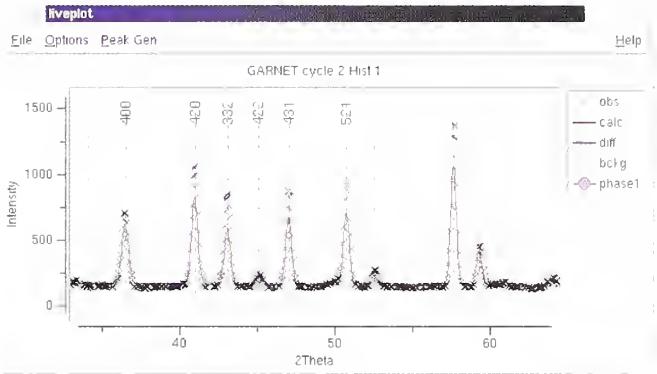

Fig. 3. Graphical display of fit in EXPGUI. This plot has been "zoomed" in to show details. Several features of this plot, for example the display of reflection indices and the location of the fitted background were not previously available in GSAS.

REFERENCES

[1] H. M. Rietfeld, J. Appl. Cryst. **2**, 65 (1965).
[2] L. W. Finger and E. Prince, National Bureau of Standards, Report No. 852 (1975).
[3] B. H. Toby, E. Prince, and J. Stalick, unpublished computer program (2000).
[4] A. C. Larson and R. B. Von Dreel, Los Alamos National Laboratory, Report LAUR 86-748, (2000).
[5] B. H. Toby, J. Appl. Cryst. **34**, 210 (2001).

Neutron Diffraction Contributes to Improving the Fatigue Life of Bridges

Welded attachments to large-scale structures such as bridges can limit the serviceability and prevent effective use of higher strength steels. To avoid this, it is desirable to enhance the fatigue resistance of common attachment details such as transverse stiffeners, cover plates, gusset plates and other welded details that – at the weld toe – are often the initiation point for crack growth.

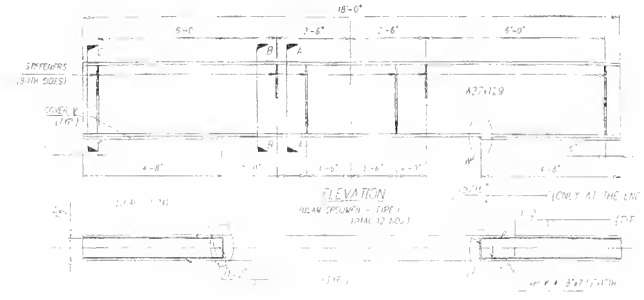

Fig. 1. Partial details of one of the beam specimens being fatigue tested at the ATLSS facility. The cover plate location is shown as "W" and "Y" on the right side.

Enhancement of fatigue resistance of welded joints by plastic deformation of the surface and by improvement of weld toe characteristics is well established [1,2]. It is known that the conventional improvement techniques such as grinding, shot peening, air hammer peening, gas tungsten arc (TIG) re-melting, and use of improved welding consumables can improve fatigue resistance of welded details [3]. However, these procedures are manpower intensive, and not always efficient or environmentally friendly. Ultrasonic Impact treatment (UIT) offers an alternative means to avoid the negative aspects of other methods [4].

The post-weld enhancement of welded details by UIT, developed by Statnikov and co-workers [4], involves deformation treatment of welds by impacts at ultrasonic frequency on the weld toe surface. The objective of the treatment is to introduce beneficial compressive residual stresses at the treated weld toe zones and to reduce stress concentration by improving the weld toe profile. UIT is claimed to involve a complex effect of strain hardening, reduction in welding strain, relaxation in residual stress, and a reduction in operating stress concentration, thereby achieving a deeper cold worked metal layer. However, virtually none of the effects ascribed to UIT have been confirmed by appropriate measurements.

Recent work at the NCNR has made significant contributions in providing new insights into how UIT actually affects residual stresses in the weld region around a full-scale cover plate for a steel girder. In Fig. 1 a typical I-beam fatigue-tested at the Center for Advanced Technology for Large Scale Structures (ATLSS) at Lehigh University is shown. In the initial phase of the NCNR-Lehigh collaboration, neutron diffraction was used to determine the effect of UIT on a simulated flange plate with attached cover plate detail having a 0.5 in. (12.7 mm) end fillet weld before and after the treatment by UIT.

The geometry and dimensions of the welded detail are the same as in the full-scale fatigue test beams of Fig. 1. Both base plate and cover plate are A572 Gr.50. This kind of cover-plate detail is largely used in steel bridges but has a low level of fatigue strength in comparison with other welded configurations.

The neutron diffraction measurements were made in a fairly complex mesh, mostly in the near vicinity of the weld toe as shown in Fig. 2. Overall, residual stresses

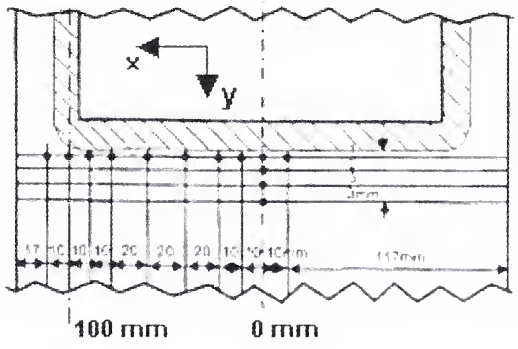

Fig. 2. Top of cover plate region of interest, and part of measurement mesh.

were determined at 30 positions in the weld region, before and after UIT. Gauge volumes of 3 x 3 x 3 mm^3 (interior) and 2 x 2 x 2 mm^3 (near surface) were used. The unstressed d-spacing, d_0, was determined from a small piece of the starting material. The depth dependence of X-direction stresses is shown in Fig. 3. The

H. J. Prask, T. Gnäupel-Herold[1] , and V. Luzin[2]
NIST Center for Neutron Research
National Institute of Standards and Technology
Gaithersburg, MD 20899-8560
and
[1] University of Maryland
College Park, MD 20742
[2] State University of New York
Stony Brook, NY 11794

J. W. Fisher and Xiaohua Cheng
Department of Civil and Environmental Engineering
Lehigh University
Bethlehem, PA 18015-4793

near-surface residual stresses determined, nominally 1 mm below the actual surface, are shown in Fig. 4.

To our knowledge this is the first determination of the triaxial stress distribution in the vicinity of a weld treated

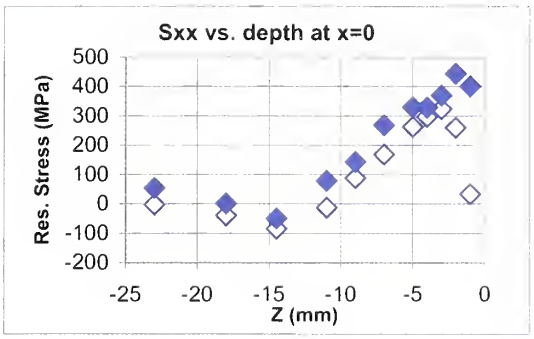

Fig. 3. X-direction residual stresses vs. depth at the weld center. Closed symbols are pre-UIT. Uncertainties are typically ± 20 MPa.

with UIT. In Fig. 4 both the anisotropy of stresses around the untreated weld metal, and the additional anisotropy introduced by UIT are seen. Before UIT, the stresses just beneath the weld toe are comparable and highly tensile in the X and Y directions, which reach and are beyond the minimum yield stress of base plate material, whereas those normal to the surface are generally only ≈ 100 MPa tensile. After UIT the X-direction stresses become compressive, changing in magnitude by about 400 MPa. The Y-direction stresses are reduced by ≈ 150 MPa or less but remain in tension except at one point, and the normal stresses (Z-direction) are essentially unchanged. The UIT effect on X-direction stresses (Fig. 3) is significant only near the plate surface, but deeper than, for example, shot peening. The depth dependence of the Y- and Z-direction stresses was also obtained.

Current neutron diffraction studies in this collaboration are focusing on the mapping of stress gradients within and near weld joints in sections of actual fatigue-tested I-beams, information not obtainable by any other technique.

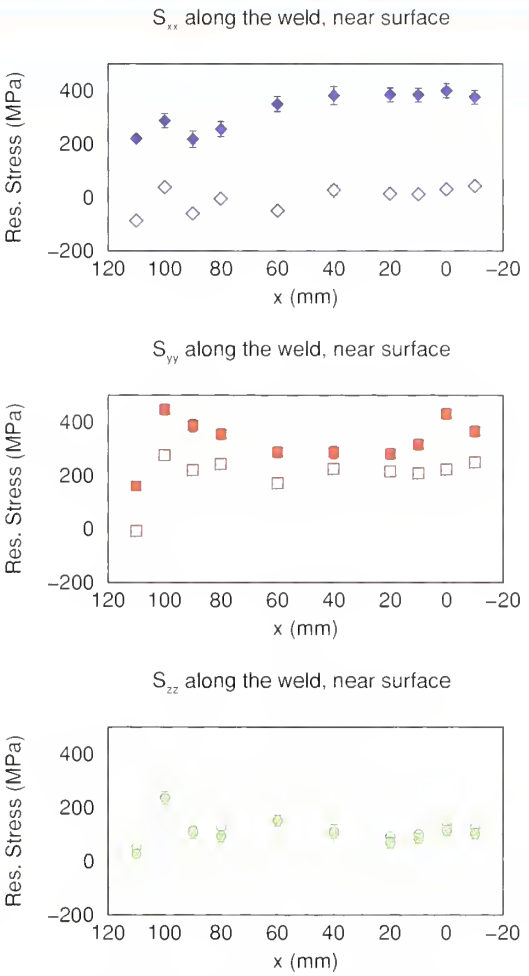

Fig. 4. The residual stresses determined by neutron diffraction for the "near-surface" points. Uncertainties due to counting statistics are typically about ± 20 MPa. Solid symbols are before UIT.

REFERENCES

[1] J. W. Fisher, K. H. Frank, M. A. Hirt, and B. M. McNamee, *Effect of Weldments on the Fatigue Strength of Steel Beams*, NCRP Report 102, Highway Research Board, Washington DC, 1970.

[2] J. W. Fisher, P. A. Albrecht, B. T. Yen, D. J. Klingerman, and B. M. McNamee, *Fatigue Strength of Steel Beams with Transverse Stiffeners and Attachments*, NCHRP Report 147, Highway Research Board, Washington DC, 1974.

[3] J. W. Fisher, H. Hausammann, M. D. Sullivan, and A. W. Pense, *Detection and Repair of Fatigue Damage in Welded Highway Bridges*, NCHRP Report 206, Transportation Research Board, Washington, DC, 1979.

[4] Reviewed in Statnikov, Esh, *Applications of Operational Ultrasonic Impact Treatment (UIT) Technologies in Production of Welded Joints*, Welding in the World **44**, 11 (2000).

Neutron Imaging and Prompt Gamma Activation Analysis Using a Monolithic Capillary Neutron Lens

Glass polycapillary fibers with hundreds of hollow micrometer-wide channels have been used for guiding and changing the direction of slow neutrons [1]. The use of a monolithic lens for PGAA has been explored earlier [2]. In addition, the converging nature of a focused beam can provide magnified images for neutron radiography [3]. We have combined these two uses of the focused beam from a monolithic lens and have implemented an alignment procedure for PGAA aided by neutron imaging.

The measurements have been performed at the end of the NG-0 beam line [4]. The average wavelength of the incident beam with a Be filter is about 0.6 nm. Neutrons are imaged with a camera that consists of a ZnS(Ag)/^{6}LiF scintillator coupled with a CCD camera with an average pixel size of 50 μm. The gamma-ray spectrometry system [5] consists of a p-type germanium photon detector with a virtual pulser "loss free" counting module. The two monolithic lenses used in this study are both fabricated from a bundle of capillaries that is 50 mm long and with a hexagonal cross section of 10 mm wide (flat-to-flat) at the entrance and tapered to 3 mm at exit. The distance from the exit to the focus is 8.8 mm for lens A and 9.8 mm for lens B. Each lens is installed on x-y-z translation stages with two directions of tilt motion. The experimental layout is shown schematically in Fig. 1.

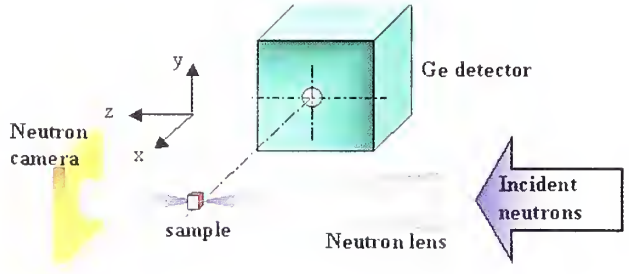

Fig. 1. Schematic experimental layout.

An optimum focal spot from lens A is recorded with the imaging detector. Line profiles across the focal spot in both the horizontal and vertical directions are taken to determine the intensity distribution and the FWHM (H: 87 μm, V:100 μm) of the focus (Fig. 2 a). The gain in neutron current density within the 100 μm x 100 μm area is 46 ± 2, and within a 50 μm x 50 μm area it is 71 ± 5. Images and their sizes and intensities as a function of z are shown in Fig. 2b.

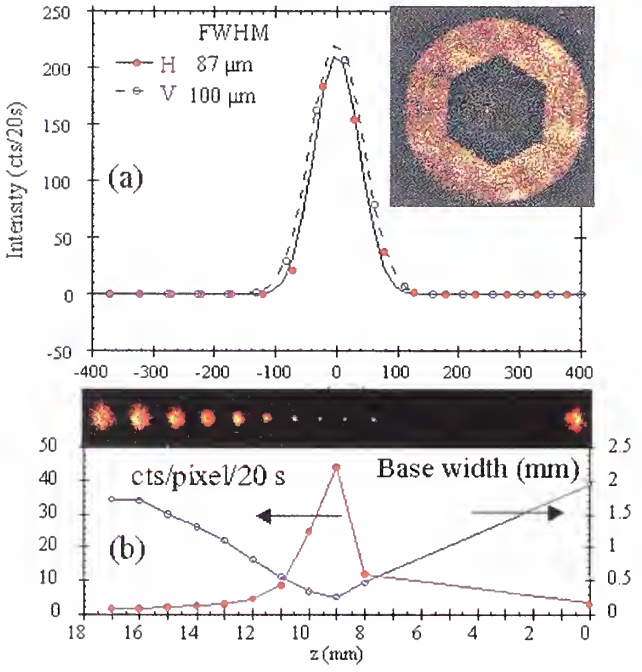

Fig. 2. (a) Line profiles of the focal spot intensity in the horizontal and vertical directions. Insert: Focused beam image - the focus is near the center of the hexagonal shadow cast by the lens entrance, surrounded by the background of unguided neutrons. (b) Intensity and base width of the spot along the beam path, and images of the focused beam "foot print". A linear fit to the region between 10 and 16 mm gives a slope of 0.233 (rad), or a 13.3° convergence angle.

The focused beam creates a neutron "point source", with neutrons departing the focus within a cone of about 13°. Any neutron-absorbing object within the path of the divergent beam will cast a magnified shadow at some further distance. We make use of this effect in order to align a small sample, a Gd foil (thickness 25 μm) of size 2 mm x 0.9 mm, at the focus for PGAA (Fig. 3a). We vary the distance L_1 between the sample and the lens focus by translating the lens along the direction of the beam. The magnified image enables a better alignment of the sample with respect to the focus. From the earlier

H. H. Chen-Mayer, G. P. Lamaze, D. F. R. Mildner and R. Zeisler
Analytical Chemistry Division
Chemical Science and Technology Laboratory
National Institute of Standards and Technology
Gathersburg, MD 20899-8395

W. M. Gibson
X-Ray Optical Systems, Inc.
Albany, NY 12203

measurement of the lens focus image, we determine the location of the focus with respect to the large hexagonal shadow cast by the lens entrance. We then move the lens such that the image of the sample is now superimposed on the image of the focus. This guarantees that the focal point is indeed on the sample. Once the image is centered, the lens is translated to $L_1 = 0$ such that the focus is on the sample, ready for prompt gamma measurements.

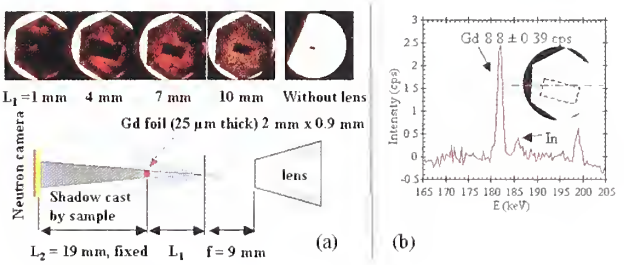

Fig. 3. (a) Magnified image of the sample at various L_1. The image of the sample without the lens is also shown for comparison. (b) Prompt gamma spectrum for Gd (182 keV) and for In (186 keV) measured with the lens, and the corresponding image of the sample.

At the center of the same Gd sample described above, there is an additional indium foil of about 1 mm x 1 mm in cross section, in contact with the Gd strip. The prompt gamma measurement without the lens gives a peak intensity for Gd at 182 keV of 2.1 counts per second (cps), but the In peak at 186 keV is not visible even for a 20 min measurement. When the lens is used in a 10 min measurement, not only has the Gd peak intensity increased, but the In peak has also become visible (Fig. 3b). Since the Gd piece is much larger than the focal spot size, the gain in sensitivity for Gd is only a factor of 4. The gain for In is not estimated.

We have also used lens B for an even smaller sample – a Gd piece of 128 μm x 103 μm x 25 μm in size and 2.59 μg in mass (effective mass ≈ 1 μg taking into account self-absorption). The images from optical microscope and from neutron measurements are shown in Fig. 4a. Without the lens, the neutron camera cannot resolve the 100 μm particle. The gamma intensity with the lens is 17.4 cps with a 1.6 % 1σ counting statistics after 1 hour of counting, and with the direct beam 0.506 cps (3.9 % 1σ) after 19.5 hours. The gain, given by the ratio of the two count rates, is 34 ± 1.4. A scan of the lens in the vertical direction yields a peak, given by the convolution of the sample width with the beam width, as shown in Fig. 4b. The FWHM of the peak is 148 (± 1.5) mm, correctly corresponding to the 100 μm sample-width and the 100 μm beam-width added in quadrature.

The effort presented here is a step toward providing quantitative elemental information to traditional neutron radiography. This new tool will provide a unique capability in non-destructive analysis for industrial materials. In the future, the system will be automated to scan, giving a more efficient probe for micro-analysis with neutron beams.

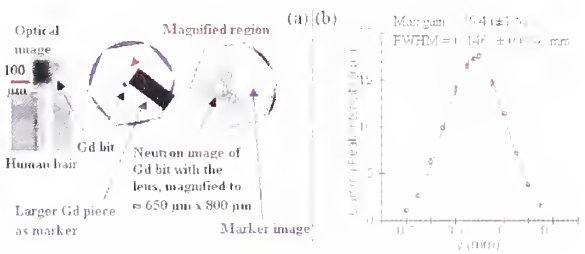

Fig. 4. (a) Optical image of the Gd piece in comparison with a strand of human hair (left), and neutron image using lens B. The large solid rectangle is a larger Gd strip marker to help locate the smaller sample more easily. (b) Gd peak intensity produced by a y-scan of the lens.

REFERENCES

[1] M. A. Kumahkov and V. A. Sharov, Nature **357**, 390 (1992), and H. Chen, R. G. Downing, D. F. R. Mildner, W. M. Gibson, M. A. Kumakhov, I. Yu. Ponomarev, and M. V. Gubarev, Nature **357**, 391 (1992).

[2] V. A. Sharov, Q. F. Xiao, I. Yu. Ponomarev, D. F. R. Mildner, and H. H. Chen-Mayer, Rev. Sci. Instrum. **71**, 3247 (2000).

[3] K. M. Podurets, D. F. R. Mildner, and V. A. Sharov, Rev. Sci. Instrum. **69**, 3541 (1998).

[4] D. F. R. Mildner, H. H. Chen-Mayer, G. P. Lamaze, and V. A. Sharov, Nucl. Instrum. & Meth. A**413**, 341(1998).

[5] R. Zeisler, G. P. Lamaze, H. H. Chen-Mayer, J. Radioanal. Nucl. Chem. **248**, 35 (2001).

Giant Anharmonicity and Theory of Surprising BCS Superconductivity in MgB_2 at 40 K

The recent surprise discovery of superconductivity in MgB_2 at 39 K has stimulated a great deal of research on this intercalated graphite-like system (see Fig. 1). Sparked by this discovery, we set out to unlock the structural secrets and, in particular, to reveal the origin of the high T_c in MgB_2: an electron-phonon or other exotic mechanism? To answer this fundamental question, we calculated T_c, its pressure dependence, and its isotope effect from the electronic band structure and lattice dynamics of MgB_2 using density functional theory within the generalized gradient approximation [1-3].

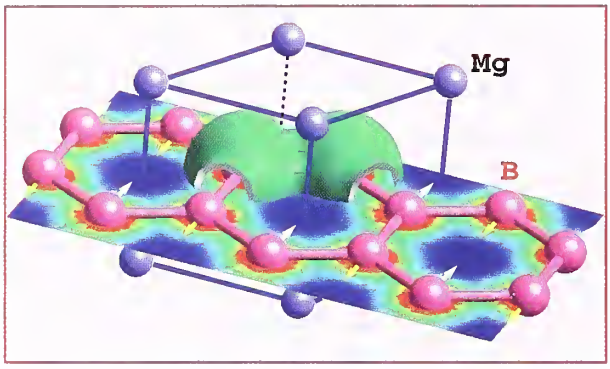

Fig. 1. The crystal structure of MgB_2 consisting of B and Mg hexagonal layers. The in-plane boron modes (shown by arrows) are strongly coupled to the boron $p_{x,y}$ σ bands shown as the green contour and isosurface plots.

Figure 2 shows that the features in the calculated phonon density of states (DOS) are in excellent agreement with the neutron data (GDOS), giving confidence that the calculations provide a sound description of the physical properties of the system. The DOS consists of two bands of phonons, one below 40 meV corresponding primarily to acoustic phonon modes, and one above 50 meV that mostly involves the boron motions. Inspection of the calculated phonon-dispersion curves that make up the high-energy band in the DOS reveals that the in-plane boron phonons (as depicted in the inset to Fig. 3) are very anharmonic. To demonstrate this, in Fig. 3 we plot the total energy as boron atoms move according to one of these zone-center in-plane phonons with E_{2g} symmetry. The potential displays a very strong anharmonic term. Numerically solving the Schrödinger equation for this anharmonic potential yields a phonon energy of $\hbar\omega(E_{2g})$ = 74.5 meV, a 25 % enhancement over the harmonic value of 60.3 meV. This value is in good agreement with recent Raman measurements. The giant anharmonicity revealed gives the first hint that the in-plane modes are strongly coupled to the $p_{x,y}$ σ bonding orbitals of boron, as shown schematically in Fig. 1. This coupling is also evident from the splitting of the boron σ bands (red lines)

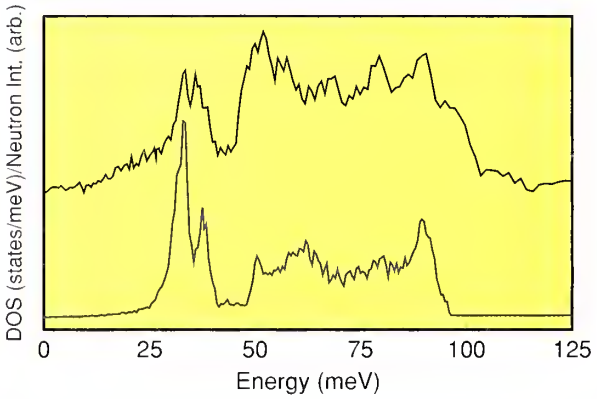

Fig. 2. Generalized (top) and the calculated (bottom) phonon density of states. The intensities of the peaks do not agree well because in DOS B and Mg ions contribute equally while in GDOS they are weighted by neutron cross-sections and inverse masses.

with the E_{2g} phonons (see Fig. 3). Note that the other bands are not affected by the E_{2g} phonons.

The splitting of the boron σ bands, when averaged over the Fermi surface, gives an electron-phonon (EP) coupling constant $\lambda \approx 1$. Using this value in the McMillan expression for T_c with $\omega(E_{2g})$ and taking a typical value for the Coulomb repulsion $\mu^* = 0.15$, we obtain a T_c of 39.4 K, in excellent agreement with experiments. We also solved the Schrödinger equation for the potential shown in Fig. 3 for different boron masses and obtained $\omega(E_{2g}) = 291.8\, M^{-0.575}$ and $\lambda = 0.615\, M^{-0.169}$, which yields the T_c-M curve shown in Fig. 4 and a boron isotope effect $\alpha = 0.21$, in good agreement with the experimental value of 0.26 ± 0.03.

Since the pressure dependence of T_c puts a stringent test on any theory of superconductivity, we repeated the calculations of phonons and electronic band structures discussed above for isotropic, uniaxial (along c-axis), and

T. Yildirim
NIST Center for Neutron Research
National Institute of Standards and Technology
Gaithersburg, MD 20899-8562

O. Gulseren
NIST Center for Neutron Research
National Institute of Standards and Technology
Gaithersburg, MD 20899-8562
and
Department of Materials Science and Engineering
University of Pennsylvania
Philadelphia, PA 19104-6202

biaxial (in the *ab*-plane) pressures [3]. We find that while $\omega(E_{2g})$ increases with increasing pressure, the density of states at the Fermi energy decreases. The EP constant λ also shows significant changes with pressure. Inserting all these competitive effects into the McMillan formula yields the pressure dependence of T_c shown in Fig. 4.

For isotropic pressure, T_c decreases with increasing pressure almost linearly at a rate of ≈ -1.0 K/GPa, in excellent agreement with the experimental value of -1.1 K/GPa. We also predict a cusp in the T_c-P curve around P ≈ 20 GPa. A similar cusp was recently observed experimentally. Our calculations indicate that T_c should increase first and then decrease with increasing c-compression, while it should decrease rapidly with ab-compression. Hence, when single crystal samples of MgB_2 become available, measurements of the ab- and c-compression dependence of T_c should provide a critical test of our theory.

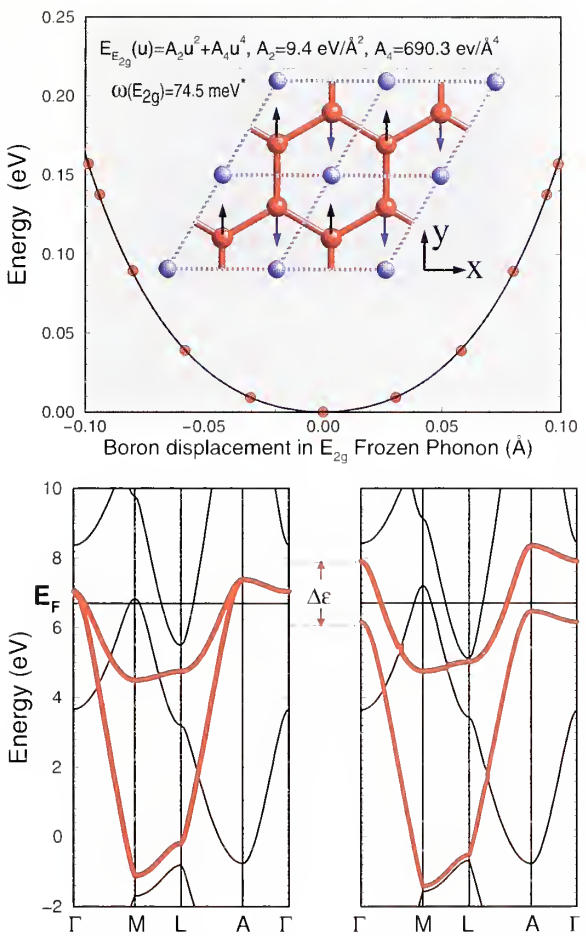

Fig. 3. Top: Total energy curve as a function of boron displacement for E_{2g} mode (shown in the inset), indicating a large anharmonic term in the potential. Bottom: Band structure of the undistorted (left) and distorted structures (right) by E_{2g} phonons (u_B ≈ 0.06 Å). See Ref. [1] for the animation of the zone center phonons and their coupling with the B σ bands.

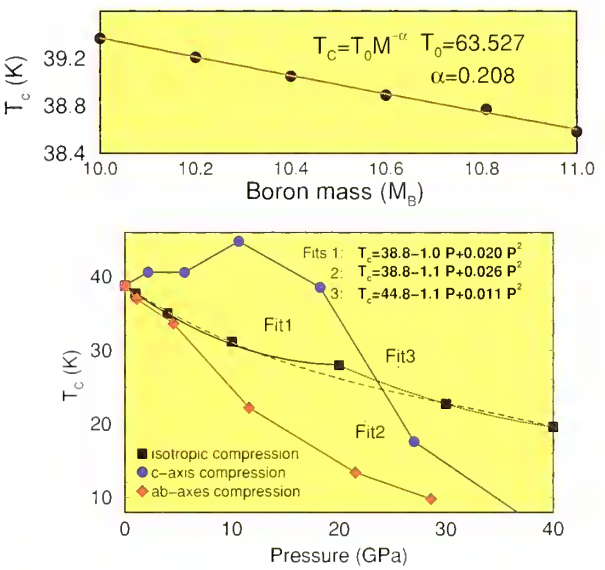

Fig. 4. Top: Boron mass dependence of the T_c. Bottom: Pressure dependence of T_c as a function of uniform, *ab*-axes, and c-axis compression, respectively.

MgB_2 may be the ultimate BCS s-wave superconductor, with parameters controlling T_c fully optimized to yield the highest possible T_c. However, even if T_c cannot be increased further, the low cost, light mass, easy fabrication, nearly isotropic high conductivity of MgB_2, which also has a large critical current, will no doubt find many important technological applications in the near future.

REFERENCES

[1] For full details of this work, see the website: http://www.ncnr.nist.gov/staff/taner/mgb2

[2] T. Yildirim, O. Gulseren, J. W. Lynn, C. M. Brown, T. J. Udovic, Q. Huang, N. Rogado, A. Regan, M. A. Hayward, J. S. Slusky, T. He, M. K. Haas, P. Khalifah, K. Inumaru, and R. J. Cava, Phys. Rev Lett **87**, 37001 (2001).

[3] T. Yildirim and O. Gulseren, J. Phys. Chem. Solids (in press, 2001).

Polaron Formation and Colossal Magnetoresistance in Manganites

The recent discovery of huge magnetoresistance effects in the manganese oxide class of materials (such as $La_{1-x}A_xMnO_3$ (A=Sr, Ca, Ba)) has rekindled intense interest in these systems for three reasons. One is that this "colossal magnetoresistance" (CMR) offers potential in a number of technologies, such as for read/write heads in magnetic recording media, sensors, and spin-polarized electronics. The second reason is that these materials are interesting from a fundamental viewpoint. In contrast to traditional isotropic ferromagnets such as Fe, Co, Ni, and EuO, where the spin system is isolated from the lattice, in the manganites the charge, spin, and lattice degrees of freedom are strongly coupled together. This leads to a delicate balance of interactions that gives rise to a rich variety of physical phenomena of current interest in condensed matter science. These include a metal-insulator transition that is juxtaposed with ferromagnetism, charge ordering, orbital ordering, polaron formation, electronic phase separation, and spin and charge stripes. The third reason is because of the similarity to the high T_C cuprate oxides. Recent progress in our understanding of the cuprates has provided insights into the manganites, and a deeper understanding of the fundamental properties of the manganites will surely elucidate the shared concepts underlying both classes of materials.

The electrical conductivity in these manganites is directly connected to the magnetic system through the double exchange mechanism, while the Jahn-Teller distortion of the $Mn^{3+}O_6$ couples the magnetic and lattice systems, resulting in the electronic, lattice, and magnetic degrees of freedom being intimately intertwined. The ferromagnetic transition then is non-conventional, and typically coincides with a metal-insulator transition to produce CMR. The present measurements on $La_{0.7}Ca_{0.3}MnO_3$, which is near optimal doping for CMR, show that polarons form as the ferro- to paramagnetic transition is traversed, self-trapping the carriers. These polarons then "melt" when a magnetic field is applied, freeing the carriers and generating the CMR.

The scattering from a lattice polaron arises from the structural distortion that surrounds a carrier and traps it.

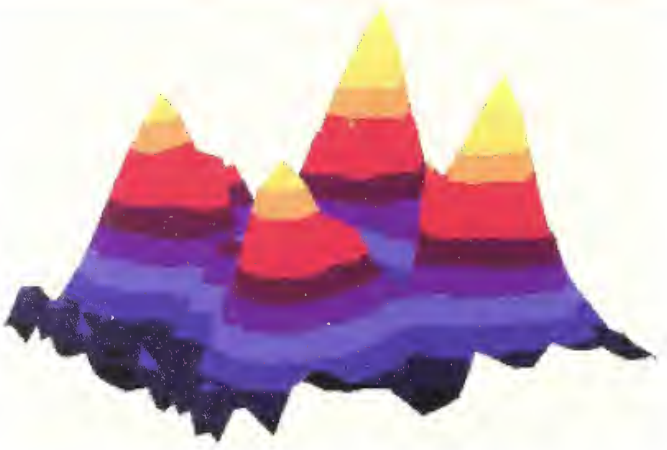

Fig. 1. Polaron correlation peaks near the 5 0 0 Bragg peak at 270 K, just above T_C = 255 K.

Individual polarons generate diffuse scattering around the fundamental Bragg peaks, while polaron correlations will give rise to additional superlattice peaks. We observe both of these effects [1], and in Fig. 1 we show the four satellite peaks at ¼ ¼ 0 positions near the 5 0 0 Bragg peak, just above T_C (255 K). The intrinsic widths of these peaks indicate that the correlations are short range (≈ 15 Å) in nature, and this range is found to be only weakly temperature dependent. Polarized neutron measurements show that these peaks originate from lattice distortions rather than from magnetic scattering. Similar direct evidence for polaron formation and correlations has been observed in the bilayer manganite $La_{1.2}Sr_{1.8}Mn_2O_7$ [2], although the ordering wave vectors and the ratios of diffuse scattering to correlated scattering are different.

A model that can explain both the ordering wave vector as well as the overall behavior of the observed intensities of the short-range correlation peaks is the CE model developed for the half-doped case. The CE model has an orbitally-ordered Jahn-Teller lattice with charge stripes in the [110] direction, and an antiferromagnetic ground state. Such ordering has been observed for $x \geq 0.5$ at low temperatures. This behavior contrasts with the present ferromagnetic system, where the orbital/charge correlations are short range in nature, occur only above

C.P. Adams[1] and J.W. Lynn
NIST Center for Neutron Research
National Institute of Standards and Technology
Gaithersburg, MD 20899-8562
and
[1]University of Maryland
College Park, MD 20742

Y.M. Mukovskii, A.A. Arsenov, and D.A. Shulyatev
Moscow Steel and Alloys Institute
Moscow, Russia

T_C, and are not accompanied by any antiferromagnetic correlations. The CE "stripes" are also consistent with stripe formation as seen in other transition metal oxides (nickelates and cuprates).

Of particular interest is how the polaron ordering is related to the metal-insulator transition and the quasielastic "central peak" [3] associated with the spin

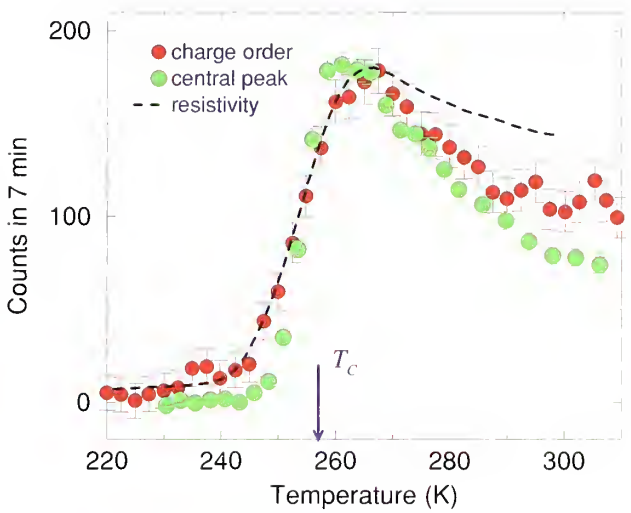

Fig. 2. Temperature dependence of the intensity of the polaron peak at 3.75 0.25 0, compared to the magnetic quasielastic central peak, and the resistivity. The data have been scaled vertically so the peak heights match. The similarity of the data indicates a common physical origin.

component of the polaron. As we see in Fig. 2, the temperature dependence of the intensity of the charge ordering is nearly identical to the quasielastic magnetic peak, and both follow the resistivity behavior. This is a very strong indication that these properties have a common origin in polaron formation.

A further indication of the strong relationship between charge ordering and resistivity is established by measurements in magnetic fields [1]. In Fig. 3 we see that the intensity of the charge ordering peaks decreases rapidly with increasing field. Thus the polarons "melt" when the magnetization develops and the conductivity increases, either by lowering the temperature (Fig. 2) or increasing the applied field, producing CMR. Identical field dependence has been observed both for the central peak in $La_{0.7}Ca_{0.3}MnO_3$ [1,3] as well as the polaron peaks in the bilayer system [2].

The above experimental results reveal that both the spin and charge correlations associated with the polarons in $La_{0.7}Ca_{0.3}MnO_3$ appear together, and have a very similar temperature dependence. This coincidence may explain the amplified magnetoresistive effects, as well as the absence of conventional magnetic critical behavior. The physical quantities that control the characteristic temperature for polaron formation, including the role that intrinsic inhomogeneities, stress, and phase separation play in their formation, still remain to be elucidated.

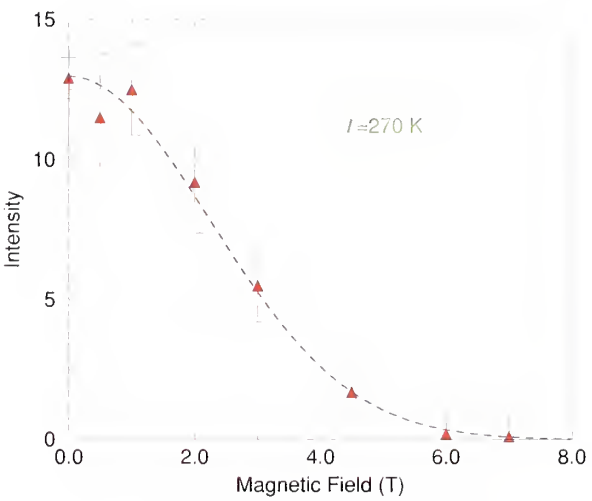

Fig. 3. Magnetic field dependence of the intensity of the polaron peak, showing that the polarons melt with increasing field.

REFERENCES

[1] C.P. Adams, J. W. Lynn, Y. M. Mukovskii, A. A. Arsenov, and D. A. Shulyatev, Phys. Rev. Lett. **85**, 3954 (2000); J. Appl. Phys. **89**, 6846 (2001).

[2] L. Vasiliu-Doloc, S. Rosenkranz, R. Osborn, S. K. Sinha, J. W. Lynn, J. Mesot, O. Seeck, G. Preosti, A. J. Fedro, and J. F. Mitchell, Phys. Rev. Lett. **83**, 4393 (1999).

[3] J.W. Lynn, R. W. Erwin, J. A. Borchers, Q. Huang, A. Santoro, J. L. Peng, and Z. Y. Li, Phys. Rev. Lett. **76**, 4046 (1996); J. Appl. Phys. **81**, 5488 (1997).

Ferromagnetism and Spontaneous Vortex Formation in Superconducting $ErNi_2B_2C$

The competition between magnetic order and superconductivity has had an interesting history. The first examples of true long range magnetic order coexisting with superconductivity were provided by the ternary Chevrel-phase superconductors and related compounds. The magnetic ordering temperatures were all low (≈ 1K), indicating that dipolar interactions dominate the energetics of the magnetic system. Similar behavior is found for the rare earth ordering in the hole-doped cuprates [1]. The first systems where exchange clearly dominates the magnetic energetics were provided by the electron-doped cuprates [1], followed by the borocarbides of central interest here [2].

Among these systems, the rare and interesting situation where ferromagnetic interactions are present has attracted special attention because of the competitive nature between the superconducting screening and the internally generated magnetic field. In the Chevrel phase materials this competition gives rise to long wavelength oscillatory magnetic states and/or reentrant superconductivity. Recently, superconducting $ErNi_2B_2C$ (T_C = 11 K) appeared to develop a net magnetization below 2.3 K, well below the onset of long range spin-density-wave order at T_N = 6 K. We have carried out a comprehensive study of the magnetic order and vortex structure in this material, and directly demonstrated that this transition does indeed correspond to the development of a net atomic magnetization that coexists with superconductivity, and this results in the spontaneous formation of vortices in the system [3].

Superconducting $ErNi_2B_2C$ orders magnetically at 6 K into a transversely polarized spin density wave structure [2,3], with the modulation wave vector d along the a axis and the spins along the b direction. A portion of a scan along the a axis is shown in Fig. 1 at three temperatures. The initial ordering is a simple spin density wave as shown in the schematic, with an incommensurate modulation of $\delta \cong 0.55\ a^*$ ($a^* = 2\pi/a$). At 2.4 K additional higher-order peaks become observable as the magnetic structure squares up, as indicated schematically at the bottom of Fig. 1. These peaks are all odd-order harmonics as expected for a square-wave magnetic structure.

Below the weak ferromagnetic transition (T_{WFM}) at 2.3 K, the data (Fig. 1) indicate that a new series of peaks has developed, which are *even* harmonics of the fundamental wave vector. Polarized neutron measurements unambiguously establish that both the odd-order peaks *and* the even-order peaks are magnetic in origin.

The integrated intensities of the odd- and even-order harmonics are shown in Fig. 2 as a function of T. The

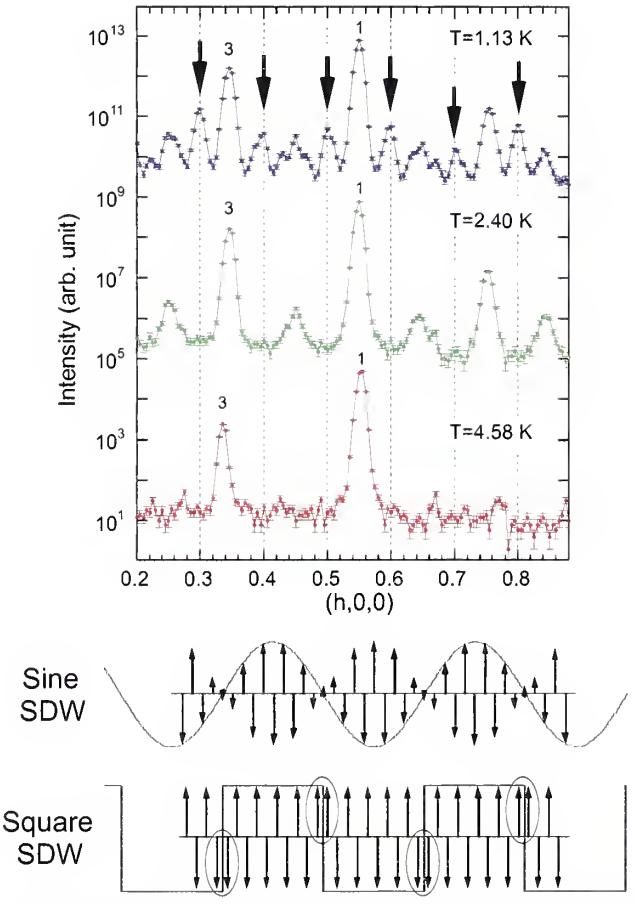

Fig. 1. Scan along the [h00] direction at T = 1.3 K, 2.4 K, and 4.58 K. The data have been offset for clarity. Above the weak ferromagnetic transition at 2.3 K we observe the fundamental peak at ≈ 0.55 along with odd-order harmonics, while below a new set of even harmonics develops (arrows). Also shown is a schematic of the spin density wave order for T just below T_N, and the (undistorted) wave when it squares up.

even-order peaks abruptly develop below 2.3 K, concomitant with the development of the new (weak) ferromagnetism at T_{WFM}. There is a substantial thermal

S.-M. Choi and J. W. Lynn
NIST Center for Neutron Research
National Institute of Standards and Technology Gaithersburg, MD 20899-8562
and
University of Maryland
College Park, MD 20742

D. Lopez, P. L. Gammel, and C. M. Varma
Bell Laboratories
Lucent Technologies
Murray Hill, NJ 07974

P. C. Canfield and S. L. Bud'ko
Ames Laboratory and Department of Physics and Astronomy
Iowa State University
Ames, IA 50011

hysteresis associated with the weak ferromagnetic transition, suggesting that this transition is first order in nature.

The present neutron results demonstrate that a net magnetization develops in $ErNi_2B_2C$ in the magnetically ordered state at low temperatures, making this the first such "ferromagnetic-superconductor" since $HoMo_6S_8$, $HoMo_6Se_8$, and $ErRh_4B_4$. For $ErNi_2B_2C$ the net magnetization is much smaller than for these earlier systems, which allows coexistence with superconductivity over an extended T range. This presents the intriguing possibility

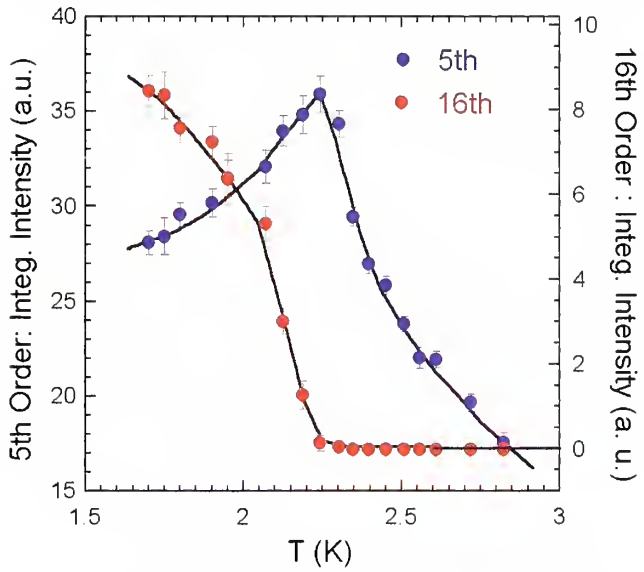

Fig. 2. Integrated intensities of the odd (open circles) and even (solid circles) order harmonics as a function of *T*.

that in an applied field vortices will form spontaneously when this net atomic magnetization is present. The small angle scattering data of the vortex structure (Fig. 3 top) show that the lattice has the expected spacing at lower applied fields. At higher fields, as the field begins to penetrate, vortices spontaneously form in addition to those expected from the applied field alone, increasing the vortex density and shifting the vortex peak. The T dependence of this shift (Fig. 3 bottom) makes it clear that this behavior is directly related to onset of the net magnetization in the system. It is also interesting to note that the vortex pinning is enhanced in both magnetic

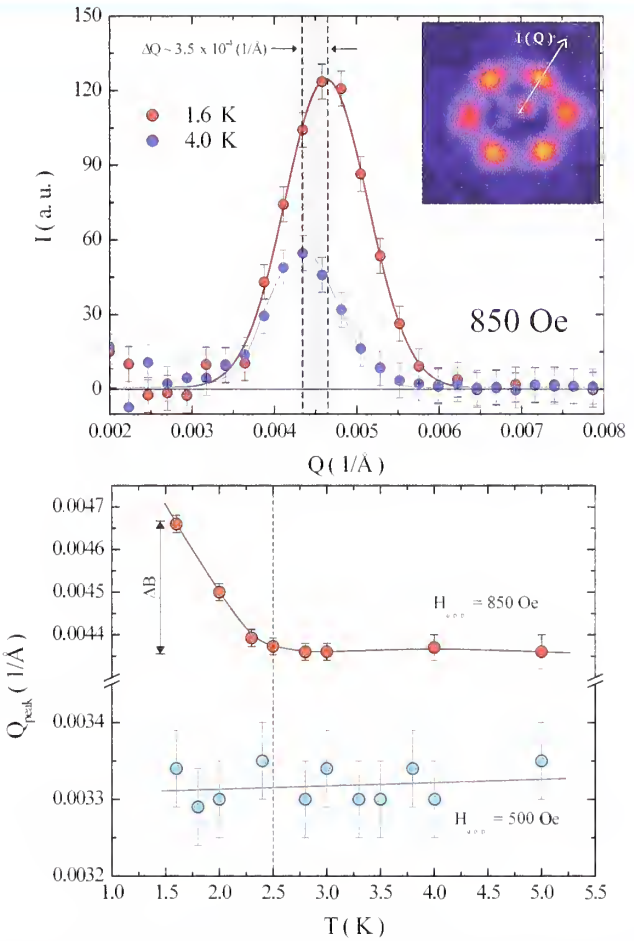

Fig. 3. Intensity of the vortex scattering vs. wave vector *Q* at 850 Oe above and below the weak ferromagnetic transition. The shift in the peak position demonstrates that additional vortices spontaneously form at low temperatures. The temperature dependence (bottom) shows that this spontaneous vortex formation is directly related to the weak ferromagnetic transition.

phases, which may prove useful in high current applications of superconductors.

REFERENCES

[1] J. W. Lynn and S. Skanthakumar, Handbook on the Physics and Chemistry of Rare Earths, Chap. 199, Vol. **31**, ed. by K. A. Gschneidner, Jr., L. Eyring, and M. B. Maple, North Holland, Amsterdam (2001), p. 313.

[2] J. W. Lynn, S. Skanthakumar, Q. Huang, S. K. Sinha, Z. Hossain, L. C. Gupta, R. Nagarajan, and C. Godart, Phys. Rev. **B55**, 6584 (1997).

[3] S.-M. Choi, J. W. Lynn, D. Lopez, P. L. Gammel, P. C. Canfield and S. L. Bud'ko, Phys. Rev. Lett. **87**, 107001 (2001).

Structure Of A Local Spin Resonance In A Geometrically Frustrated Antiferromagnet

For many crystalline magnetic materials, only a long range ordered spin configuration can satisfy all near neighbor spin interactions. Such systems generally display a finite temperature transition to a broken symmetry phase with long-range magnetic order. However, on certain lattices with weak connectivity and a triangular motif, short-range interactions can be satisfied without long-range order [1].

To explore this possibility we examined magnetic order and fluctuations in $ZnCr_2O_4$. The B-site of this spinel lattice is solely occupied by spin-3/2 Cr^{3+} and this leads to a magnet with dominant nearest neighbor interactions on the lattice of corner-sharing tetrahedra shown in Fig. 1.

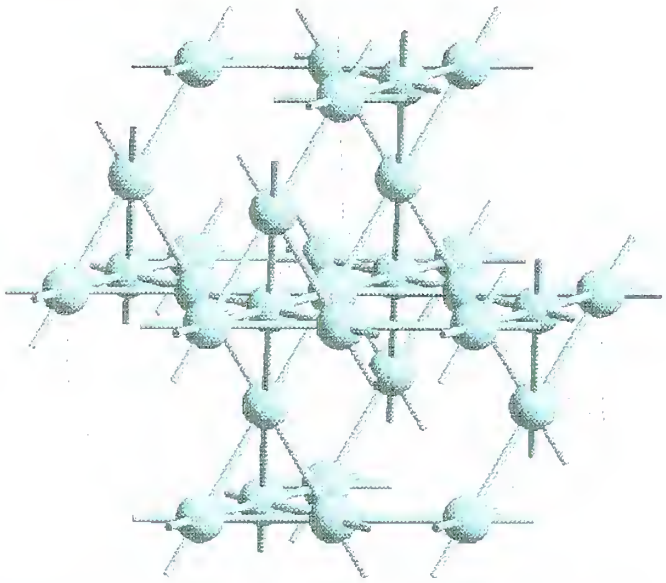

Fig. 1. Lattice of corner-sharing tetrahedra formed by the octahedrally coordinated B sites of the spinel AB_2O_4 structure.

Exchange interactions in this structure are satisfied at the mean field classical level when every tetrahedron carries zero net magnetization. Not only are there many ways that a tetrahedron can have no moment, but there are also many ways to organize such non-magnetic tetrahedra on the corner-sharing lattice. The result is a "geometrically frustrated" spin system with many ways to satisfy interactions without long-range order.

Analysis of specific spin models on the B-site spinel (or pyrochlore) lattice indicates that spin-1/2 and spin-∞ models have short-range order down to $T = 0$ [2], while long-range order is induced by quantum fluctuations for an unknown intermediate range of spin values. Experiments indicate that spin-3/2 $ZnCr_2O_4$ is "close" to the quantum critical point that separates the low spin quantum-disordered phase from the intermediate spin long-range ordered phase. Specifically, the relaxation rate for magnetic excitations, Γ, follows a power-law that extrapolates to zero as $T \rightarrow 0$ indicating quantum criticality [3]. This state of affairs however does not persist to the lowest temperatures. Instead, a first order transition at T_N = 12.5 K causes a transition from the cubic cooperative paramagnet to tetragonal Néel order.

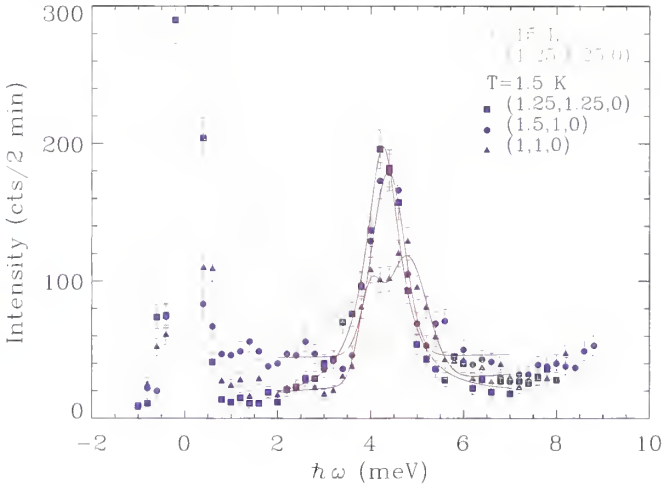

Fig. 2. Constant-Q scans above and below T_N.

Figure 2 shows that a gapless continuum of magnetic scattering above T_N is pushed into a local spin resonance at $\hbar\omega \approx 4.5$ meV $\approx J$ with remarkably little dispersion throughout the Brillouin zone. The result is analogous to the spin-Peierls transition of the uniform spin-1/2 chain, where quantum critical fluctuations are pushed into a finite energy singlet-triplet transition through structural dimerization. Our recent synchrotron X-ray and neutron powder experiments indicate that deformation of tetrahedra does indeed occur for $ZnCr_2O_4$. However, the structural changes push the system to long range order rather than to quantum disorder, as indicated by the magnetic Bragg peaks and spin wave excitations.

S.-H. Lee
NIST Center for Neutron Research
National Institute of Standards and Technology
Gaithersburg, MD 20899-8562
and
University of Maryland
College Park, MD 20742

C. Broholm and G. Gasparovic
Department of Physics and Astronomy
The Johns Hopkins University
Baltimore, MD 21218

T. H. Kim
Francis Bitter Magnet Laboratory
Massachusetts Institute of Technology
Cambridge, MA 02139

W. Ratcliff and S-W. Cheong
Department of Physics and Astronomy
Rutgers University
Piscataway, NJ 08854

Our single crystal experiment [4] also enabled unique insight into the local structure of spin-fluctuations in geometrically frustrated systems. Figure 3 shows the ***Q***-dependence of low energy magnetic scattering in two high symmetry planes above and below T_N. While the spectrum for spin fluctuations changes dramatically at the first order phase transition, the structure factor clearly does not. Also shown in the figure is the structure factor for six spins of <111> type kagomé hexagons precessing with π phase shift between neighbors. The proposal by O. Tchernyshyov *et al.* [5] that these are the dominant low energy spin fluctuation for spins on the B-site spinel lattice is clearly borne out by the data.

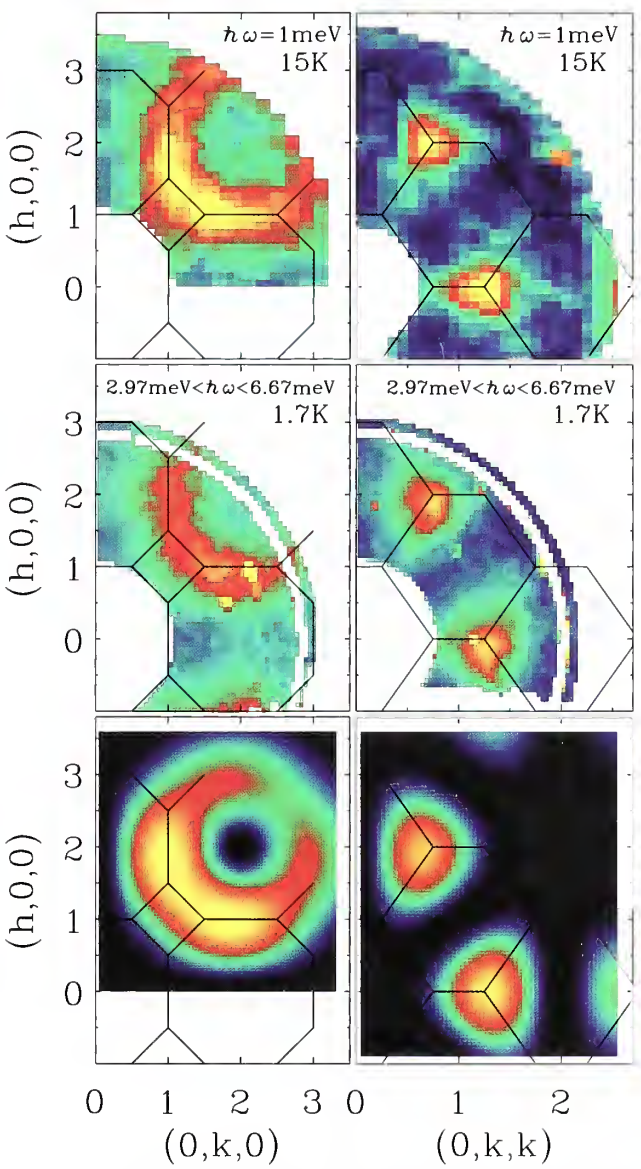

Fig. 3. Color images of inelastic neutron scattering intensities in the (hk0) and (hkk) symmetry planes. From top to bottom are shown data from below and above T_N, and the structure factor for the hexagon mode proposed by O. Tchernyshyov. T = 1.7 K data were taken integrating over the energy range $\hbar\omega$ from 3.0 meV to 6.7 meV. Data in the paramagnetic phase (T = 15 K) were taken at $\hbar\omega$ = 1 meV.

The present data for $ZnCr_2O_4$ show that geometrically frustrated lattices have composite low energy degrees of freedom analogous to rigid unit modes in certain open framework lattice structures. To better understand the unusual type of phase transition that occurs in this system, it must be determined what defines the 4.5 meV energy scale for hexagon excitation in the ordered phase. Do quantum fluctuations play a significant role or does the broken symmetry between exchange interactions within tetrahedra induce the resonance? The answer to this question is now being pursued through an accurate determination of the complex low temperature lattice and magnetic structure.

REFERENCES

[1] P. W. Anderson *et al.*, Philos. Mag. **25**, 1 (1972); J. Villain, Z. Phys. B **33**, 31 (1979).

[2] R. Moessner *et al.*, Phys. Rev. Lett. **80**, 2929 (1998); B. Canals et al., Phys. Rev. Lett **80**, 2933 (1998).

[3] S.-H. Lee, C. Broholm, T. H. Kim, W. Ratcliff II, and S-W. Cheong, Phys. Rev. Lett. **84**, 3718 (2000).

[4] S.-H. Lee *et al.*, unpublished (2001).

[5] O. Tchernyshyov *et al.*, unpublished (2001).

Pressure-Induced Phase Transition of $C_{12}E_5$ Micelles

Nonionic surfactants form a variety of microstructures in water, ranging from simple micelles at low surfactant concentrations to complex mesophases, such as hexagonal or lamellar phases at high concentrations. The effect of pressure on the structure of micelles and microemulsions has not been extensively studied. Small angle neutron scattering (SANS) is particularly well suited for such measurements because the range of length scales probed includes both the particle size and the interparticle spacing. Pressure effects observed in SANS measurements of surfactant microstructure are typically interpreted in terms of geometric packing arguments that focus on the compressible hydrophobic tails of the surfactants. In this context, increasing pressure has the single effect of decreasing the surfactant tail volume, thereby increasing the curvature of the oil-water interface. Conversely, increasing temperature dehydrates the nonionic headgroups, decreasing the headgroup area and decreasing the film curvature. Thus, temperature and pressure can be viewed as thermodynamic variables with inherently different mechanisms and opposite effects for controlling microstructure in nonionic surfactant solutions.

Here we report the results of high-pressure SANS experiments on a solution of 1 % by weight pentaethylene glycol mono-n-dodecyl ether ($C_{12}E_5$) in D_2O at 20 °C and pressures up to ≈ 300 MPa. The phase diagram for this system [1] at ambient pressure is shown in Fig.1. At this temperature and surfactant concentration, a single-phase micellar solution (L_1 phase) forms at ambient pressure, well below the lower critical solution temperature (LCST) for liquid-liquid equilibrium and far removed from the H_1 hexagonal phase at much higher $C_{12}E_5$ concentrations. The microstructure of the L_1-phase at ambient pressure is known to be a network of branched semi-flexible, cylindrical micelles with the branch points comprised of three-armed junctions.

SANS spectra were measured using the NIST high-pressure cell and neutrons of wavelength $\lambda = 6$ Å, covering a q-range of $0.012\ Å^{-1} < q < 0.22\ Å^{-1}$. The scattering curves obtained at 3.4, 241, and 255 MPa are shown in Fig. 2. The curves at 3.4 MPa and 241 MPa are virtually identical, indicating no significant change in microstructure with increasing pressure up to 241 MPa. Fitting these curves using a form factor for cylindrical micelles gives a radius of (21.0 ± 0.2) Å and a length greater than 600 Å, independent of pressure. However, a small increase in pressure from 241 MPa to 255 MPa leads to the appearance of a peak in the scattering intensity at $q \approx 0.130\ Å^{-1}$, indicative of a locally ordered system. A similar transition has been reported in high-pressure SANS studies of tetradecyldimethylaminoxide (TDMAO) micelles in D_2O at pressures up to 300 MPa, but the high-pressure microstructure was never determined [2].

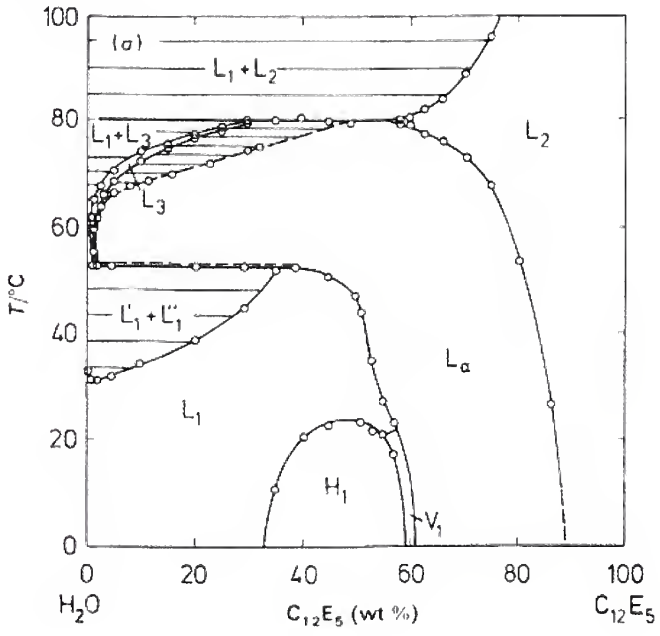

Fig. 1. Temperature-composition phase diagram for $C_{12}E_5$/water solutions at ambient pressures [1].

Shown in Fig. 2 is the scattering curve for the H_1 hexagonal phase at 49 % by weight $C_{12}E_5$ at 20 °C, and ambient pressure. The peak at $q \approx 0.120\ Å^{-1}$, arising from the hexagonal lattice of cylindrical micelles, is similar to the peak for the 1 % by weight $C_{12}E_5$ solution at 255 MPa, suggesting that this new high-pressure phase may resemble a slightly compressed state of the H_1 hexagonal phase at ambient pressure. The formation of a lamellar

D. P. Bossev and M. E. Paulaitis
Department of Chemical Engineering
Johns Hopkins University
Baltimore, Maryland 21228-2694

J. N. Israelachvili
Department of Chemical Engineering
University of California, Santa Barbara
Santa Barbara, CA 93106

S. R. Kline
NIST Center for Neutron Research
National Institute of Standards and Technology
Gaithersburg, MD 20899-8562

phase from cylindrical micelles is unlikely, since this corresponds to increasing the hydrophobic core volume-to-surface-area ratio per surfactant molecule, or equivalently, decreasing the spontaneous curvature of the surfactant film. The application of pressure would have the opposite effect. We conclude, therefore, that the observed change in microstructure corresponds to a pressure-induced L_1-H_1 phase transition from a network

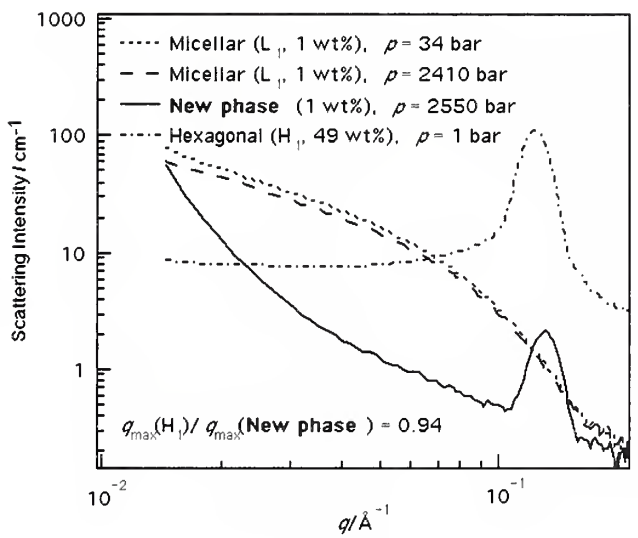

Fig. 2. Measured SANS spectra at 20 °C for 1 % by weight $C_{12}E_5$ in D_2O as a function of pressure and 49 % by weight $C_{12}E_5$ in D_2O at ambient pressure.

of branched semi-flexible, cylindrical micelles to hexagonally ordered bundles of cylindrical micelles.

To further understand the SANS results, we have measured the temperature dependence of the L_1-H_1 transition pressure and find that the *p-T* curve follows the *p-T* freezing curves for liquid *n*-alkanes of comparable hydrocarbon chain length. *N*-decane solidifies at a pressure of ≈ 250 MPa at 20 °C, which is close to the pressure for the observed L_1-H_1 phase transition. We propose that the $C_{12}E_5$ micelle hydrophobic core, equivalent to *n*-decane, does solidify at these conditions, such that the micelles lose flexibility, and hence conformational entropy. An analysis of the geometric packing constraints for three-arm junctions coexisting with cylinders shows that when the surfactant tail volume decreases with increasing pressure, the fraction of surfactant forming junction points also decreases. This indicates that the formation of three-arm junctions becomes increasingly unfavorable at higher pressures due to the compression of the $C_{12}E_5$ micelle hydrophobic core. Our calculations predict that no junctions should be present at $P > 275$ MPa at 20 °C, which is in good agreement with our observation of a structural transition between 241 MPa and 255 MPa at this temperature. Consequently, the network of branched threadlike micelles becomes globally unstable. The formation of hexagonally ordered bundles of cylindrical micelles follows as the attractive van der Waals forces between the micelles are not offset by entropic repulsive undulation interactions that are not present in the now-solidified hydrophobic core.

The practical significance of these results is to show that pressure allows access to regions of the $C_{12}E_5$/water phase diagram that are virtually inaccessible to temperature. Thus, the use of pressure may offer unique approaches for directing and stabilizing certain surfactant microstructures that, in turn, could prove useful for creating novel soft materials.

REFERENCES

[1] R. Strey, R. Schomäcker, D. Roux, F. Nallet, U. Olsson, J. Chem. Soc. Faraday Trans. **86**, 2253 (1990).

[2] N. Gorski, J. Kalus, D. Schawhn, Langmuir **15**, 8080 (1999).

Probing The Structure Of Aerosol Nanodroplets

Nanodroplet aerosols form readily in the supersonic expansions that occur, for example, in turbomachinery, jet exhausts, and volcanic eruptions. Thus, understanding particle formation and growth when cooling rates approach 10^6 K/s is of broad scientific interest.

From a fundamental point of view, particles with radii < 10 nm are important because they lie in the critical transition zone between large molecular clusters and bulk material. In multicomponent droplets, there is also strong theoretical evidence for surface enrichment, i.e., that the surface and interior compositions can differ significantly. Surface enrichment is important because it affects nucleation, growth and evaporation kinetics, and the heterogeneous chemistry of aerosol droplets. A major goal of our work is to use small angle neutron scattering to find direct evidence for surface enrichment in nanodroplets.

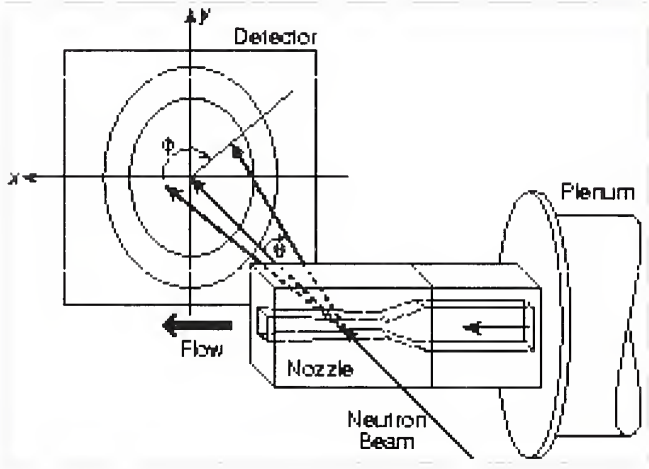

Fig. 1. The nozzle is placed in the sample chamber at right angles to the neutron beam.

We produce nanodroplets with radii between 5 nm and 12 nm and number densities in the range of 10^{11} cm^{-3} to 10^{12} cm^{-3} by rapidly expanding a dilute vapor mixture of D_2O (or other condensible) and N_2 in a supersonic nozzle apparatus (Fig. 1) [1]. The volume fraction of droplets is always less than 10^{-5} and, thus, the scattering signals are close to the instrument background. Furthermore, the high velocity of the droplets (400 m/s to 500 m/s) is comparable to the speed of the neutrons. This leads to a Doppler shift in the momentum of the scattered neutrons [2,3], and the 2-D scattering patterns are anisotropic (Fig. 2) even though spherical droplets at rest

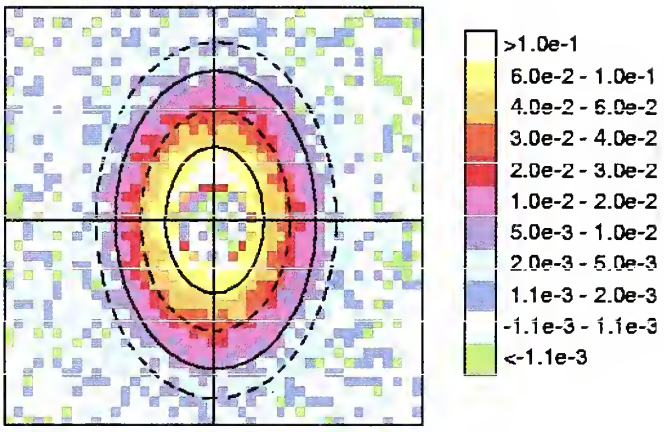

Fig. 2. The observed 2-D scattering pattern for an aerosol with an average particle velocity v_p = 435 m/s measured using a neutron wavelength of λ = 1.0 nm (v_n = 400 m/s). The contour levels correspond to absolute intensities of 0.08, 0.03, 0.008 and 0.003 cm^{-1}, respectively.

scatter isotropically. This Doppler shift can be used to directly measure the velocity of the particles, and, in a test case, this velocity was within 2 % of the average velocity derived from the pressure trace measurements [2].

Rather than simply examine nanodroplets for which segregation of the components is severe, we use different materials to observe the transition between well-mixed and fully segregated droplets. Thus, our experiments include binary mixtures of H_2O, D_2O, ethanol, and n-butanol, or its fully deuterated analog d-butanol. Almost

B. E. Wyslouzil, C. H. Heath, U. M. Dieregsweiler, and K. A. Streletzky
Department of Chemical Engineering
Worcester Polytechnic Institute
Worcester, MA 01609

R. Strey and J. Wölk
Institut für Physikalische Chemie
Universität zu Köln
Cologne, Germany

G. Wilemski
Physics Department
University of Missouri – Rolla
Rolla, MO 65409

J. Barker
NIST Center for Neutron Research
National Institute of Standards and Technology
Gaithersburg, MD 20899-8562

degenerate mixtures, such as $D_2O - H_2O$, appear to form well-mixed droplets [4]. In contrast, binary nanodroplets containing H_2O (or D_2O) and a low molar concentration of d-butanol (or h-butanol) should consist of a water-rich core and an alcohol-rich shell. Our recent SANS experiments with H_2O – d-butanol nanodroplets clearly demonstrate for the first time the existence of the alcohol-rich shell. As illustrated in Fig. 3, for these droplets the scattered intensity falls off as q^{-2} in the high q region, as is characteristic for scattering by a shell. Furthermore, the feature in the region 0.4 $nm^{-1} < q < 0.5$ nm^{-1} cannot be reproduced by a well-mixed droplet model that matches the low q data. Also shown in Fig. 3 is the scattering spectrum from the complementary D_2O – h-butanol experiment. As expected, the scattered intensity is much higher, and the signal intensity decreases as q^{-4} in the high q region. In this case, the D_2O-rich core dominates the scattering.

In summary, SANS provides us with a powerful new way to study the properties of nanometer sized liquid droplets in the environment in which they form. To date, it is the only technique to directly probe the microstructure of aerosol nanodroplets. Combined with pressure trace measurements and modeling, SANS provides information critical to our understanding of droplet formation and growth in the nanometer size regime.

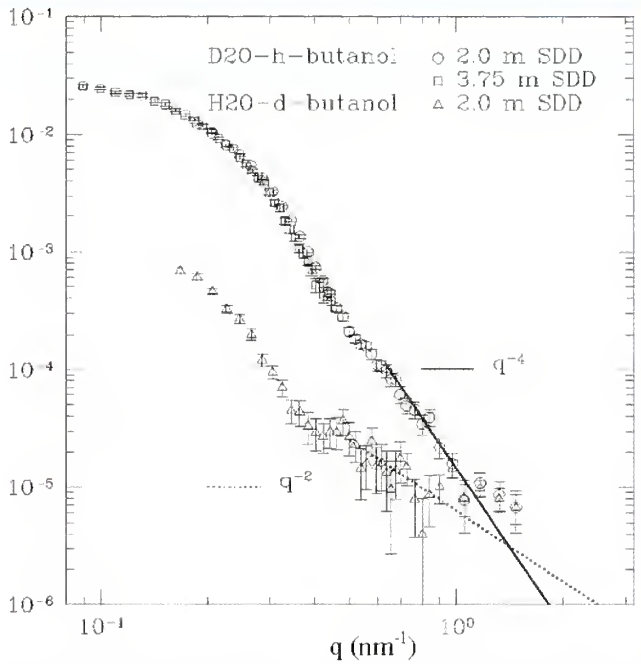

Fig. 3. Scattering from a D_2O – h-butanol aerosol is compared to that from a H_2O – d-butanol aerosol formed under identical conditions in the nozzle. Both aerosols contain ≈ 6 mol % butanol. In the high q region, the intensity falls off as q^{-4} for the D_2O-rich droplets, but only as q^{-2} for the H_2O-rich droplets. Our preliminary modeling shows that the feature in the region 0.4 $nm^{-1} < q <$ 0.5 nm^{-1} of the H_2O – d-butanol spectrum cannot be reproduced by a well mixed droplet model. SDD is the sample-to-detector distance.

REFERENCES

[1] B. E. Wyslouzil, J. L. Cheung, G. Wilemski, and R. Strey, Phys. Rev. Lett. **79**, 431 (1997).

[2] B. E. Wyslouzil, G. Wilemski, J. L. Cheung, R. Strey, and J. Barker, Phys. Rev. E **60**, 4330 (1999).

[3] G. Wilemski, Phys. Rev. E **61**, 557 (2000).

[4] C. H. Heath, K. A. Streletzky, J. Wolk, B. E. Wyslouzil, and R. Strey, in Nucleation and Atmospheric Aerosols, 2000, ed. by B. N. Hale and M. Kulmala, American Institute of Physics, New York (2000) p.59.

Nanoporous Ultra-Low Dielectric Constant Materials

The next generation of interlayer dielectric materials for microelectronics must have an ultra-low dielectric constant of less than 2.0 to meet the *National Technology Roadmap for Semiconductors* [1]. In addition, the material must have excellent thermal stability and mechanical properties [2,3]. One route is to introduce nanometer sized pores into a material with an initially low dielectric constant ($k \approx 2$ to 3). The presence of the pores lowers the dielectric constant of the nanoporous film as the dielectric constant of air is 1.0. One class of materials that is receiving significant attention is based on poly(methylsilsesquioxane) (PMSSQ) which has a dielectric constant between 2.7 and 2.8 (lower than conventional SiO_2) and good thermal stability up to 500 °C [4, 5]. The dielectric constant is a function of the level of porosity and detailed knowledge of the morphology is required for implementation in electronic packaging.

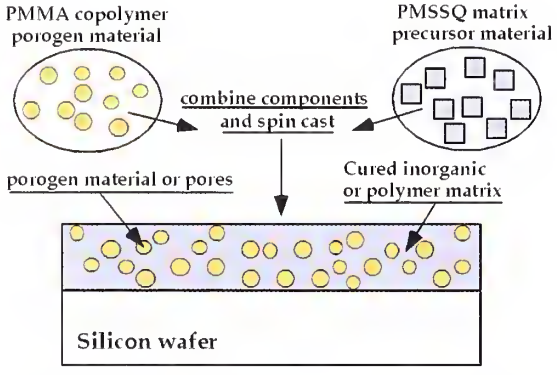

Fig. 1. Schematic showing the generation of nanoporous PMSSQ films.

A schematic diagram of the synthesis process is shown in Fig. 1. The materials are based on an inorganic matrix of PMSSQ containing a porogen (i.e. a labile pore generating material) based on a poly(methylmethacrylate) copolymer (coPMMA) as a template for creating the pores [6,7]. A film is prepared by dissolving the PMSSQ matrix precursor material and the coPMMA porogen in a common solvent and spin casting onto a silicon substrate.

The film is then slowly ramped up in temperature to 450 °C. During this temperature ramp, the matrix film fully cures by about 225 °C, resulting in microphase separation of the coPMMA polymer. Above about 350 °C the coPMMA polymer degrades leaving nanometer sized pores. Neutron scattering was used with a deuterated coPMMA polymer to understand the morphological development of the films during the cure. The use of the deuterated porogen provides contrast for neutron scattering in the hybrid (polymer containing) system that is not available with x-ray scattering.

In situ studies of the curing process by small angle neutron scattering (SANS) were performed. To provide sufficient scattering signal, four or more samples on Si wafers were stacked to increase the scattering volume.

Figure 2 shows a set of SANS data from a PMSSQ thin film containing 20 % porogen at various cure temperatures. The scattered intensity varies as a function

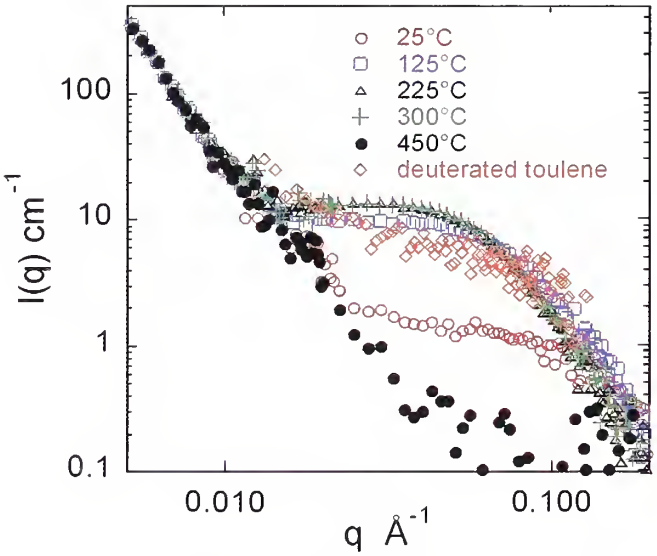

Fig. 2. SANS data taken during cure of a nanoporous PMSSQ thin film.

of curing temperature due to morphology changes occurring in the sample. For the as-spun materials there is a shoulder at high q from which a radius of gyration (R_g) of 12 Å was obtained by Guinier analysis. After heat treatment at 225 °C the shoulder in $I(q)$ becomes more pronounced and shifts to about $q = 0.06$ Å^{-1}. The shift to smaller q indicates a coarsening of the microphase separated porogen domain structure. A radius of gyration

G.Y. Yang and R.M. Briber
Department of Materials and Nuclear Engineering
University of Maryland
College Park, MD 20742

E. Huang, H.-C. Kim, W. Volksen, and R.D. Miller
IBM Almaden Research Center
San Jose, CA 95120

K. Shin
Department of Materials Science and Engineering
State University of New York
Stony Brook, NY 11794

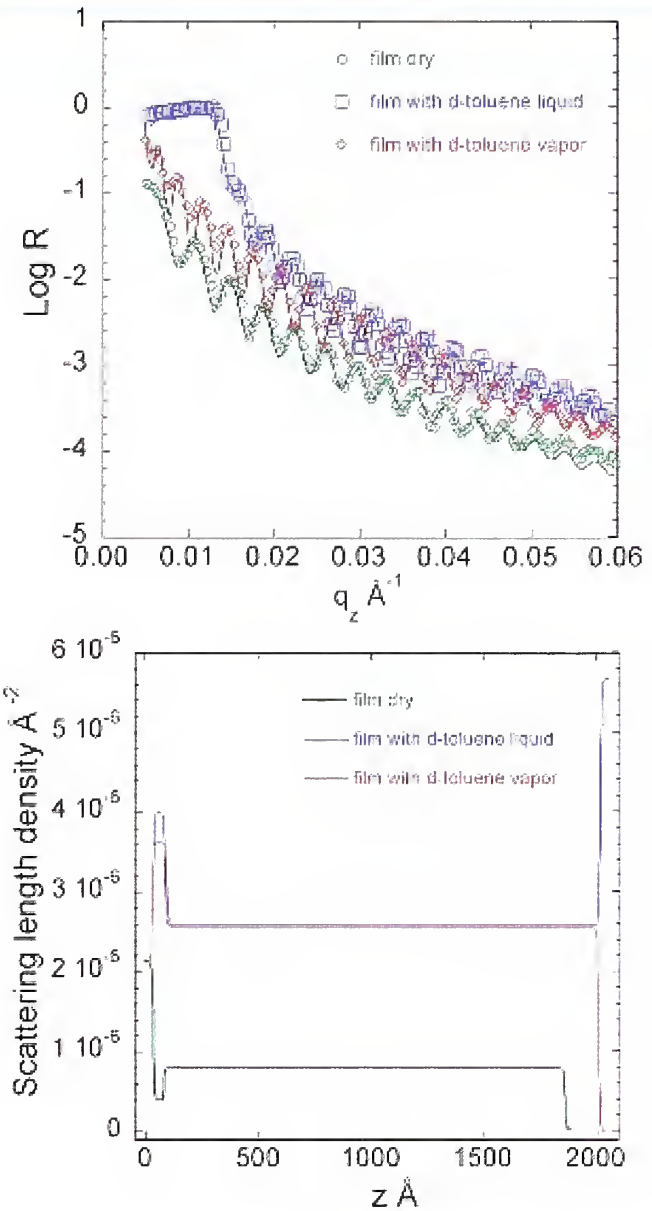

Fig. 3. Above, neutron reflectivity data (symbols) and best fit (lines) calculated from the scattering length density profiles shown below for a nanoporous PMSSQ thin film under various conditions.

of R_g = 23 Å for the domains was obtained for the cured materials . The scattering curves do not change significantly between 225 °C and 300 °C, indicating that the morphology remains fixed until the degradation of the polymer at 450 °C. The dramatic decrease in intensity of the SANS curve at 450 °C is due to a loss of neutron scattering length density contrast because of the degradation of the porogen and the formation of pores in the film.

To provide neutron contrast between the pores and the matrix, the fully cured sample was exposed to deuterated toluene. These data are also shown in Fig. 2. The scattering is largely recovered after exposure to deuterated toluene, indicating that the porous structure is maintained with no collapse after degradation of the polymer.

Figure 3 shows a set of neutron reflectivity profiles and scattering length density (SLD) profiles of a nanoporous PMSSQ thin film prepared with 20 % porogen and deposited on a silicon substrate. The film was exposed to deuterated toluene liquid and vapor to examine solvent swelling. The film thickness is observed to increase upon exposure to both liquid and vapor. A higher porosity is observed in a 50 Å region next to the silicon surface. This is probably due to porogen surface segregation at the substrate interface and is in agreement with results from transmission electron microscopy.

REFERENCES

[1] *The National Technology Roadmap for Semiconductors: Technology Needs*, SIA. Semiconductor Industry Association, **1997** Edition, 101.

[2] R. D. Miller, J. L. Hedrick, D. Y. Yoon, R. F. Cook, and J. P. Hummel, Mater. Res. Soc. Bulletin **22**, 44 (1997).

[3] C. Jin, J. D. Luttmer, D. M. Smith, and T. A. Ramos, Mater. Res. Soc. Bulletin **22**, 39 (1997).

[4] C. V. Nguyen, R. B. Beyers, C. J. Hawker, J. L. Hedrick, R. L. Jaffe, R. D. Miller, J. F. Remenar, H. W. Rhee, M. F. Toney, M. Trollsas, and D. Y. Yoon, Polymer Preprint **40** (1), 398 (1999).

[5] R. F. Cook, E. G. Liniger, D. P. Klaus, E. E. Simonyi, and S. A. Cohen, Mater. Res. Soc. Symp. Proc. **511**, 33 (1998).

[6] C. V. Nguyen, K. R. Carter, C. J. Hawker, J. L. Hedrick, R. L. Jaffe, R. D. Miller, J. F. Remenar, H. W. Rhee, P. M. Rice, M. F. Toney, M. Trollsas, and D. Y. Yoon, Chem. Mater. **11**, 3080 (1999).

[7] C. Nguyen, C.J. Hawker, R. D. Miller, E. Huang, and J. L. Hedrick, Macromolecules **33**, 4281 (2000).

Neutron Reflectivity Studies of Surfactants at Electrode Surfaces

Knowledge of the forces that control the assembly of surfactant molecules at the solid-liquid interface is vital for traditional fields such as detergency, flotation, oil recovery and tribology [1]. Thin organic films deposited at solid surfaces also find application in the fabrication of optoelectronic devices, sensors, biosensors and chemically modified electrodes [2]. It has long been established that the assembly of surfactants at the solid-liquid interface depends on the charge at the solid surface [3,4]. For example, the spreading of vesicles into a phospholipid bilayer requires that surface of the solid support be negatively charged and hydrophilic.

However, the present understanding of the role played by charge on the interaction of a surfactant molecule with the electrified solid surface is far from being complete. Electrochemistry provides a unique opportunity to study the effect of the charge on the properties of amphiphilic and ionic surfactants at the charged solid-liquid interface [5]. When an organic film is deposited on a gold electrode the charge density at the metal surface may be varied, from about 30 $\mu C/cm^2$ to about 40 $\mu C/cm^2$. This magnitude of charge generates fields on the order of 10^{10} V/m. Such a field interacts with polar molecules in the membrane. By changing the sign of the charge one can use attractive or repulsive forces. In this manner, by turning a knob on a control instrument one can force phase transitions in the film of organic molecules or force surfactants to desorb or re-adsorb on the surface.

We have recently employed electrochemical techniques, atomic force microscopy and neutron reflectivity to study the field driven transformations of thin films formed by a model anionic surfactant sodium dodecyl sulfate (SDS) at the surface of a gold electrode [6]. Figure 1 shows how the surface concentration of SDS at the gold electrode surface changes with the electrode potential. A convenient way to interpret these data is to treat the electrode potential as an operational variable that can be easily adjusted using a control instrument.

Figure 1 shows that the character of SDS adsorption is strongly influenced by the charge on the metal. At sufficiently negative potentials SDS molecules are totally desorbed from the electrode surface. At moderate

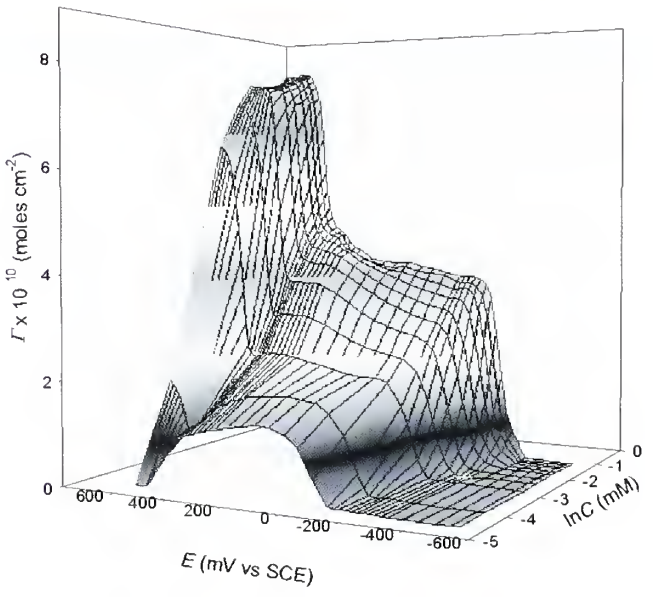

Fig. 1. Three dimensional plots of the surface concentration of SDS as a function of electrode potential measured versus the calomel reference electrode and the logarithm of the bulk SDS concentration.

negative charge densities SDS forms a film characterized by a limiting surface concentration 4.0 x 10^{-10} mol cm^{-2}. When the metal surface is positively charged the surface concentration of SDS increases to 8.1 x 10^{-10} mol cm^{-2}.

Neutron reflectivity was employed to determine the structure of the film formed by SDS at different charge densities at the gold surface. Neutron reflectivity experiments were carried out on the NG-7 reflectometer. Thin layers of chromium (≈ 20 Å) and gold (≈ 80 Å) were sputtered onto the crystal quartz substrate. After cleaning, the crystal was mounted on a specially constructed Teflon cell [7]. The cell had ports for the counter (gold foil) and reference electrodes (Ag/AgCl, $E \approx$ - 40 mV versus SCE). D_2O (99.9 %) was used as a solvent in reflectivity studies.

Figure 2a shows the neutron reflectivity data determined for SDS adsorption at various electrode potentials, and Fig. 2b shows the scattering length density profiles calculated from the reflectivity curves. The neutron reflectivity data are consistent with electrochemical measurements. They show that at very negative potentials

I. Burgess, V. Zamlynny, G. Szymanski, and J. Lipkowski
Department of Chemistry and Biochemistry
University of Guelph
Guelph, ONT N1G 2W1, Canada

J. Majewski and G. Smith
Los Alamos National Laboratory
Los Alamos, NM 87545

S. Satija and R. Ivkov
NIST Center for Neutron Research
National Institute of Standards and Technology
Gaithersburg, MD 20899-8562

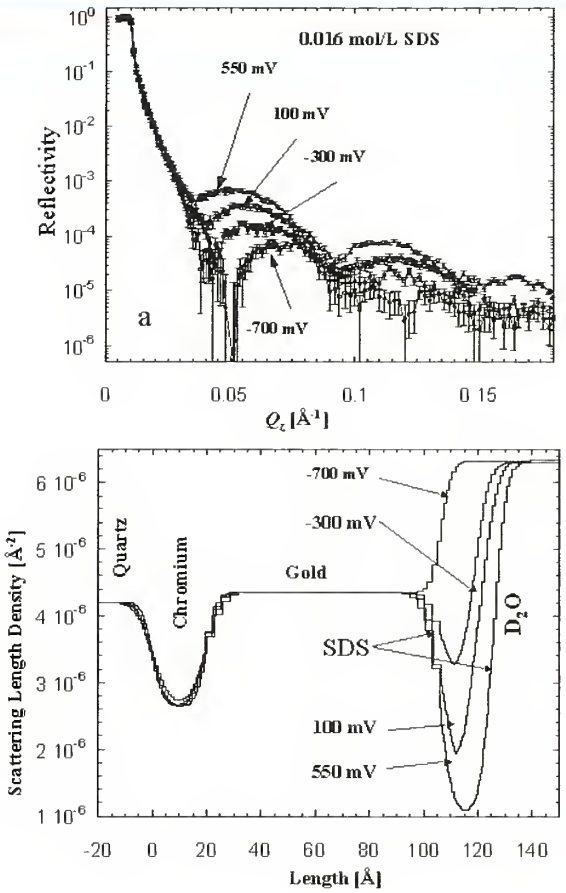

Fig. 2. (a) Normalized neutron reflectivity curves for a Au/Cr-coated quartz substrate in 16 mM SDS in D_2O. (b) Scattering length density profiles of the interface as determined from the fitting procedure.

the gold solution interface is free from hydrogenated species. When the potential increases the film of hydrogenated species appears at the electrode surface. The thickness of this film increases and the scattering length density progressively decreases with increasing potential. When combined with the results of electrochemical measurements and atomic force imaging, the neutron reflectivity data allow the determination of the structure of the film formed at different charge densities. At small or moderate negative charge densities, SDS molecules form a hemimicellar film that consists of hemicylindrical stripes, as first observed by Manne [4]. The packing of SDS molecules in a cross section of that hemicylinder is shown schematically in Fig. 3 (top). At positive charge densities the hemimicellar state is transformed into the interdigitated bilayer schematically shown in Fig. 3 (bottom).

The results of this study demonstrate the need for the use of neutron reflectometry to explore adsorption and phase transitions in films of surfactants adsorbed at the solid-solution interface. Specifically, they show that when neutron reflectivity measurements are combined with electrochemical studies and atomic force microscopy, they provide unique opportunities to explore different stages involved in the interaction of surfactants with solid surfaces.

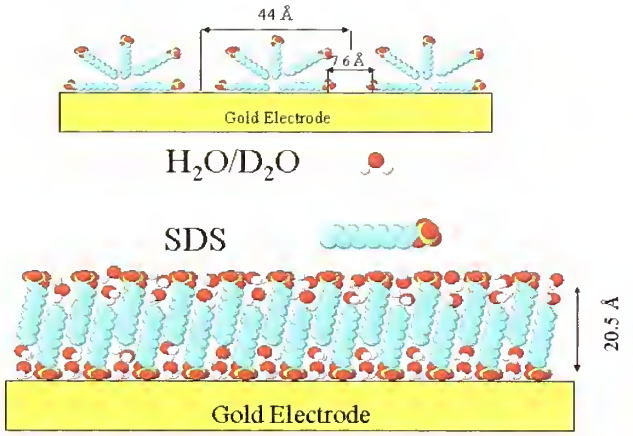

Fig. 3. Models of SDS adsorption at the Au- solution interface: a cross section of hemicylindrical aggregates observed at moderately negative charge densities (top); interdigitated bilayer observed at positive charge densities (bottom).

REFERENCES

[1] A.W. Adamson, Physical Chemistry of Surfaces, 5th ed., John Wiley & Sons, New York (1990).

[2] E. Sackmann, Science **271**, 43 (1996).

[3] P. Chandar, P. Somasundaran, N. J.Turro, J. Colloid Interface Sci **117**, 31 (1987).

[4] S. Manne, Progr. Colloid Polym. Sci. **103**, 226 (1997).

[5] D. Bizzotto, J. Lipkowski, J. Electroanal.Chem. **409**, 33 (1996).

[6] V. Zamlynny, I. Burgess, G. Szymanski, J. Lipkowski, J. Majewski, G. Smith, S. Satija, and R. Ivkov, Langmuir **16**, 9861 (2000).

[7] I. Burgess, V. Zamlynny, G. Szymanski, J. Lipkowski, J. Majewski, G. Smith, S. Satija, and R. Ivkov, Langmuir **17**, 3355 (2001).

Magnetic Semiconductor Superlattices

Currently a great deal of attention is being focused on spintronics, a new area of solid-state electronics. In spintronics not only the current magnitude but also its spin state is controlled. Spin valves and spin injectors are the first practical applications of spintronics. Further progress in developing new devices hinges critically on the availability of suitable materials. Such materials need to be "good" semiconductors, easy to integrate in typical integrated circuits, and their electronic properties should exhibit strong sensitivity to the carrier's spin, ferromagnetism being an especially desirable property.

EuS is one of the very few natural ferromagnetic (FM) semiconductors. Since it becomes FM at a low temperature (T_C = 16.6 K) it is an unlikely choice for applications. However, studying the properties of heterostructures made on its base may give an important insight into fundamental processes taking place in all classes of materials under consideration.

GaMnAs is a man-made FM semiconductor. It is an example of a diluted magnetic semiconductor (DMS) in which a fraction of nonmagnetic cations (Ga) is substituted with magnetic ions (Mn). Such a material can readily be incorporated into modern GaAs-based semiconductor devices. Its T_C is still below room temperature, but this limitation may be lifted in other materials of this class [1].

Interlayer exchange coupling (IEC) in superlattices (SL), composed of ferromagnetic and nonmagnetic layers, is a crucial element of all spin-valve type devices that utilize the giant magnetoresistance effect. In metallic SLs currently being used, conduction electrons transfer the interlayer interactions through nonmagnetic spacers [2]. Here we address the question whether IEC phenomena are possible in all-semiconductor superlattices, like EuS/PbS and GaMnAs/GaAs, where the carrier concentrations are many orders of magnitude lower than in metals.

The nonmagnetic spacer in EuS/PbS SLs is a narrow gap semiconductor with electron concentration of the order of 10^{17} cm^{-3} to 10^{18} cm^{-3}. For thin PbS layers (d_{PbS} < 70 Å) neutron reflectivity spectra, shown in Fig. 1, have revealed a pronounced maximum of magnetic origin at the position corresponding to the doubled structural SL periodicity, thus indicating the existence of antiferromagnetic (AFM) interlayer arrangements [3].

For much thicker PbS spacers (d_{PbS} > 120 Å) the only magnetic peaks visible in the reflectivity profiles, see e.g. Fig. 2, coincide with the chemical ones, thus leading to the conclusion that the magnetization vectors in adjacent EuS layers are parallel which indicates FM IEC.

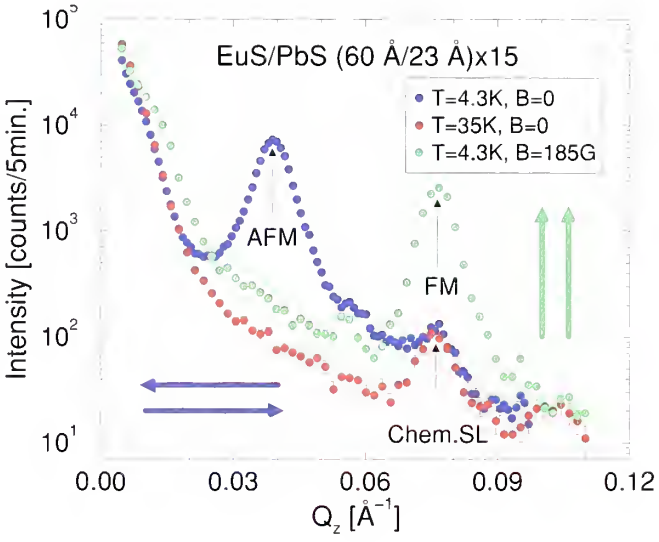

Fig. 1. Unpolarized neutron reflectivity spectra for EuS/PbS SL with thin (23 Å) PbS spacer. Antiferromagnetic interlayer exchange coupling below T_C and at zero external field is clearly visible (blue curve). Applying a strong enough magnetic field (185 G in this case) parallel to the SL surface forces all the EuS layer's magnetizations to ferromagnetic configuration (green curve). Above T_C the system is nonmagnetic, the only Bragg peak comes from the chemical SL periodicity.

In the intermediate PbS thickness range (70 Å < d_{PbS} < 120 Å), both types, AFM as well as FM, peaks are present. Polarized neutron analysis of these maxima gives evidence that the magnetization vectors of adjacent EuS layers are not collinear. Hence, the IEC found in EuS/PbS SLs has an oscillatory character similar to that occurring in metallic SLs, although the oscillation period is much longer than the one in metallic systems.

In order to confirm that the free carriers, present in the PbS layer in such a small amount, are the cause of the observed oscillatory IEC, a series of analogous measure-

H. Kepa, J. Kutner-Pielaszek, and A. Twardowski
Institute of Experimental Physics,
Warsaw University
Warsaw, Poland

A. Yu. Sipatov, V. Volobuev
Kharkov State Polytechnical University
Kharkov, Ukraine

T. Story, J. Sadowski
Institute of Physics,
Polish Academy of Sciences
Warsaw, Poland

T. M. Giebultowicz
Physics Department
Oregon State University
Corvallis, OR 97331

C. F. Majkrzak
NIST Center for Neutron Research
National Institute of Standards and Technology
Gaithersburg, MD 20899-8562

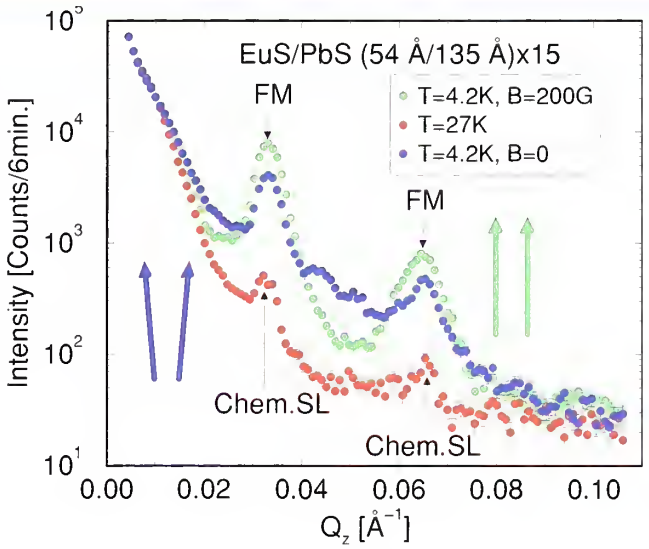

Fig. 2. The sample with thick (135 Å) PbS layers is almost ferromagnetically coupled. Application of an external magnetic field enhances the FM Bragg peaks and lowers the intensity between them (in AFM peak position).

ments have been carried out on EuS/YbSe SLs. The structure and lattice constant of YbSe are the same as those of PbS. In contrast to PbS, YbSe is a semi-insulator with a negligible carrier concentration. Neutron reflectivity profiles have shown no evidence of any interlayer coupling in the all investigated samples. That finding, together with the oscillatory character of coupling in SLs with PbS spacer, strongly points to the leading role of PbS free electrons in providing the necessary IEC mechanism, similar to that discovered in metallic multilayers.

Ferromagnetic ordering in GaMnAs is carrier (holes) induced; the Mn atoms, apart from being the magnetic element in the system, act also as acceptors providing the holes responsible for transferring exchange interactions between them. The details of the magnetic ordering, in particular its range, are still being disputed.

To address the latter issue, polarized neutron reflectometry has been performed on a number of GaMnAs/GaAs superlattices. Figure 3 shows an example of the reflectivity profile obtained in the vicinity of the first SL Bragg peak for one of the samples. The very presence of the magnetic contribution to the structural SL Bragg peak is a strong confirmation of the FM IEC between consecutive GaMnAs layers. The absence of any spin-flip scattering shows that the sample is in a one-domain state, i.e., the FM ordering in GaMnAs is long range, and the sample is spontaneously saturated. The peak in (--) cross section, and its absence in the (++), is proof that the magnetization is directed oppositely to the external

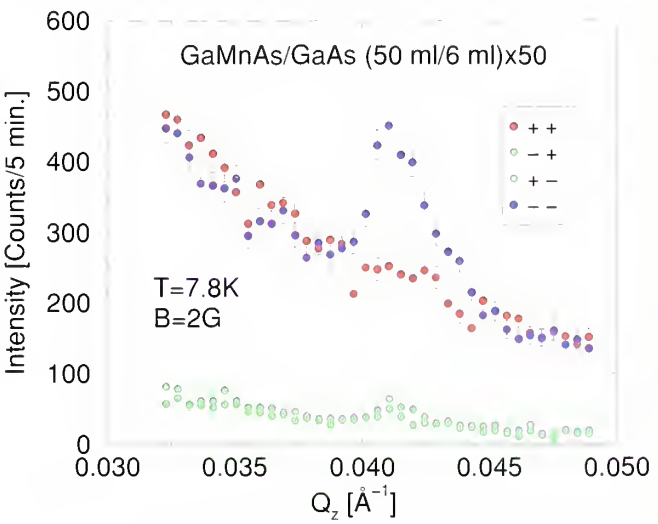

Fig. 3. Polarized neutron reflectivity spectra for GaMnAs/GaAs superlattice.

magnetic guide field, hence the long range ordering has formed spontaneously, without the influence of the external field. More details can be found in [4].

REFERENCES

[1]. T. Dietl, H. Ohno, F. Matsukura, J Cibert, D. Ferrand, Science **287**, 1018 (2000).

[2]. P. Bruno, Phys. Rev. **B52**, 411 (1995).

[3]. H. Kepa, J. Kutner-Pielaszek, J. Blinowski, A. Twardowski, C. F. Majkrzak, T. Story, P. Kacman, R. R. Galazka, K. Ha, H. J. M. Swagten, W. J. M de Jonge, A. Yu. Sipatov, V. Volobuev, T. M. Giebultowicz, Europhys. Lett. (2001), in print.

[4]. H. Kepa, J. Kutner-Pielaszek, A. Twardowski, C. F. Majkrzak, J. Sadowski, T. Story, T. M. Giebultowicz, Phys. Rev. **B**, (2001), in print.

Pinpointing Chiral Structures with Front/Back Polarized Neutron Reflectometry

We have developed a new method of using polarized neutron reflectometry (PNR) to extract the structure of buried magnetic spirals in magnetic films. This technique improves upon earlier methods by being particularly sensitive to the presence of magnetic twists vis-à-vis structures in which the magnetization direction does not vary appreciably. Tracking the formation and growth of twists may solve a number of puzzles that hamper the development of magnetic thin film devices.

In collaboration with IBM scientists, we have applied the technique to a thin-film exchange-spring magnet and confirmed that the results may violate the current theory regarding the behavior of such magnets. It has been predicted that exchange-spring magnets, comprised of soft and hard ferromagnets in close proximity, are a composite that has a strong moment and does not readily demagnetize [1]. Therefore, exchange-spring magnets should give industry the ability to make much smaller permanent magnets for use in the magnetic recording devices, and elsewhere. As a side effect, when a small external magnetic field is opposed to that of the magnet, the portion of the soft ferromagnet farthest from the hard ferromagnet may twist into alignment with the field. When the field is removed, the soft ferromagnet untwists. The film provided by IBM consists of the hard ferromagnet $Fe_{55}Pt_{45}$ topped by the soft ferromagnet $Ni_{80}Fe_{20}$ [2].

Figure 1 shows a simplified diagram of the behavior predicted by current theories [1]. A magnetic field of 0.890 T, provided by an electromagnet, is sufficient to align both the soft and the hard layers of our exchange-spring magnet, as shown on the left. When a modest reverse field (on the order of 0.025 T) is applied to the exchange spring magnet, only the top of the soft layer will realign with the magnetic field. The hard layer remains pinned in the original direction, and a continuous twist is induced in the soft layer, as the direction of magnetization changes smoothly between the reverse field direction to the aligning field direction.

Although there are many alternatives to PNR to measure the magnetization, typically they measure only the average orientation of the magnetic spins, and cannot readily distinguish a spiral from a structure in which all

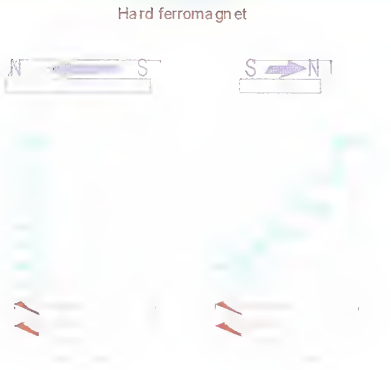

Fig. 1. Model for field behavior of exchange-spring magnets. On the left the magnet has been aligned by a large external magnetic field. On the right a smaller field opposed to the first field causes a twist to form in the soft ferromagnet, while the hard ferromagnet remains aligned.

the spins are canted with respect to an external field. PNR can extract the depth-dependence of the magnetic and chemical structure. We have studied the sample over a wide range of external magnetic fields, and can track the development of the spiral with field [3].

A PNR experiment begins with neutrons whose magnetic moments are aligned parallel (+) or opposite (-) to the external magnetic field. When the magnetization of the sample is perpendicular to this magnetic field, the neutron moment precesses as it interacts with the sample. When this happens the spin-flip (SF) reflectivities R^{+-} and R^{-+} are strong. If the magnetization of the sample is parallel to the external magnetic field, no precession occurs, but the non-spin-flip (NSF) reflectivities R^{++} and R^{--} will differ. The NSF reflectivities also provide information about the chemical structure of the film.

Our new modification of the PNR method greatly enhances the contrast between collinear and certain noncollinear magnetic structures [4]. We first measure the reflectivity with neutrons glancing off the front surface of the material, and then repeat with neutrons glancing off the back surface. The experiment is akin to holding the plane of the film up to a "magnetic mirror" to see whether the mirror image is the same as the original structure. In a collinear structure, all the spins are aligned along a common direction, and the mirror image is very much like the original structure. But the mirror image of

K. V. O'Donovan, J. A. Borchers, and C. F. Majkrzak
NIST Center for Neutron Research
National Institute of Standards and Technology
Gaithersburg, MD 20899-8562

O. Hellwig, E. E. Fullerton
IBM Almaden Research Facility
San Jose, CA 95120-6001

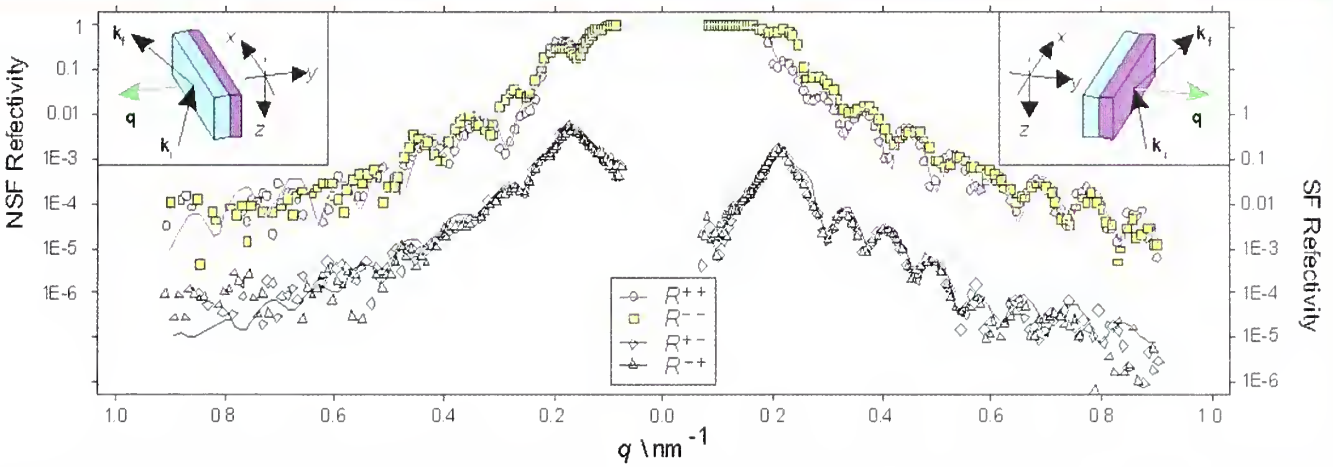

Fig. 2. Reflectivity of a $Ni_{80}Fe_{20}|Fe_{55}Pt_{45}$ bilayer. The front reflectivity is plotted on the right while the back reflectivity is plotted on the left. The SF reflectivities R^{+-} and R^{-+} are plotted against the right ordinate axis. The NSF reflectivities R^{++} and R^{--} are plotted against the left ordinate axis.

a magnetic twist to the right is a magnetic twist to the left. Therefore, if the front and back reflectivities are significantly different, we can deduce the presence of a spiral. Fitting the data confirms the spiral's existence.

Figure 2 shows data collected at 0.026 T after aligning in -0.89 T. Fits to the data are shown as solid lines. The data from the front reflectivity are shown on the right, and the data from the back reflectivity are shown on the left. The spin-flip (SF) reflectivities R^{+-} and R^{-+} plotted against the right-hand axis, have been shifted relative to the NSF reflectivities R^{++} and R^{--} that are plotted against the left axis. At $q = 0.2$ nm^{-1}, there is a splitting in the front NSF reflectivity that is much more pronounced than that of the back reflectivity at the same q. This is a hallmark of the spiral structure.

Figure 3 shows the magnetic structure that gives the excellent fit to the data plotted in Fig. 2. The location of the hard/soft interface is marked in Fig. 3. Surprisingly, we discover the spiral invades the hard ferromagnet even at extremely low fields. Current theory predicts that when this occurs, the soft ferromagnet will not be able to untwist fully. Yet, other magnetic studies show that our exchange-spring magnet does untwist when this field is removed. Thus, our PNR measurements have identified a shortcoming of current theory.

With this new technique, NIST is now able to better characterize the magnetic properties of thin films, which can improve the capability and reliability of industrial devices for magnetic recording and sensing.

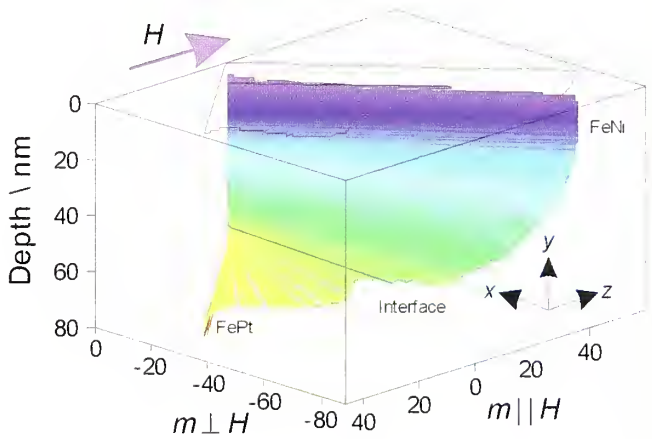

Fig. 3. Fitted magnetization of the data presented in Fig. 2. The front of the sample is at a depth of 0 nm and the back is at a depth of 70 nm. The red curve is a projection of the magnetic structure into the plane of the front surface.

REFERENCES

[1] E. F. Kneller and R. Hawig, IEEE Trans. Magn. **27**, 3588 (1991).

[2] O. Hellwig, J. B. Kortright, K. Takano, and E. E. Fullerton, Phys. Rev. **B 62**, 11694 (2000).

[3] K. V. O'Donovan, *et al.*, in preparation.

[4] K. V. O'Donovan *et al.*, submitted to Applied Physics A

The Nature of Vibrational Softening in α-Uranium

The standard textbook explanation for phonon softening with increasing temperature in a single phase is that the potentials are not perfectly harmonic, but it has been suggested that phonon softening can also occur if the potential itself can change with temperature, while remaining harmonic. For example, a large softening of the vibrational properties of α-uranium has been observed [1] that cannot be explained in terms of the anharmonic lattice contribution alone. In the present work a harmonic contribution to the phonon softening is made evident by treating inelastic neutron scattering spectra as an expansion of the vibrational power spectrum of the atomic motion.

Earlier diffractometry measurements by Lawson *et al.* [2] suggested that the Debye temperature decreased by 40 % in going from 300 K to the β-phase transition temperature at 940 K. In terms of entropy this corresponds to an additional $\Delta S = -3k_B ln(0.6) = 1.5\ k_B/atom$. The usual thermodynamic argument is that this increase in vibrational entropy compensates for the elastic energy generated by thermal expansion. However, from heat capacity data, the entropy needed to compensate for the elastic energy is nearly an order of magnitude too small at 0.16 $k_B/atom$.

All experiments used uranium powder. High temperature measurements were made using the Fermi-Chopper Spectrometer (FCS) at the NCNR. Low temperature measurements were performed with the Low Resolution Medium Energy Chopper Spectrometer (LRMECS) at Argonne National Laboratory. Figure 1 shows the phonon density of states obtained from the measured spectra, corrected for the incoherent multiphonon scattering using a procedure described elsewhere [3]. There is a redistribution of intensity in the main features at ≈ 8 meV and ≈ 12 meV, with the higher energy peak gaining extra weight with increasing temperature. These features also show an overall softening of around one meV for every 200 K increase in temperature.

The Q-summed one phonon scattering function was used to calculate a quantity proportional to the square of the power spectrum and hence to the average potential energy per oscillator, $\langle U \rangle$. In Fig. 2 we show $\langle U \rangle$ for α-uranium at the four highest temperatures scaled so that the lowest point is at the harmonic energy $k_B T/2$. The effects of anharmonicity on $\langle U \rangle$ would be evident as nonlinearity in the plot of $\langle U \rangle$ vs. temperature. For comparison, attempts were made to calculate the

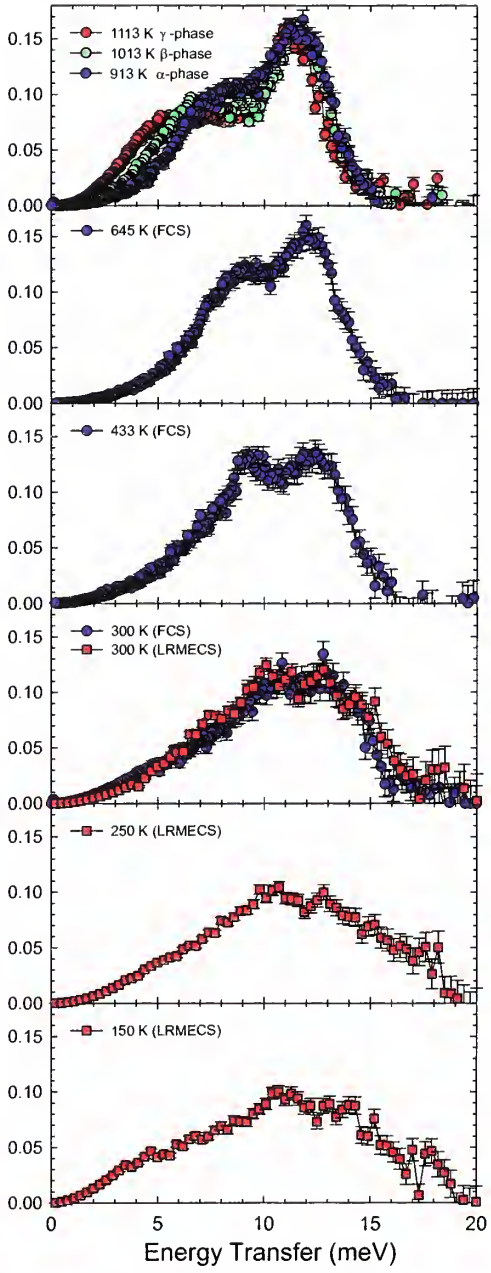

Fig. 1. The phonon density of states of uranium. Data from 300 K and above were obtained from spectra acquired with FCS. Data from 300 K and below were measured on LRMECS.

M. E. Manley and B. Fultz
California Institute of Technology
Pasadena, CA 91125

M. E. Manley, R. J. McQueeney, W. L. Hults, J. L. Smith, and D. J. Thoma
Los Alamos National Laboratory
Los Alamos, NM 87545

C. M. Brown
NIST Center for Neutron Research
National Institute of Standards and Technology
Gaithersburg, MD 20899-8562
and
University of Maryland
College Park, MD 20742

R. Osborn
Argonne National Laboratory
Argonne, IL 60439

J. L. Robertson
Oak Ridge National Laboratory
Oak Ridge, TN 37831

temperature dependence of the potential energy of Morse and Lennard-Jones potentials with the appropriate vibrational softening for uranium [1]. The result shown in Fig. 2 indicates that, in the high temperature limit, the potential energy has nearly a linear dependence on temperature, i.e. the phonon softening in α-uranium occurs while the potential remains primarily harmonic. Evidently the interatomic force constants are decreasing

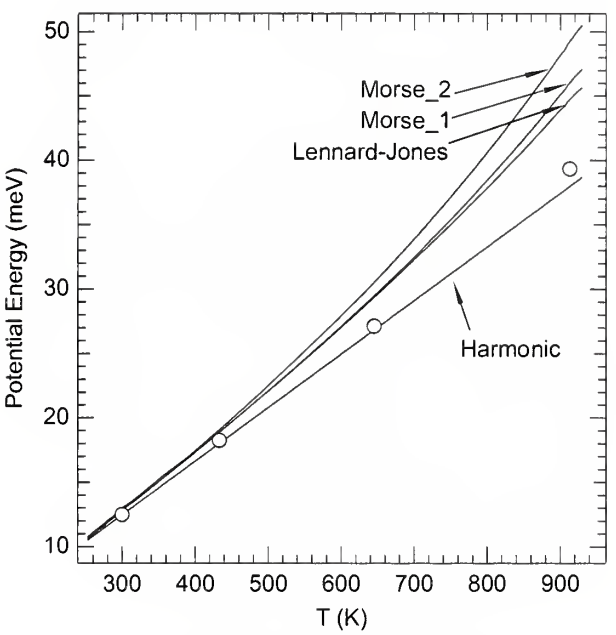

Fig. 2. Vibrational potential energy of α-uranium (○). The Lennard-Jones, Morse_1 and Morse_2 curves were calculated from potentials described in the text. The Harmonic curve is the result for a harmonic potential in the classical limit.

with increasing temperature. Since the force constants originate from the change of the electronic energy with atom displacements, it must be that *thermal excitations of the electronic states* are altering the force constants.

The phonon density of states of the three solid state phases of uranium, orthorhombic (α), tetragonal (β) and body centered cubic (γ) are compared in the top panel of Fig. 1. The γ-uranium phonon density of states was statistically identical at 1113 K and 1213 K. Evidently, the thermal softening mechanism seen in α-phase does not operate in the γ-phase. The β-phase was not stable over a wide enough temperature range to obtain a reliable temperature dependence. The phonon softening between each phase accounted for vibrational entropy changes of $0.15 \pm 0.01\ k_B$/atom and $0.20 \pm 0.01\ k_B$/atom for the α→β and β→γ transitions, respectively. Both of these values make up only about 35 % to 40 % of the total entropy changes predicted from latent heat measurements; $(S^{\beta}\text{-}S^{\alpha})_{tot} = 0.37\ k_B$/atom and $(S^{\gamma}\text{-}S^{\beta})_{tot} = 0.55\ k_B$/atom. The remaining 60 % of the entropy increases must be electronic in origin. So not only does the phonon softening disappear in the high temperature γ-phase, but also it does so with a large increase in electronic entropy.

Electronic band structure calculations used to predict phonon frequencies are based on the assumption that thermal effects can be neglected when compared to volume effects. The actinides, however, show the need for more sophisticated treatments of the role of temperature on interatomic interactions.

REFERENCES

[1] M. E. Manley, B. Fultz, R. J. McQueeney, C. M. Brown, W. L. Hults, J. L. Smith, D. J. Thoma, R. Osborn, J. L. Robertson, Phys. Rev. Lett. **86**, 3076 (2001).

[2] A. C. Lawson, B. Martinez, J. A. Roberts, B. I. Bennett and J. W. Richardson, Jr., Phil. Mag. B **80**, 53 (2000).

[3] M. E. Manley, R. J. McQueeney, J. L. Robertson, B. Fultz and D. A. Neumann, Phil. Mag. Lett. **80**, 591 (2000).

Dynamics of Native and Partially Unfolded Proteins by Inelastic Neutron Scattering and Molecular Dynamics Simulations

A molten globule (MG) is a partially folded protein that is compact with native-like secondary structure and overall backbone-folding topology but which lacks the extensive specific side-chain packing interactions of the native-like structure. Such partially folded states have been shown to resemble the kinetic folding intermediate states along the protein-folding pathway. In addition, partially folded proteins are important in cell functioning. A full understanding of the mechanism of protein folding requires the knowledge of the structures, relative energetics, and dynamics of the species populating the folding pathway. Incoherent inelastic neutron scattering (INS), which makes use of the large incoherent cross section of hydrogen nuclei, is a technique well suited to the study of protein internal molecular motion on the picosecond time scale. Molecular dynamics (MD) simulations on the other hand are a potentially valuable tool for interpreting neutron data on proteins [1,2], and may provide atomic level description of the motions taking place.

In this study, we have explored the dynamics of bovine α-lactalbumin, a calcium-binding protein, in the native and molten globule states, using both techniques. INS data were collected on the Disk-Chopper Spectrometer at ≈ 32 μeV resolution for native and molten globular bovine α-lactalbumin. The simulations results were generated from ≈ 1 ns constant temperature and pressure MD trajectories. The model systems consisted each of a single protein monomer, immersed in a large water box (60 Å x 50 Å x 80 Å). For the native state, the α-lactalbumin configuration was initiated from the crystal structure. The model molten globule state was generated by partially unfolding the protein at 500 K at atmospheric pressure until the radius of gyration reached the experimental value determined for the molten globule state (10 % expansion). A 1 ns trajectory was then generated at 300 K for data analysis and comparison with experiment.

Figure 1 shows the structure of the α-lactalbumin in the native and molten globule states obtained from the MD simulations in solution at 300 K. The overall structural change, manifested by the conservation of the helical α-domain and the loss of the β sheets in the β-domain, is consistent with NMR data [3]. We therefore regard this structure as a reasonable model of a member of the MG ensemble for comparison with the INS data.

In Fig. 2 we report the incoherent structure factors $S(Q,\omega)$ as a functions of energy transfer $\hbar\omega$ for selected momentum transfer Q, measured and calculated from the MD simulations trajectories. In both systems the agreement with experiment is remarkable, assessing the ability of the simulations to reproduce the picosecond dynamics of the protein. In agreement with previous INS data collected at lower resolution [4], the molten globule has a broader quasi-elastic spectra compared to the native state,

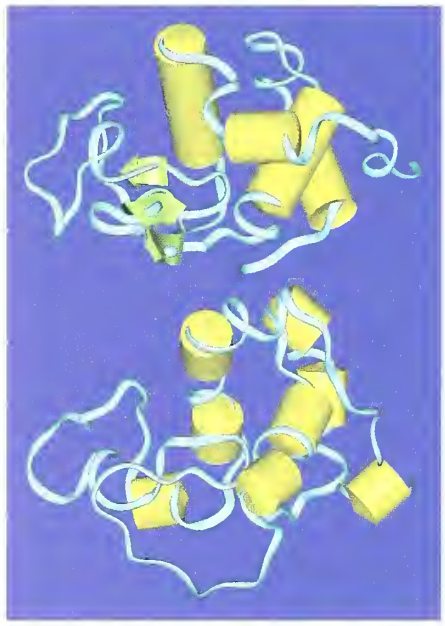

Fig. 1. α-lactalbumin structure in the native (top) and molten globule (bottom) state from MD simulations. Note the loss of the β-domain structure, with most the α domain (helix) being conserved.

which indicates that the protein atoms are more mobile in the MG state. The additional motion is large enough to be detected at the length scale probed by the DCS spectrometer, *i.e.*, in the range 3 Å to 60 Å.

To investigate the relationship between the structure of the protein and the motion of its side chains, we have used the MD trajectories to follow the motion of these side chains quantitatively. Figure 3 reports the fluctuations per residue along the backbone for the native and the molten globule states, as a function of residue. These

M. Tarek
NIST Center for Neutron Research
National Institute of Standards and Technology
Gaithersburg, MD 20899-8562
and
Center for Molecular Modeling and Department of Chemistry,
University of Pennsylvania
Philadelphia, PA 19103

D. J. Tobias
Department of Chemistry
University of California Irvine, CA 92697-632

Z. Bu and D. A. Neumann
NIST Center for Neutron Research
National Institute of Standards and Technology
Gaithersburg, MD 20899-8562

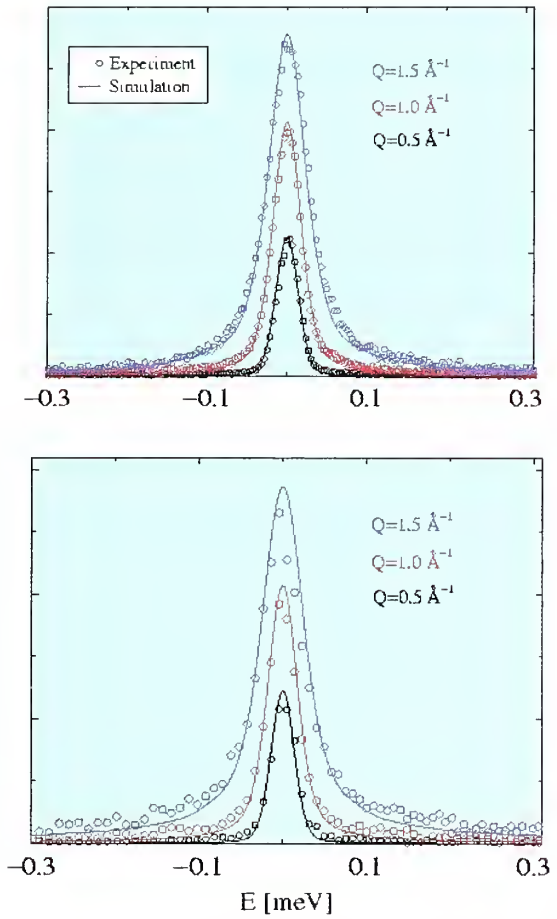

Fig. 2. Incoherent structure factor *S(Q,ω)* at selected wavevectors *Q*, measured and calculated from the simulation for the native (top) and molten globule (bottom) states.

correspond to the 100 ps root-mean- square amplitudes of motion of the backbone atoms, averaged over the simulation trajectories. First, for the native state, the backbone fluctuations appear to correlate with the secondary structure of the protein, showing much smaller amplitudes in the α-helix and β-sheet regions. For the molten globule state, a significant increase in the protein fluctuation amplitudes is observed, in agreement with the broadening of the INS spectra. Figure 3 shows clearly that most of the additional motion occurs in the region of the protein that "unfolds", *i.e.,* the β-domain. The results indicate also that the motion of the side chains is by no means homogeneous. Differences in amplitudes up to 10

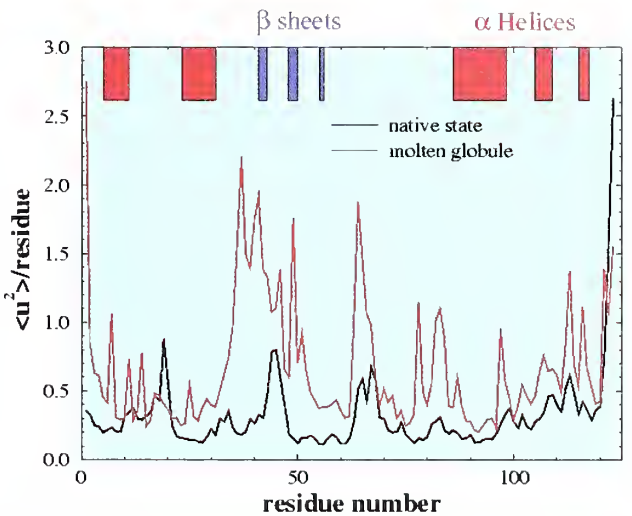

Fig. 3. 100 ps mean squared fluctuations of the backbone atoms computed from the MD simulations of the native state (black) and the molten globule state (red).

folds are observed between parts of the proteins, regardless of exposure to the solvent.

The MD study of the dynamics of partially folded states of the protein should in principle be extended to explore a large portion of the conformational space, *i.e.,* be extended to a large ensemble of non-native conformers. At any rate, the present results, though limited, combined with neutron experiments are believed to capture the essence of the structural and dynamical changes taking place as the protein partially unfolds. They demonstrate the utility of the MD simulations for qualitatively elucidating the dynamical behavior of native and non-native proteins at the atomic level.

REFERENCES

[1] M. Tarek, G. J. Matryna, and D.J. Tobias, J. Amer. Chem Soc. **122**, 10450 (2000).

[2] M. Tarek and D. J. Tobias, Biophys. J. **79**, 3244 (2000).

[3] J. Baum *et al.*, Biochemistry, **28** 7 (1989).

[4] Z. Bu *et al.*, J. Mol. Biol. **301**, 525 (2000).

Dynamics in Confined Polymer Films

Material properties at surfaces and interfaces often deviate from their bulk values. This has ramifications in a range of polymer thin film applications such as chemically amplified photoresists, lubricants, adhesives, etc. Of particular interest are changes in the glass transition temperature, T_g, and the viscoelastic properties that are related to T_g. A viscosity increase of liquid polymeric films, like those used for hard disc lubricants, could have deleterious consequences. Likewise, a T_g decrease in a thin photoresist film could enhance photoacid diffusion and create image blur. Clearly, it is of great interest to characterize the molecular level mobility in thin polymer films.

It is well known that thermal motions lead to a decrease in the intensity of the elastically scattered neutrons. In a harmonic solid this is related to the amplitude of the motion through the Debye-Waller factor: $I_{inc}(Q) \sim \exp(-^1/_3 Q^2 \langle u^2 \rangle)$ where Q is the scattering vector and $\langle u^2 \rangle$ is the mean-square displacement. In a logarithmic plot of I_{inc} as a function of Q^2, $\langle u^2 \rangle$ is proportional to the slope of a linear fit to the data. This approximation has proven very useful in studying dynamics of polymers, both synthetic [1] and biological [2], despite the fact that their motions are typically anharmonic.

The elastic incoherent neutron scattering intensities can be measured as a function of temperature on the NCNR's High Flux Backscattering Spectrometer (HFBS), using the "Fixed Window" mode. Polycarbonate (PC) films, seen in Fig. 1, are spin cast onto Si wafers, sectioned into small rectangles, and stacked into an Al sample cell. The scattering from the Si substrates and Al cell are negligible because their Bragg peaks are beyond the Q range of the instrument ($0.25 < Q$ (Å^{-1}) < 1.75); the scattering is dominated by the large incoherent cross-section of the amorphous PC.

Ideally there should be 200 mg of PC per cell to maximize the signal and minimize multiple scattering effects (90 % transmission). For the Si-supported films we are limited by (10 to 0.5) mg of PC per cell and thus a very weak signal (99 % transmission). However, the HFBS is sufficiently sensitive, as seen in Fig. 2 where the temperature dependence of the elastic scattering is

Fig. 1. A stack of 1014 Å PC films (notice the blue tint) on thin slabs of Si ready to go into the HFBS spectrometer.

shown. The relative magnitude of the intensity change is diminished with decreasing film thickness, a clear indication of reduced mobility in the thin PC films. Given the HFBS energy resolution of 0.85 μeV, these changes reflect atomic motions at 200 MHz or faster.

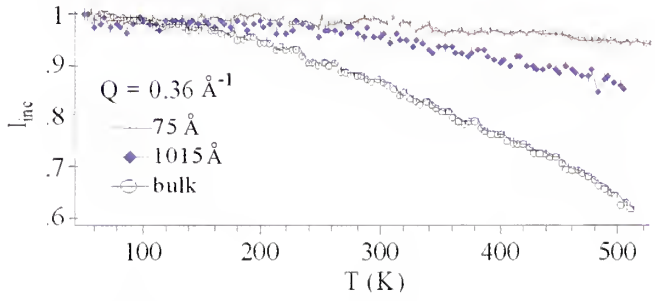

Fig. 2. The normalized elastic intensities in the HFBS detector at Q = 0.36 Å^{-1}. The decrease in intensity at high temperatures reflects dynamics in the thin polymer films.

This reduced mobility is qualitatively reflected in Fig. 3 as a strong suppression of $\langle u^2 \rangle$. We emphasize qualitatively because $\langle u^2 \rangle$ is derived from the harmonic approximation. Nevertheless, there is a clear reduction in the amplitude of the thermal motions both above and below the calorimetric T_g as the film thickness approaches the rms end-to-end length of PC (R_{ee} = 160 Å).

C. L. Soles, J. F. Douglas, and Wen-li Wu
Polymers Division
National Institute of Standards and Technology
Gaithersburg, MD 20899-8541

R. M. Dimeo
NIST Center for Neutron Research
National Institute of Standards and Technology
Gaithersburg, MD 20899-8562

At temperatures below 200 K, $<u^2>$ is small and the harmonic approximation is reasonable. In this regime the thermal evolution of $<u^2>$ (i.e., slope) defines an elastic force constant κ. The inset of Fig. 3 displays a dramatic stiffening of κ with confinement. This implies that the atoms or molecules in PC become strongly caged by their environment in the exceedingly thin films.

Similar $<u^2>$ measurements on thin films of polymethyl methacrylate (PMMA; R_{ee} = 915 Å) and polyvinyl

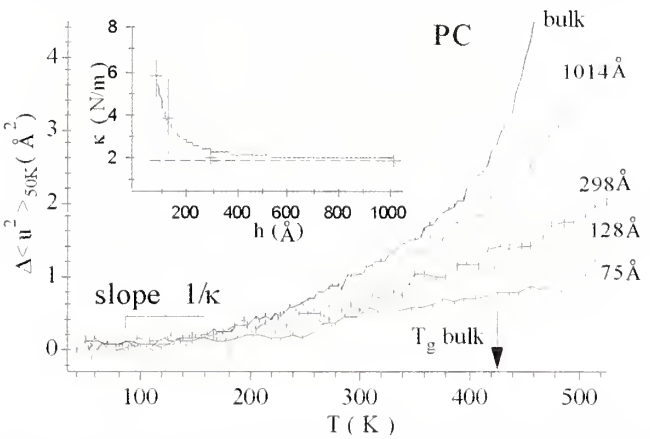

Fig. 3. $<u^2>$ as a function of temperature for the PC thin films. The inset reveals a stiffening of the harmonic (low temperature) force constant *k* with decreasing film thickness *h*.

chloride (PVC; R_{ee} = 437 Å) are shown in Figs. 4(a) and 4(b). There is a suppression of $<u^2>$ with decreasing film thickness above the bulk T_g that is qualitatively consistent with the PC films. However, below T_g bulk the suppression is less pronounced in PMMA, and not observed in the PVC films. Careful inspection of Figs. 3 and 4 suggests a relation between the magnitude of $<u^2>$ at T_g in the bulk and the degree of $<u^2>$ suppression in the thin glassy films.

Bulk PC has the largest $<u^2>$ at T_g, indicating extensive mobility. In fact, PC is renowned for is segmental mobility in the glassy state, which is in part related to its superior impact resistance (bullet proof glass); molecular mobility helps dissipate strain energy. This extensive mobility is also susceptible to thin film confinement, as is also seen through the stiffening of the elastic constants from 1.9 N/m in bulk PC to 5.8 N/m in the 75 Å film (stronger molecular caging). At the other extreme, bulk PVC has the smallest $<u^2>$ at T_g, indicating a lack of

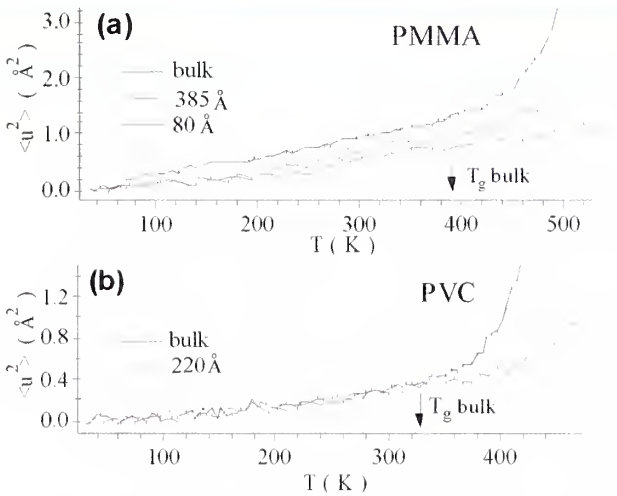

Fig. 4. $<u^2>$ as a function of thickness and temperature for similar PMMA (a) and PVC (b) films.

motions that can be affected by confinement. This is also consistent with the strong intermolecular caging at low temperatures; both bulk PVC and the 220 Å film have large elastic force constants of 4.6 N/m. This lack of mobility reflects the observation that PVC is a brittle polymer that needs high levels of plasticization for practical use. Only when PVC is taken above the bulk T_g, where long-range motions dominate, do the effects of confinement become evident.

In short, we have seen two different responses to thin film confinement. While there is a general suppression of $<u^2>$ and fast dynamics, polymers with greater mobility are more susceptible to confinement, especially below the calorimetric T_g. In contrast, polymers with strongly localized motions appear bulk-like, even in highly confined glassy films. More details of these studies can be found in our upcoming publications [3-5].

REFERENCES

[1] B. Frick, D. Richter, Science **267**, 1939 (1995).

[2] G. Zaccai, Science **288**, 1604 (2000).

[3] C. Soles, J. Douglas, W. Wu, R. Dimeo, submitted to Phys Rev E.

[4] C. Soles, J. Douglas, W. Wu, H. Peng, D. Gidley, submitted to Euro. Phys. J. E.

[5] C. Soles, E. Lin, J. Lenhart, R. Jones, W. Wu, D. Goldfarb, M Angelopoulos, J. Vac. Sci. Tech. B, in press.

Intimate Relationship Between Structural Deformation and Properties of Carbon Nanotubes

Carbon nanotubes continue to surprise scientists with their novel properties. Recently we have discovered many intimate relationships between structural deformation and the properties of single-walled nanotubes (SWNT) [1, 3] that could be important in technological applications. These observations were made using state-of-the-art first-principles total energy calculations within the pseudo-potential and the generalized gradient approximations (GGA). Here we present a brief review of our findings.

SWNTs are basically rolled graphite sheets which are characterized by two integers *(n,m)* defining the rolling vector of graphite. Therefore, the electronic properties of SWNTs, to first order, can be deduced from that of graphite by mapping the band structure from a 2D hexagonal lattice onto a cylinder. Such an analysis indicates that *(n,n)* armchair nanotubes are always metallic and *(n,0)* zigzag nanotubes are metallic only if n is an integer multiple of three. From our first-principles calculations we find that these electronic properties can be significantly modified by radial strain, which distorts the circular cross section to an elliptical one. Figure 1 shows that the energy gap of an insulating SWNT decreases and eventually vanishes at an insulator-metal transition with increasing applied elliptical strain. The density of states at the Fermi level $N(E_F)$, of a metallized SWNT increases with increasing deformation. More interestingly, the elliptical deformation necessary to induce metallicity is found to be in the elastic range. Therefore, all strain induced changes in electronic and also in mechanical properties are reversible.

Another significant effect of the elliptical distortion of SWNTs is the change in the uniformity of their charge distribution. This, in turn, imposes changes in the chemical reactivity and hence on the interaction of the tube surface with foreign atoms and molecules. To demonstrate this, we calculate the binding energies of H and a simple metal atom, Al, on SWNTs as functions of nanotube radius (R), type, and elliptical deformation. We find that the binding energy, E_B, is positive (i.e. stable) and follows a remarkably simple $1/R$ scaling for *(n,0)* SWNTs for both H and Al, even though H prefers to sit

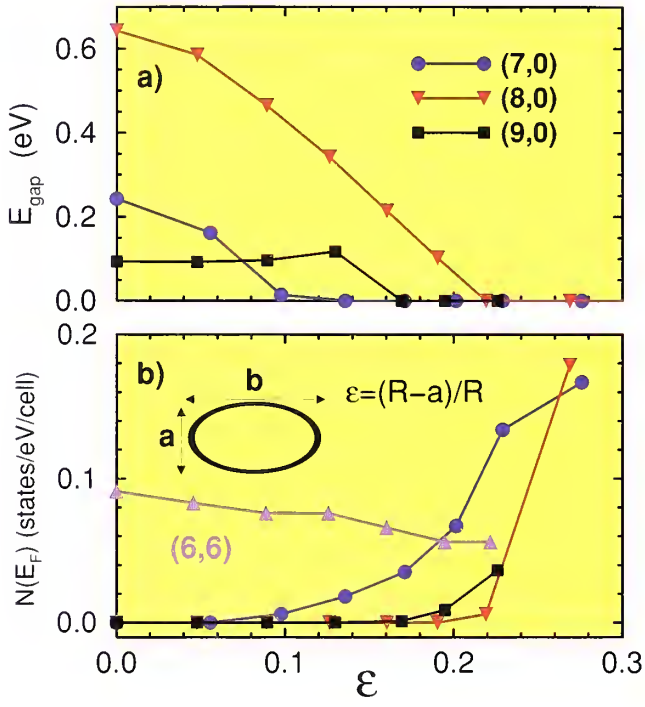

Fig. 1. Variation of the energy band gap E_{gap}(a) and density of the states at the Fermi energy (b) as a function of elliptical deformation

on top of C atoms and Al favors the hollow sites (i.e. top of hexagons). Increasing binding energy with increasing curvature (i.e. decreasing R) suggests that E_B can be modified by elliptical deformation.

Figure 2 shows the variation with elliptical distortion of the binding energy E_B of a single hydrogen atom adsorbed on the sharp and flat edges of the (8,0) surface. With increasing distortion, the binding energy of the sharp site increases, while it decreases for the flat site, creating an energy difference of ≈ 1.1 eV at the distortion value $\varepsilon = 0.3$. This value is 44 % of the binding energy of H on the undeformed SWNT.

The binding energy of Al exhibits a behavior similar to that of H, despite H and Al favoring different sites on the (8,0) tube. Elliptical deformation increases the binding energy of the both flat and sharp sites for Al, given an energy difference of 0.5 eV at the deformation $\varepsilon = 0.3$. It is remarkable that Al, which is not bound to the

T. Yildirim
NIST Center for Neutron Research
National Institute of Standards and Technology
Gaithersburg, MD 20899-8562

O. Gulseren
NIST Center for Neutron Research
National Institute of Standards and Technology
Gaithersburg, MD 20899-8562
and
Department of Materials Science and Engineering
University of Pennsylvania
Philadelphia, PA 19104-6202

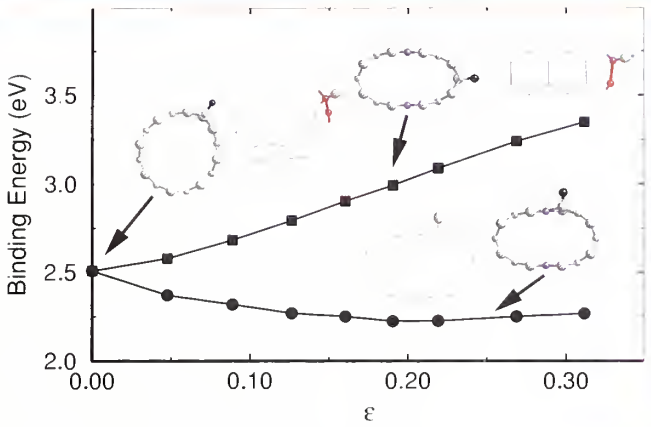

Fig. 2. Binding energies of the sharp (top) and the flat sites (bottom) versus elliptical deformation for a hydrogen adsorbed on a (8,0) SWNT.

graphite, can be adsorbed at the sharp site of the distorted SWNT with a binding energy of 1.8 eV. Hence, we conclude that not only band gap engineering but also chemical reactions taking place on the surface of a SWNT can be engineered through radial deformation.

Explanation of this remarkable change of the binding energy with elliptical deformation is sought in the electronic structure of SWNTs. Figure 3 shows the response of the first conduction band to elliptical distortion. It is clear that the distortion disturbs the uniformity of the charge distribution of the SWNT and pushes the chemically most active electrons from the flat to the sharp site of the nanotube, increasing the adsorption energy of the sharp site significantly. Surprisingly the effect of distortion on metallic armchair *(n,n)* nanotubes is found to be very small due to the metallic bands of the tubes [2]. This could be important in selective functionalization of nanotubes. See Ref.[1] for animation of this effect.

We believe that the tunable electronic and chemical properties reported here can have important implications for metal coverage and for selective adsorption and desorption of atoms and molecules on carbon nanotubes. This could allow the fine tuning of the properties of SWNTs via reversible deformation and can ultimately lead to a wide variety of technological applications such

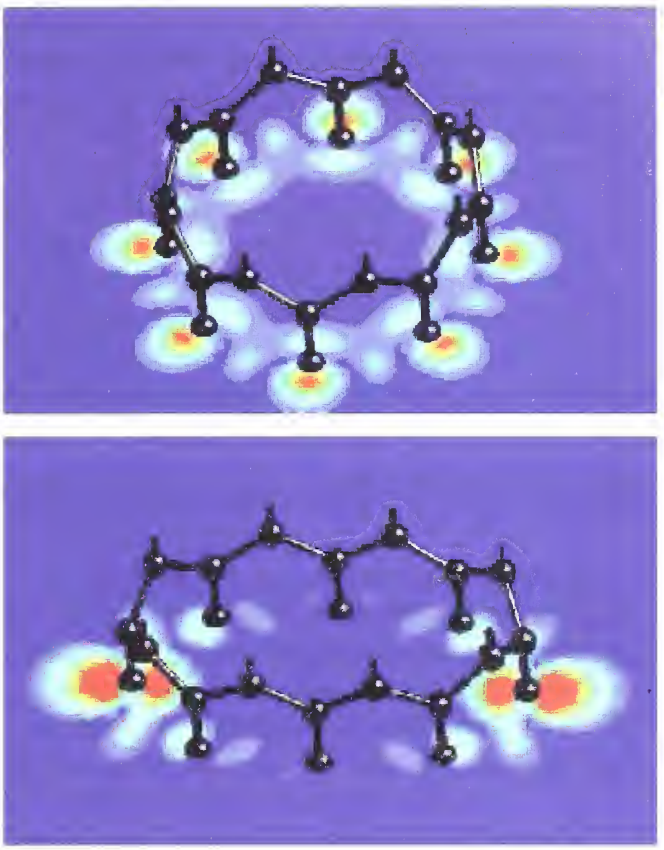

Fig. 3. Contour plot of the first conduction band of an undeformed (top) and elliptically deformed (bottom) (8,0) SWNT.

as variable metal-insulator junctions, quantum wells, catalysts, hydrogen storage devices, magnetic tubes (by absorbing magnetic ions), etc.

REFERENCES

[1] See http://www.ncnr.nist.gov/staff/taner/nanotube

[2] O. Gulseren, T. Yildirim, and S. Ciraci, Phys. Rev. Lett. **87**, 116802 (2001).

[3] C. Kilic, S. Ciraci, O. Gulseren, and T. Yildirim, Phys. Rev. **B 62**, R16345 (2000).

Serving the Scientific and Technological Communities

The role of the NCNR as a national user facility has expanded significantly over the past few years, as the last of the instruments envisioned in the original cold neutron project have become operational. The Disk-Chopper Spectrometer, the Filter-Analyzer Neutron Spectrometer, the High Flux Backscattering Spectrometer, and the Neutron Spin-Echo spectrometer now permit U.S. scientists to carry out neutron spectroscopy with greatly improved resolution and sensitivity. The thermal perfect-crystal small angle neutron scattering instrument (USANS) has expanded the length scale available by this technique to 10^4 nm. User experiments show a steadily increasing diversification in subject area and technique, enabled by the new instruments. We anticipate that the trend will continue over the next few proposal cycles.

User participation over the past 15 years shows continuing growth (see Fig. 1). The NCNR currently accommodates more than half of all neutron users in the United States. While the Spallation Neutron Source is being built at Oak Ridge, the NCNR continues to be the nation's premier facility for providing neutrons to the U.S. research community.

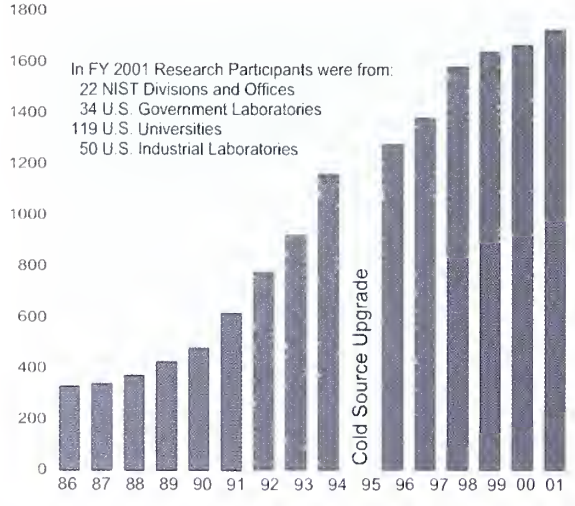

Fig. 1. Research Participants at the NCNR.

The NCNR User Program

Researchers may obtain use of NCNR neutron beam instruments in several ways, the most direct being through the formal proposal system. Approximately twice a year, a Call for Proposals is issued. After a thorough review process by external referees and by the NCNR Program Advisory Committee (PAC), approved proposals are allocated beam time. The PAC is a panel of distinguished scientists with expertise across a broad range of neutron methods and scientific disciplines. It is the body primarily responsible for proposal review and recommending user policies for the NCNR, working closely with the Center's Director and staff. Its current membership includes Sanat Kumar (Penn State University, chair), Robert Briber (University of Maryland), Michael Crawford (DuPont), Dieter Schneider (Brookhaven National Laboratory), Kenneth Herwig (Oak Ridge National Laboratory), Yumi Ijiri (Oberlin College), Michael Kent (Sandia National Laboratories, John Tranquada (Brookhaven National Laboratory), and Andrew Allen (NIST).

At the recent PAC meeting in January 2001, the PAC considered 121 proposals for SANS and reflectometry, in addition to 49 for inelastic neutron scattering. Although we expect that both categories will see increased user demand in future proposal rounds, the latter area is likely to see more growth, since the new inelastic scattering spectrometers have added capabilities previously unavailable at US neutron facilities.

The Center for High Resolution Neutron Scattering

Several NCNR instruments are supported by the National Science Foundation (NSF) through the Center for High Resolution Neutron Scattering (CHRNS), a very important component of the user program. Until the present, CHRNS instruments included a 30 m SANS machine, the SPINS triple-axis spectrometer, and USANS. Approximately 40 % of the instrument time allocated by the PAC went to experiments carried out on CHRNS instruments. During the past year, the NSF

approved a proposal to provide support for a substantial enlargement of CHRNS, enabling us to offer more beam time to users on the three new high-resolution inelastic scattering instruments. In the near future, another SANS diffractometer, the 8 m machine on neutron guide NG-1, which is presently used primarily for NIST programmatic research, will be upgraded to a more powerful 9 m instrument with a new detector, and made available to users through CHRNS. The expanded suite of CHRNS instruments will provide enhanced technical support and accessibility to the user community.

Summer School on Methods and Applications of Neutron Spectroscopy

The NCNR's seventh annual Summer School on neutron scattering, held on June 18-22, 2001, focused on high-resolution neutron spectroscopy. Most of the 32 participants were graduate and postdoctoral students; we also had an undergraduate student and a professor.

In a radical departure from the format of previous NCNR summer schools, plenary lectures were presented on the first morning only. After lunch the students were divided into four groups of eight, and each group performed an experiment using a different instrument (in one case a pair of instruments). Students learned the scientific motivation for the experiment, how the instrument works, and how to set up measurements. The instruments collected data overnight and on the following morning the data were analyzed. After lunch on each of the second, third and fourth days the groups rotated to new experiments. After lunch on the final day, eight of the students gave short presentations describing an experiment.

Students used the following instruments: the Spin Polarized Inelastic Neutron Spectrometer, the Disk Chopper Spectrometer, the High-Flux Backscattering Spectrometer, the Neutron Spin Echo spectrometer, and the Filter Analyzer Neutron Spectrometer. Together these instruments probe motions in materials over six decades in time (from approximately 10^{-7} s to 10^{-13} s) and two orders of magnitude in distance (0.1 nm to 10 nm). Test

Fig. 2. Seventh annual Summer School on Neutron Scattering participants analyze results with NCNR's Seung-Hun Lee (bottom left).

samples included a geometrically frustrated antiferromagnet, a transition metal compound with organic ligands, a "symmetric top" molecule, and a system of spherical micelles. The experiments illustrated coherent scattering, incoherent scattering, magnetic scattering, and tunneling. In evaluating the school more than 80 % of the participants described it as "excellent", and generally high ratings were received in all areas. The lectures and experiment handouts have been placed on the Web (www.ncnr.nist.gov/programs/spectroscopy/SS01/SS01_materials.html.) A short report about the summer school will appear in "Neutron News". As in the past, the summer school was jointly sponsored with the National Science Foundation, which provided financial assistance to many of the university participants.

Collaborations

Direct collaborations on specific experiments remain a common way for users to pursue their ideas using NCNR facilities, accounting for approximately half of the number of instrument-days. The thermal-neutron triple-axis spectrometers are mainly scheduled in this way. Most of the time reserved for NIST on these and all other NCNR instruments is devoted to experiments that are collaborations with non-NIST users. Collaborative research involving external users and NIST scientists

often produces results that could be not obtained otherwise.

Another mode of access to the NCNR is through Participating Research Teams (PRTs). In this case, groups of researchers from various institutions join forces to build and operate an instrument. Typically, 50 % to 75 % of the time on the instrument is then reserved for the PRT, and the remaining time is allocated to general user proposals. For example, a PRT involving ExxonMobil, the University of Minnesota, and NIST cooperates on the NG-7 30 m SANS instrument. Similar arrangements involving other PRTs apply for the horizontal-sample reflectometer, the high-resolution powder diffractometer, the filter-analyzer spectrometer, and the neutron spin-echo spectrometer.

Independent Programs

There are a number of programs of long standing located at the NCNR that involve other parts of NIST, universities, industrial laboratories, or other government agencies.

The **Polymers Division** of the Materials Science and Engineering Laboratory has two major program elements at the NCNR. In the first, the purpose is to help the U.S. microelectronics industry in addressing their most pressing materials measurement and standards issues. In today's integrated circuits and packages the feature size on a chip is ever shrinking, approaching 250 nm, while the size of a polymer molecule is typically 5 nm to 10 nm. As feature size shrinks, the structure and properties of interfaces play an increasingly important role in controlling the properties of the polymer layers used in interconnects and packages. NIST scientists use both neutron reflectivity and other neutron scattering methods to characterize polymer/metal interfaces with regard to local chain mobility, moisture absorption, glass transition temperature and crystalline structure.

In the second program element, the objective is to understand underlying principles of phase behavior and phase separation kinetics of polymer blends, both in the bulk and on surfaces, in order to help control morphology and structure during processing. SANS and reflectivity measurements in equilibrium, in transient conditions, and under external fields, provide essential information for general understanding as well as for specific application of polymer blend/alloy systems. Customers include material producers and users, ranging from chemical, rubber, tire, and automotive companies, to small molding and compounding companies. The focus of research on polymeric materials includes commodity, engineering and specialty plastic resins, elastomers, coatings, adhesives, films, foams, and fibers.

The **ExxonMobil Research and Engineering Company** is a member of the Participating Research Team (PRT) that operates, maintains, and conducts research at the NG-7 30 m SANS instrument and the recently commissioned NG-5 Neutron Spin Echo Spectrometer. The mission is to use those instruments, as well as other neutron scattering techniques, in activities that complement research at ExxonMobil's main laboratories as well as at laboratories of its affiliates around the world. The aim of these activities is to deepen understanding of the nature of ExxonMobil's products and processes, so as to improve customer service and to improve the return on shareholders' investment. Accordingly, and taking full advantage of the unique properties of neutrons, most of the experiments use SANS or other neutron techniques to study the structure and dynamics of hydrocarbon materials, especially in the fields of polymers, complex fluids, and petroleum mixtures. ExxonMobil regards its participation in the NCNR and collaborations with NIST and other PRT members not only as an excellent investment for the company, but also as a good way to contribute to the scientific health of the Nation.

The **Nuclear Methods Group** (Analytical Chemistry Division, Chemical Science and Technology Laboratory) has as its principal goals the development and application of nuclear analytical techniques for the determination of

elemental compositions with greater accuracy, higher sensitivity and better selectivity. A high level of competence has been developed in both instrumental and radiochemical neutron activation analysis (INAA and RNAA). In addition, the group has pioneered the use of cold neutron beams as analytical probes with both prompt gamma activation analysis (PGAA) and neutron depth profiling (NDP). PGAA measures the total amount of a particular analyte present throughout a sample by the analysis of the prompt gamma-rays emitted during neutron capture. NDP, on the other hand, determines concentrations of several important elements (isotopes) as a function of depth within the first few micrometers of a surface by energy analysis of the prompt charged-particles emitted during neutron bombardment. These techniques (INAA, RNAA, PGAA, and NDP) provide a powerful combination of complementary tools to address a wide variety of analytical problems of great importance in science and technology, and are used to help certify a large number of NIST Standard Reference Materials.

During the past several years, a large part of the Group's efforts has been directed towards the exploitation of the analytical applications of the guided cold-neutron beams available at the NIST Center for Neutron Research. The Group's involvement has been to design and construct state-of-the-art cold neutron instruments for both PGAA and NDP and provide facilities and measurements for outside users, while retaining and utilizing our existing expertise in INAA and RNAA.

The **Center for Food Safety and Applied Nutrition**, U.S. Food and Drug Administration (FDA), directs and maintains a neutron activation analysis (NAA) facility at the NCNR. This facility provides agency-wide analytical support for special investigations and applications research, complementing other analytical techniques used at FDA with instrumental, neutron-capture prompt-gamma, and radiochemical NAA procedures, radioisotope x-ray fluorescence spectrometry (RXRFS), and low-level gamma-ray detection. This combination of analytical techniques enables diverse multi-element and radiological information to be obtained for foods and related materials. The NAA facility supports agency quality assurance programs by developing in-house reference materials, by characterizing food-related reference materials with NIST and other agencies, and by verifying analyses for FDA's Total Diet Study Program. Other studies include the development of RXRFS methods for screening foodware for the presence of Pb, Cd and other potentially toxic elements, use of instrumental NAA to investigate bromate residues in bread products, and use of prompt-gamma NAA to investigate boron nutrition and its relation to bone strength.

The **Neutron Interactions and Dosimetry Group** (Physics Laboratory) provides measurement services, standards, and fundamental research in support of NIST's mission as it relates to neutron technology and neutron physics. The national and industrial interests served include scientific instrument calibration, electric power production, radiation protection, defense nuclear energy systems, radiation therapy, neutron radiography, and magnetic resonance imaging.

The Group's activities may be represented as three major activities. The first is Fundamental Neutron Physics including magnetic trapping of ultracold neutrons, operation of a neutron interferometry and optics facility, development of neutron spin filters based on laser polarization of ^{3}He, measurement of the beta decay lifetime of the neutron, and investigations of other coupling constants and symmetries of the weak interaction. This project involves a large number of collaborators from universities and national laboratories.

The second is Standard Neutron Fields and Applications utilizing both thermal and fast neutron fields for materials dosimetry in nuclear reactor applications and for personnel dosimetry in radiation protection. These neutron fields include thermal neutron beams, "white" and monochromatic cold neutron beams, a thermal-neutron-induced ^{235}U fission neutron field, and ^{252}Cf fission neutron fields, both moderated and unmoderated.

The third is Neutron Cross Section Standards including experimental advancement of the accuracy of neutron cross section standards, as well as evaluation, compilation and dissemination of these standards.

Several universities have also established long term programs at the NCNR. The **University of Maryland** is heavily involved in the use of the NCNR, and maintains several researchers at the facility. **Johns Hopkins University** participates in research programs in solid-state physics and in instrument development at the NCNR. The **University of Pennsylvania** is working to help develop biological applications of neutron scattering. It is also participating in the second stage construction of the filter analyzer neutron spectrometer, along with the **University of California at Santa Barbara, DuPont, Hughes,** and **Allied Signal.** The **University of Minnesota** participates in two PRTs, the NG-7 30 m SANS and the NG-7 reflectometer. The **University of Massachusetts** also participates in the latter PRT.

Reactor Operation and Engineering

The reactor operated for 240 full power (20 MW) days during the past year, or 100 % of the scheduled time. Routinely, the reactor is scheduled to operate a seven week cycle, seven times a year. Each operating cycle includes 38 days on-line and 11 days shutdown for refueling, routine maintenance, and surveillance tests. (Figure 1 shows the reactor operations staff adjusting the reactor power regulatory rod). This year four days in March were required for maintenance on the Thermal Column Cooling System. The reactor was shutdown on August 26, 2001 for a planned maintenance period of three months. During this time the cold source will be replaced, building transformers and switchgear will be replaced to provide additional electrical capacity, and the new cooling tower will undergo final hookup and testing. (Figure 2 shows the new cooling tower in the final stages of construction. For comparison the old cooling tower is seen on the left).

Analysis has been completed to verify that the thermal-hydraulic characteristics of the NBSR, as was predicted using correlations and simple models available when the licensed power level was raised to 20 MW, are conservative relative to results obtained using newer correlations that better represent research reactor characteristics. Calculations show that the heat transfer coefficient, onset of flow instability, and critical heat flux are all conservative. In addition, the NBSR also has an adequate margin before the onset of nuclear boiling.

The above results are for extreme yet still conceivable conditions of operation. The Energy Sciences and Technology Department at the Brookhaven National Laboratory has been tasked to perform transient analysis with state-of-the art methods. Monte Carlo neutronics calculations will be used to accurately predict parameters that are used in the transient analysis.

Work is also continuing in the preparation of an updated license renewal submittal to the NRC. In conjunction with this effort, an in-service inspection of reactor internals and ultrasonic testing of the primary cooling system are planned for the summer/fall shutdown.

Fig. 1. Bill Mueller and Greg Heller of the reactor operations staff adjust the reactor power regulatory rod.

Fig. 2. The new plume-abated cooling tower (right) nears completion. It will replace the lower capacity and less efficient system that had no abatement ability (left).

Instrumentation Developments

The Advanced Cold Neutron Source

After 6 years of safe and reliable operation, the liquid hydrogen cold source cryostat at the NIST reactor is being replaced with a new advanced design. Based on extensive operating experience and sophisticated Monte Carlo calculations of the cold source and NIST reactor core, the new design improves the neutron coupling between the reactor fuel and moderator and the cold source cryostat. The advanced source, (called Unit 2), will differ from the original in many key respects, as can be seen in Fig. 1. The most important change is the addition of 60 liters of D_2O, partially surrounding the moderator chamber, reducing the moderator void volume and increasing the thermal neutron flux in the cryostat region by about 40 %.

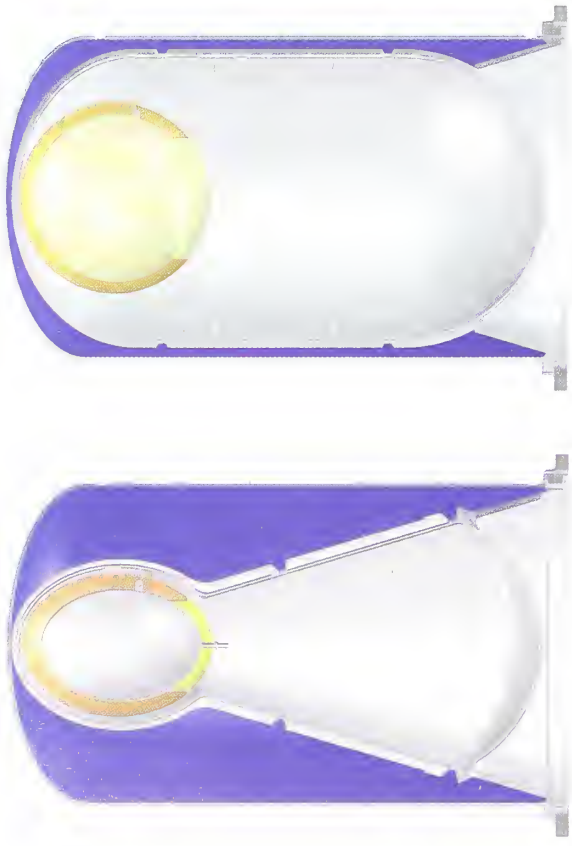

Fig. 1. Comparison between the original (top) and new designs for the liquid hydrogen cold source cryostat at NIST. Heavy water volume is indicated in blue, liquid hydrogen in orange, and hydrogen vapor in yellow.

The new cryostat is shaped like an ellipsoidal shell, rather than a spherical one. This results in a smaller volume so that more D_2O can be introduced in the cryostat assembly. The center of the inner ellipsoid is offset, so the liquid hydrogen shell is 30 mm thick near the reactor core. This change results in an additional 50 % increase in flux. Finally, in contrast to the original design, the inner ellipsoid will be evacuated through a small port, removing most of the hydrogen vapor. This change will add another 15 % to 20 % gain. Based on these changes, users can expect an overall intensity

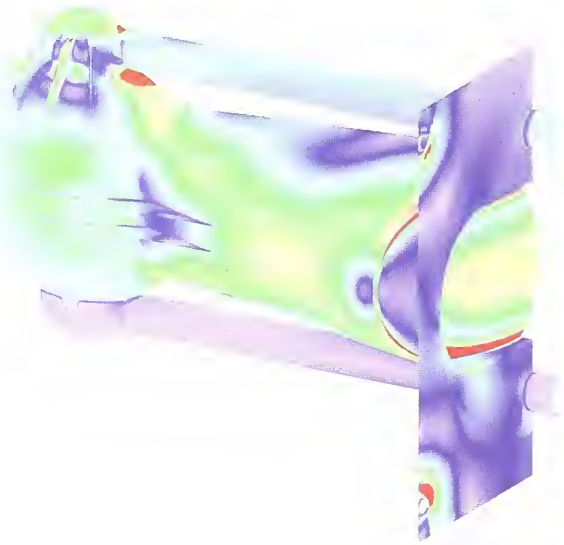

Fig. 2. False color representation of stresses from finite element calculations of the helium containment jacket with an internal pressure of 82 atmospheres.

increase of 50 % to 80 % between 2 Å and 20 Å with this design.

The complex geometry of the advanced source posed many engineering challenges. The moderator chamber is surrounded by a vacuum vessel, which is surrounded by a helium containment vessel, strong enough to withstand the design basis accidental detonation of liquid hydrogen and solid oxygen. These vessels determine the extent of the D_2O volume, so they were designed to partially surround the moderator chamber, allowing an opening just large enough to fully illuminate the neutron guides.

This "hour-glass" shape created regions of very high mechanical stress, analyzed and ultimately mitigated with the aid of finite element analysis (see Fig. 2). During the three month period beginning at the end of August 2001, we are removing the old cryostat and installing Unit 2.

Development of an Air-pad and Floor System for New Neutron Spectrometers

The NCNR is currently developing several new neutron triple axis spectrometers with a key design feature that allows interchangeability of the back-end detector/analyzer systems. Exchanging the back-end system on these instruments requires a universal connection and positioning system between it and the sample position of the instrument. This interface must be capable of achieving an angular accuracy of 0.1 degrees, an angular precision of 0.01 degrees and a vertical positional accuracy of less than a millimeter.

The design approach adopted uses a commercial air-pad system with a precision-leveled floor. After considering several different types of floors we chose to use epoxy as our sub-floor with precision cut and anodized aluminum plates as our contact surface. Epoxy will self-level, fill in holes, and mask over any imperfections in the concrete floor and results in a highly smooth and level surface to build on. The epoxy is also low cost, relatively easy to use, and provides great flexibility for repair or maintenance. The aluminum plates provide protection to the epoxy from cryogenic spills, increased wear resistance, and an easily removable/reusable floor.

Fig. 3. Michael Murbach and Colin Wrenn conduct tests on the prototype floor system for a triple axis spectrometer.

We have developed and tested a prototype single air-pad system that has successfully demonstrated the construction techniques for the floor system and the ability of the air pad positioning system to meet the accuracy and repeatability requirements for a 1 ton test load. Currently, a three-pad prototype system is under development which will allow us to test control system concepts needed in a final design.

Development of an Intercalated Graphite Monochromator

As part of an ongoing collaboration between NIST and Harvard University to measure the neutron lifetime using magnetically trapped ultracold neutrons (UCNs), a new monochromator has been developed. In the lifetime experiment, ultracold neutrons (UCN: neutrons with energies $\approx$ 100 neV) are produced in a superfluid ^{4}He bath inside the trapping apparatus using the "superthermal process." A beam of cold neutrons is introduced into the helium, in which neutrons with wavelength near 0.89 nm scatter to UCN energies by creation of a single phonon. Only neutrons within a narrow wavelength band ($\pm$ 0.01 nm for our current magnetic trap) participate in this single-phonon production mechanism. Since the wavelength band for UCN production occupies only a small fraction of the neutron spectrum produced by the cold source (see Fig. 4), a significant signal-to-background improvement is possible with appropriate wavelength filtering of neutrons that enter the apparatus. Bragg reflection from a crystalline monochromator with a lattice spacing, d, can be used to select a narrow wavelength band for neutrons with wavelengths up to $2d$. Unfortunately, widely used materials for neutron monochromatization, such as pyrolytic graphite, have insufficiently large d-spacings for reflecting 0.89 nm neutrons. One attractive class of materials for producing long wavelength monochromators is the intercalated graphites. Intercalation is the

process of inserting foreign atoms or molecules between the layers of the graphite, and results in a crystal with a larger d spacing Intercalated graphites are formed in "stages", where the stage number defines the number of planes of graphite between layers of intercalant atoms.

We have designed, fabricated, and tested a new 0.89 nm monochromator using stage-2 potassium-intercalated graphite. Nine pieces of intercalated graphite

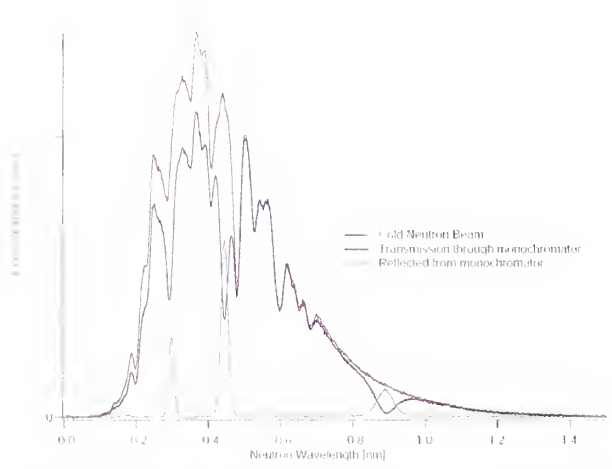

Fig. 4. Neutron wavelength spectra were measured using a time-of-flight technique. Only 1% of the neutrons emerging from guide NG-6 (red) lie within the wavelength band (between the orange vertical bars) available for production of UCN. The spectra of neutrons transmitted (blue) and reflected (green) by the monochromator are also shown.

are tiled to form the monochromator, which has a total size of 6 cm x 15 cm. Each tile is produced by heating potassium and graphite to two different temperatures in an evacuated glass cell. Performance of the assembled monochromator was determined using time-of-flight techniques (see Fig. 4). The monochromator reflects more than 80 % of the neutrons incident upon it in the wavelength band relevant for UCN production. However, only 3 % of all incident neutrons are reflected. When combined with additional techniques that filter out neutrons from higher order Bragg reflections, the monochromator results in an improvement of the ratio of useful to total neutrons of almost two orders of magnitude while sacrificing few trapped neutrons. During the summer of 2001, this new monochromator was used in conjunction with the trapping apparatus in a temporary setup. Presently, we are permanently installing the monochromator at the fundamental physics station at NG-6. This installation will place the monochromator much closer to the end of the neutron guide and will result in an increase by an additional factor of 2 in the number of trapped UCNs.

NCNR Computer and Software Environment

The NCNR's computerized data acquisition and reduction environment encompasses all stages of research: experiment preparation, data collection and analysis of results. NCNR provides site-specific tools that augment the tools in researchers' own scientific arsenal. Some specific areas of recent activity are described below:

- NCNR is providing simulation tools that model the behavior of our instruments, to evaluate the feasibility of proposed experiments. They can be used by prospective users, especially those who aren't already familiar with neutron scattering experiments, to explore 'what-if' scenarios with different sample and instrument configurations. Currently, we have simulations of small angle scattering experiments, with reflectivity and stress measurement simulations being developed.
- Researchers who plan to use NCNR instrumentation must submit their proposals for review. We have created a web-based proposal submission system that tracks user proposals from submission to review and ranking, to the final instrument time allocation.
- All instruments available at NCNR are computer-controlled. The control software running on these computers must satisfy two seemingly contradictory needs: simplicity, for straightforward use, and sophistication, for power uses. New, more complex instruments, such as the spin echo spectrometer, require carefully designed graphical user interfaces (GUIs) that hide unnecessary detail, while still providing access to all functions, if needed. Since the NCNR instruments run around the clock, the data acquisition functions must be capable of automation and unattended operation. To this end, the experiment control software is scriptable, in

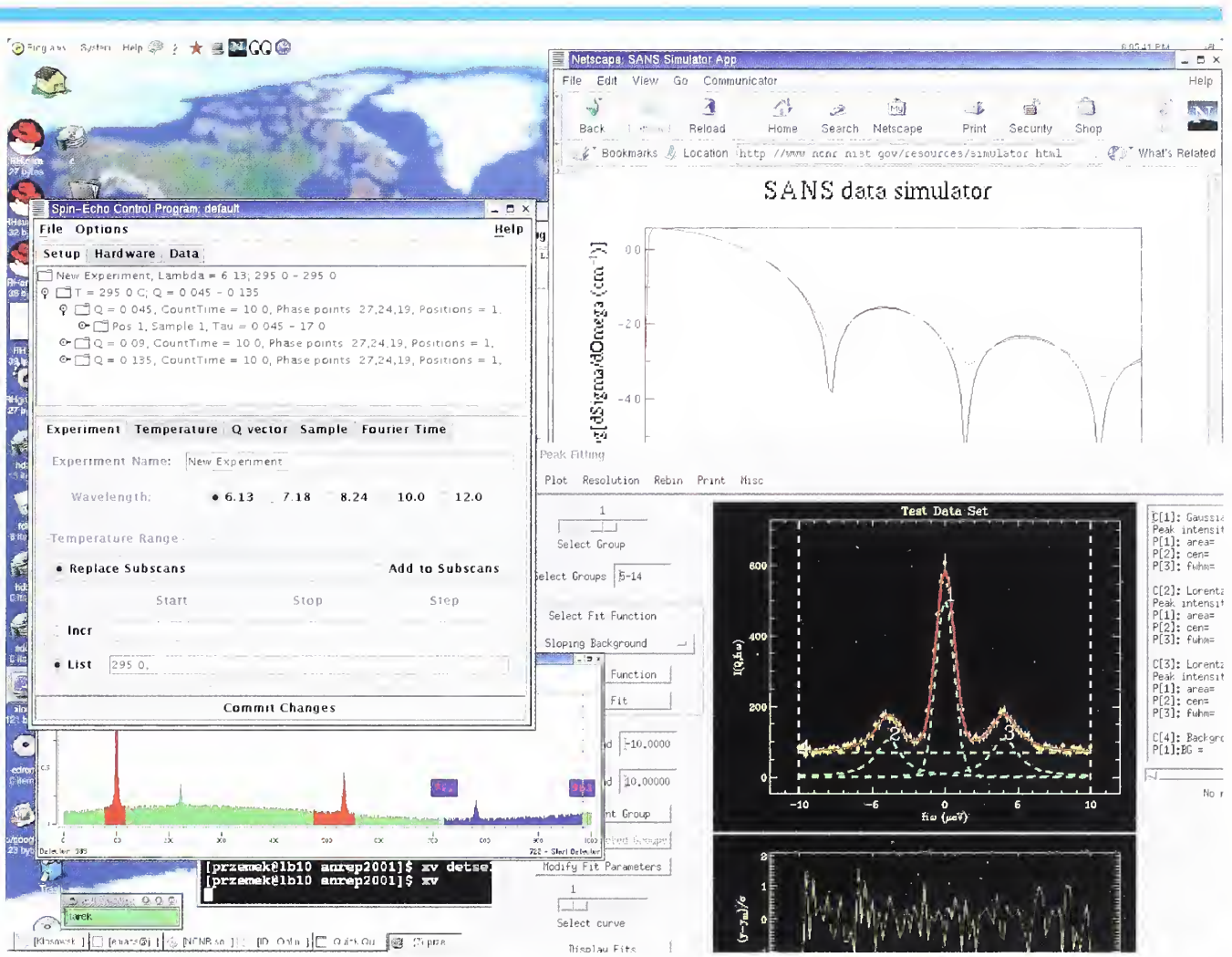

Fig. 5. A screenshot of several NCNR applications. Clockwise from top left corner: the web-based simulator of a SANS experiment, peak analysis application, Time-of-flight detector selection, and a Neutron Spin Echo instrument control panel.

addition to the GUI interface. The scriptable, command-based interface fulfills "power-user" needs, while a simplified GUI interface tends to be easier to learn and use.

- Rapid post-acquisition data reduction is important to guide the ongoing experiments, and, later, to aid in the processing of data to obtain the scientific results. Many data reduction procedures are common to all the instruments. The Data Visualization and Analysis Environment (DAVE) is a set of tools commonly used by NCNR scientific community; these tools include programs to manipulate and compare data, extract parameters of theoretical models by data fitting, etc.
- NCNR maintains a sophisticated computer infrastructure including a modern network installation, and an ensemble of nearly 400 computers and other IT equipment, for scientific and office computing, ranging from email servers to supercomputer-style parallel computing clusters.
- NCNR participates in inter-laboratory collaborations developing software for specialized domains.

Perhaps the best known of these is the GSAS software for crystallographic data reduction. Another ongoing NCNR collaboration is in international scattering data exchange format, NeXuS.

Sample Environment Team

The sample environment team expanded by two new members this year, bringing the total number to four employees that are actively working to ensure that the needs of researchers working at the NCNR are met. This team works to improve the infrastructure sample environment equipment and to support neutrons scattering instruments at the NCNR. A principal objective is to provide safe and easy to use equipment to the research staff. Equipment development activities are done in collaboration with the engineering and technical staff, with input from both staff and guest scientists. As an example, a new superconducting magnet/dilution refrigerator system needed modifications for use on the Disk Chopper Spectrometer (DCS) for an experiment. The impracticality of separating the cryostat from its support pumps and electronics led to the decision to lift the entire system onto the instrument for use. A new adjustable lifting frame was design and manufactured to lift the various components of the magnet (see Figure 6).

Another experiment required the development of a system capable of going to temperatures as high as 675 K with a high voltage applied to the sample. The design goal was to be able to achieve a 5 kV potential difference across the sample. After continued development work, we were able to apply a potential difference of 8 kV to the sample while at the maximum temperature of 675 K. In addition to the human safety features designed in from the beginning, a circuit was developed which prevents the continued arcing that can occur if the sample breaks down during the course of the experiment.

Fig. 6. Superconducting magnet/dilution refrigerator as it is being lifted onto the DCS spectrometer. The adjustable lifting frame compensates for the lifting point shifting in case liquid cryogens are added.

Publications

Abdurashitov, J. N., Gavrin, V. N., Kalikhov, A. V., Matushko, V. L., Shikhin, A. A., Yants, V. E., Zaborskaia, O. S., Adams, J. M., Nico, J. S., Thompson, A. K., "A High Resolution Low Background Fast Neutron Spectrometer," in Proceedings of the International Workshop on Neutron Field Spectrometry in Science, Technology and Radiation Protection, (Pisa, Italy, June 2000), in press.

Adams, C. P., Lee, Y. S., Lee, Lee, S.-H., Lynn, J. W., "Triple-Axis Research at NIST," Neutron News **12**, 15 (2001).

Adams, C. P., Lynn, J. W., Mukovskii, Y. M., Arsenov, A. A., Shulyatev, D. A., "Charge Ordering and Polaron Formation in the Magnetoresistive Oxide $La_{0.7}Ca_{0.3}MnO_3$," Phys. Rev. Lett. **85** (18), 3954 (2000).

Adams, J. M., "Results From the NIST Round Robin Test of Fissionable Dosimeters in a Reactor Leakage Spectrum," *REACTOR DOSIMETRY, Radiation Metrology and Assessment*, edited by J. Williams, D. Vehar, F. Ruddy, D. Gilliam, (ASTM, West Conshohocken, PA, Feb. 2001).

Adams, J. M., Greenhouse, L. A., "Nuclear Science at the National Institute of Standards and Technology: A Historical Overview," in *Proceedings of Transactions of the American Nuclear Society, Winter Meeting, November 2000*, (Washington, DC), in press.

Agnew, S. R., Elliott, B. R., Youngdahl, C. J., Hemker, K. J., Weertman, J. R., "Structure and Mechanical Properties of Nanocrystalline Metals—With Opportunities for Modeling," 19th Risφ International Symposium on Materials Science, Risφ National Laboratory, Roskilde, Denmark, in press.

Akpalu, Y. A, Karim, A., Satija, S., Balsara, N. P., "Suppression of Lateral Phase Separation in Thin Polyolefin Blend Films," Macromol. **34** (6), 1720 (2001).

Allen, A. J., Ilavsky, J., Long, G. G., Wallace, J. S., Berndt, C. C., Herman, H., "Microstructural Characterization of Yttria-Stabilized Zirconia Plasma-Sprayed Deposits Using Multiple Small-Angle Neutron Scattering," Acta Mater. **49** (9), 1661 (2001).

Allen, A. J., Livingston, R. A., "The Effect of Fly Ash on the Microstructure of Portland Cement," in press.

Allen, A. J., Thomas, J. J., Jennings, H. M., "Small Angle Scattering Measurements of the C-S-H Gel Phase in Cements via Deuterated Exchange Experiments," Langmuir, in press.

Allman, B. E., McMahon, P. J., Nugent, K. A., Paganin, D., Jacobson, D. L., Arif, M., Werner, S. A., "Quantitative Phase Radiography with Neutrons," Nature, in press.

Amis, E. J., Fanconi, B. M., "Polymers Division Technical Activities-1999" NISTTR 6435.

Anderson, C. R., Andersen, K. H., Stirling, W. G., Sokol, P. E., Dimeo, R. M., "Dynamics of Superfluid ^{4}He Confined in Xerogel Glass," Phys. Rev. B, in press.

Anderson, D. L., Capar, S. G., "Identification of Lead in Metal Food Can Seams Using ^{57}Co RXRFS," J. Radioanal. Nucl. Chem., in press.

Anderson, D. L., Cunningham, W. C., Capar, S. G., Baratta, E. J., Mackill, P., "Nuclear Methods for Food Analysis at the U. S. Food and Drug Administration," J. Radioanal. Nucl. Chem., in press.

Bao, W., Aeppli, G., Lynn, J. W., Pagliuso, P. G., Sarrao, J. L., Hundley, M. F., Thompson, J. D., Fisk, Z., "Anisotropic Three-Dimensional Magnetic Fluctuations in Heavy Fermion $CeRhIn_5$," Phys. Rev. Lett., in press.

Bao, W., Christianson, A. D., Pagliuso, P. G., Sarrao, J. L., Thompson, J. D., Lacerda, A. H., Lynn, J. W., "Effect of La Doping on Magnetic Structure in Heavy Fermion $CeRhIn_5$," Physica B, in press.

Bao, W., Pagliuso, P. G., Sarrao, J. L., Thompson, J. D., Fisk, Z., Lynn, J. W., "Magnetic Structure of Heavy Fermion Ce_2RhIn_8," Phys. Rev. B **64** (2), 0401 (2001).

Bao, W., Pagliuso, P. G., Sarrao, J. L., Thompson, J. D., Fisk, Z., Lynn, J. W., Erwin, R. W., "Incommensurate Magnetic Structure of $CeRhIn_5$," Phys. Rev. B **6321** (21), 9901 (2001).

Barnes, K. A., Morrison, F. A., Nakatani, A. I., "The Effects of Steady Shear on the Order and Orientation of Diblock Copolymer Melt Using In-Situ Small-Angle Neutron Scattering," SPE ANTEC, in press.

Bateman, F. B., Boukharouba, N., Brient, C. E., Carlson, A. D., Grimes, S. M., Haight, R. C., Massey, T. N., Wasson, O. A., "New Measurements of the H(n,n)H Angular Distribution," *REACTOR DOSIMETRY, Radiation Metrology and Assessment*, edited by J. Williams, D. Vehar, F. Ruddy, D. Gilliam, (ASTM, West Conshocker, PA, Feb. 2001).

Bauer, B. J., Amis, E. J., "Characterization of Dendritically Branched Polymers by SANS, SAXS, and TEM," Tomalia/Frechet. Dendritic Polymers. 2000, in press.

Bauer, B. J., Lin, E. K., Lee, H. J., Wang, H., Wu, W. L., "Structure and Property Characterization of Low-k Dielectric Porous Thin Films," J. Electron. Mater **30** (4), 304 (2001).

Becker, P. R., Mackey, E. A., Demiralp, R., Epstein, M. S., Donais, M. K., Goessler, W. A., Porter, B. J., Wise, S. A., "Heavy Metals and Other Trace Elements Measured in Tissues of Marine Mammals Archived by the Alaska Marine Mammal Tissue Archival Project from the Bering Sea and Cook Inlet, Alaska," in *Proceedings of The AMAP Heavy Metals Workshop*, in press.

Becker, P. R., Pugh, P. R., Schantz, M. M., Mackey, E. A., Oflaz, R. D., Epstein, M. S., Donais, M. K., Porter, B. J., Wise, S. A., Mahoney, B. A., "Persistent Chlorinated Compounds and Elements in Tissues of Cook Inlet Beluga Whales, Delphinapterus leucas, Banked by the Alaska Marine Mammal Tissue Archival Project," NISTIR, in press.

Bellitto, C., DiMarco, M. G., Branford, W. R., Green, M. A., Neumann, D. A., "Cation Distribution in Ga-Doped $Li_{1.02}Mn_2O_4$," Solid State Ionics **140** (1), 77 (2001).

Benenson, R. E., Chen-Mayer, H. H., Lynn, J. W., "Search for Effects on Neutron Transmission Due to Multiple Reflection by Glass Capillary Walls," in *Proceedings of SPIE Annual Meeting*, **3767** (1999), in press.

Bianco-Peled, H., Dori, Y., Satija, S., Schneider, J., Sung, L., Tirrell, M., "Structural Study of Langmuir Monolayers Containing Lipidated Poly (Ethylene Glycol) and Peptides," Langmuir, in press.

Blackman, M. J., Badaljan, R. S., Kikodze, Z. K., Kohl, P. L., "Chemical Characterization of Caucasian Obsidian: Geological Sources," in *Synthese Sur l'Obsidienne au Proche-Orient: Du Volcan a l'Outil*, (BAR Publication, London), in press.

Blackman, M. J., Redford, S., "Northern Syrian Luster and Fruitware: Petrographic and Chemical Implications for Productions and Distribution," Antiquity, in press.

Bode, P., de Nadai Fernandes, E. A., Greenberg, R., "INAA as a Primary Method in Metrology for Chemical Measurements," in *Proceedings Metrolsul '99*, in press.

Borchers, J. A., Ijiri, Y., Lind, D. M., Ivanov, P. G., Erwin, R. W., Qasba, A., Lee, S.-H., O'Donovan, K. V., Dender, D. C., "Detection of Field-Dependent Antiferromagnetic Domains in Exchange-Biased Fe_3O_4/NiO Superlattices," Appl. Phys. Lett. **77** (25), 4187 (2000).

Bossev, D. P., Ferdinand, S., Paulaitis, M. E., "Effect of Pressure on Microstructure in Water-in-Oil and Oil–in-Water Microemulsions for $C_{12}E_5$ n-Octane/D_2O Mixtures," in press.

Bossev, D., Kline, S., Paulaitis, M. E., "Pressure-Induced Aggregation of $C_{12}E_5D_2O$ Wormlike Micelles," in press.

Bourdarot, F., Lynn, J. W., Baggio-Saitovitch, E., Huang, Q., Sanchez, D. R., Skanthakumar, S., "Magnetic Behavior of the Rare Earth Compounds RNiBC by Neutron Scattering," Phys. Rev. B **64**, 1044 (2001).

Brome, C. R., Butterworth, J. S., Dzhosyuk, S. N., Mattoni, C. E. H., McKinsey, D. N., Doyle, J. M., Huffman, P. R., Dewey, M. S., Wietfeldt, F. E., Golub, R., Lamoreaux, S. K., Coakley, K. J., "Magnetic Trapping of Ultracold Neutrons," Phys. Rev. C **6305** (5), 5502 (2001).

Bu, Z., Chowdhuri, Z., Callaway, D. J. E., "Coexistence of Fluctuating Secondary Structure and Long-Range Tertiary Interaction in Highly Denatured Alpha-Lactalbumin – A Neutron Scattering Study," Protein Sci., in press.

Bu, Z., Cook, J., Callaway, D. J. E., "Dynamics Regimes and Correlated Structural Dynamics in Native and Denatured Alpha-Lactalbumin," J. Mol. Biol., in press.

Bu, Z., Neumann, D. A., Lee, S.-H., Brown, C. M., Engleman, D. M., Han, C. C., "A View of Dynamical Changes in the Molten Globule-Native Folding Step by Quasielastic Neutron Scattering," J. Mol. Biol. **301**, 525 (2000).

Buckley, C. E., Birnbaum, H. K., "Characterization of the Charging Techniques Used to Introduce Hydrogen in Aluminum," Scripta Mat., in press.

Buckley, C. E., Birnbaum, H. K., Lin, J. S., Spooner, S., Bellmann, D., Staron, P., Udovic, T. J., Hollar, E., "Characterization of H Defects in the Aluminium-Hydrogen System Using Small-Angle Scattering Techniques," J. Appl. Crystallogr. **34**, 119 (2001).

Caliskan, G., Kisliuk, A., Tsai, A. M., Soles, C. L., Sokolov, A. P., "Protein Dynamics in Viscous Solvents," J. Biophys., in press.

Cappelletti, R. L., "The National Institute of Standards and Technology Center for Neutron Research (NCNR)," Neutron News, in press.

Cappelletti, R. L., Clutter, L. K., edited by, "NIST Center for Neutron Research Accomplishments and Opportunities, NCNR 2000," NIST SP 962.

Cappelletti, R. L., Clutter, L. K., edited by, "NIST Center for Neutron Research, Programs and Accomplishments," NISTIR 6598.

Cappelletti, R. L., Glinka, C. J., Krueger, S., Lindstrom, R. A., Lynn, J. W., Prask, H. J., Prince, E., Rush, J. J., Rowe, J. M., Satija, S. K., Toby, B. H., Tsai, A., Udovic, T. J., "Materials Research With Neutrons at NIST," J. Res. Natl. Inst. Stand. **106** (1), 187 (2001).

Carpenter, J. M., Iverson, E. B., Mildner, D. F. R., "Time Focusing of Pulsed-Neutron Source Crystal Analyzer Spectrometers," Nucl. Instrum. Meth. A, in press.

Cava, R. J., Yamaura, K., Loureiro, S., Huang, Q., Erwin, R. W., Lynn, J. W., Young, D., "Magnets, Mischief and Metals in Cobalt Analogs of the Superconducting Cuprates," Physica C **341**, 351 (2000).

Chen, W. C., Heuser, B. J., King, J. S., "SANS Investigation of Deuteride (Hydride) Precipitation and Decomposition Morphology in Single Crystal Pd," J. Appl. Crystallogr., in press.

Chen, Y.Y., Honda, Z., Zheludev, A., Broholm, C., Katsumata, K., Shapiro, S. M., "Field-Induced Three-and Two-Dimensional Freezing in a Quantum Spin Liquid," Phys. Rev. Lett. **86** (8), 1618 (2001).

Chen, Y. Y., Lodge, T. P., Bates, F. S., "Entropically Driven Phase Separation of Highly Branched Linear Polyolefin Blends," J. Polym. Sci. Pol. Phys. **22**, 2965 (2000).

Cheng, Y. T., Mildner, D. F. R., "A Sensitive High Resolution Neutron Imaging Detector," Nucl. Instrum. Meth. A, **454** (2), 452 (2000).

Cheng, Y. T., Mildner, D. F. R., Chen-Mayer, H. H., Sharov, V. A., Glinka, C., "An Imaging Plate Detector for Small-Angle Neutron Scattering," J. Appl. Crystallogr. **33**, 1253 (2000).

Chen-Mayer, H. H., Lamaze, G. P., Satija, S. K., "Characterization of BPSG Films Using Neutron Depth Profiling and Neutron/X-ray Reflectometry," in *2000 International Conference on Characterization and Metrology for the ULSI Technology*, edited by D. G. Seiler, A. C. Diebold, W. M. Bullies, T. J. Shaffner, R. McDonald, E. J. Walters (AIP Press, Woodbury, NY), **550**, 407 (2001).

Choi, S. M., Lynn, J. W., Lopez, D., Gammel, P. L., Varma, C. M., "Direct Observation of Spontaneous Weak-Ferromagnetism in the Superconductor $ErNi_2B_2C$," Phys. Rev. Lett. **87**, 107001 (2001).

Christianson, R. J., Leheny, R. L., Birgeneau, R. J., Erwin, R. W., "Critical Dynamics of a Spin-5/2 Two-Dimensional Isotropic Antiferromagnet," Phys. Rev. B **6314** (14), 0401 (2001).

Coakley, K. J., Chen-Mayer, H. H., Lamaze, G. P., Simons, D. S., and Thompson, P. E., "Calibration of a Stopping Power Model for Silicon Based on Analysis of Neutron Depth Profiling and Secondary Ion Mass Spectrometry Measurements," J. Nucl. Instrum. & Meth. B, in press.

Cohen, R. E., Gulseren, O., "Thermal Equation of State of Tantalum," Phys. Rev. B. **63**, 224101 (2001).

Copley, J. R. D., "NIST Recommended Practice Guide: The Fundamentals of Neutron Powder Diffraction," NIST SP 960-2, in press.

DeWall, J., Dimeo, R. M., Sokol, P. E., "Diffusion and Phase Transitions of Molecular Hydrogen in Zeolites," Phys. Rev. B, in press.

Dimeo, R. M., Chowdhuri, Z., Meyer, A., Gehring, P. M., Neumann, D. A., "The NIST High Flux Backscattering Spectrometer," Appl. Phys. A, in press.

Dimeo, R. M., Neumann, D. A., "Low Temperature Dynamics of Confined Methyl Iodide," Phys. Rev. B. **63** (1), 4301 (2001).

Dimeo, R. M., Neumann, D. A., "The Effects of Confinement on Rotational Tunneling," Appl. Phys. A, in press.

Douglas, J. F., Kent, M. S., Satija, S. K., Karim, A., "Swelling of Grafted Polymer 'Brushes,'" in *Proceedings Encyclopedia of Materials: Science and Technology*, in press.

Downing, R. G., Iyengar, G. V., "Methodological Issues in the Analytical Determination of Boron," Environ. Health Perspect., in press.

Dubsky, J., Prask, H. J., Matejicek, J., Gnäupel-Herold, T., "Stresses in Plasma Sprayed Cr_2O_3 Coatings Measured by Neutron Diffraction," in *Proceedings of the International Conference on Neutron Scattering*, (Munich, Germany, Sept. 2001) in press.

Fid, K., Portner, D., Borchers, J. A., Loloee, R., Tsoi, M., O'Donovan, K. V., Pratt, W. P., Bass, J., "Mean-Free Path Effects in CPP Magnetoresistance of Magnetic Multilayers," Phys. Rev. B, in press.

Elliot, J., Meuse, V., Silin, V., Krueger, S., Woodward, J. T., Petralli-Mallow, T. P., Plant, A. L., "Biomedical Membranes on Metal Supports: Opportunities and Challenges," *in Biomolecular Films: Design, Function, and Application*, edited by J. Rusling (New York, Marcel Dekker, Inc.), in press.

En, Z., Brenizer, J. S., Hostica, B., Becker, D. A., "Nitrogen Distribution Measurements by Neutron Induced Autoradiography," J. Radioanal Nucl. Chem., in press.

Evmenenko, G., Bauer, B. J., Kleppinger, R., Forier, B., Dehaven, W., Amis, E. J., Miscehnko, N., Reynaers, H., "The Influence of Molecular Architecture and Solvent Type on the Size of Structure of Poly (Benzyl Ether) Dendrimers by SANS," Chem. Phys. **202** (6), 891 (2001).

Farrow, R. F. C., Marks, R. F., Toney, M. F., Hannibal, K., David, S., Kellock, A., Borchers, J. A., O'Donovan, K. V., Smith, D. J., "Spontaneous Chemical Ordering and Exchange Bias in Epitaxial $Mn_{0.52}Pd_{0.48}$/Fe (001) Bilayers Prepared at Room Temperature," Appl. Phys. Lett., in press.

Feeney, M., Brown, C. M., Tsai, A., Neumann, D. A., Debenedetti, P. G., "Incoherent Quasi-Elastic Neutron Scattering From Fructose-Water Solutions," J. Phys. Chem., in press.

FitzGerald, S. A., Thomas, J. J., Neumann, D. A., Livingston, R. A., "A Neutron Scattering Study of the Role of Diffusion in the Hydration of Tricalcium Silicate," Cement and Concrete Res., in press.

Freeman, K. S., Beck Tan, N. C., Trevino, S. F., Kline, S., McGown, L. B., Kiserow, D. J., "Size and Polydispersity Determinations of AOT/Bile Salt Reversed Micelles Obtained by Small-Angle Neutron Scattering," Langmuir **17** (13), 3912 (2001).

Gehring, P.M., Park, S.-E., Shirane, G., "Dynamical Effects of the Nanometer-Sized Polarized Domains in $Pb(Zn_{1/3}Nb_{2/3})O_3$," Phys. Rev. B **63** (22), 4109 (2001).

Gentile, T. R., Jones, G. L., Thompson, A. K., Rizi, R. R., Dimitrov, I. E., Roberts, D., Gefter, W., Schnall, M. D., Leigh, J. S., "A Compact Compressor for Application of Metastability-Exchange Optical Pumping of ^{3}He to Human Lung Imaging," Magn. Reson. Med., in press.

Gentile, T. R., Rich, D. R., Thompson, A. K., Bailey, C., Gericke, M., Hussey, D., Neff, B., Snow, W. M., Jones, G.L., Wildman, E., "The NIST-Indiana-Hamilton Polarized ^{3}He Spin Filter Program," in *Proceedings of the Fundamental Physics with Pulsed Neutron Beams Conference*, TUNL, Durham, NC, June 1-2, 2000, (World Scientific Inc.), in press.

Geissler, E., Hecht, A. M., "Treatment of Incoherent Signal Subtraction" Frontiers in SAXS and SANS, ESRF-ILL-CEA Workshop (Grenoble, France, February 12-13, 1999), in press.

Geissler, E., Horkay, F., Hecht, A. M., Deschamps, P., "Neutron Scattering From Elastomer Gels," Kautschuk, Gummi, and Kunstoffe, in press.

Geissler, E., Horkay, F., McKenna, G. B., Deschamp, P., "Osmotic and Mechanical Observations of Swollen Polyisoprene Rubber and its Microscopic Structure," Worldwide Amazon Rubber Conference (Manus, Brazil, October 31 - November 4, 1999), in press.

Gibbons, M. R., Richards, W. J., Shields, K., Paul, R. L., Lindstrom, R. M., "Correction of Scattering and Beam Hardening in Thermal Neutron Topography for Quantitative Detection of Hydrogen," IEEE Trans. Nucl. Sci., in press.

Gibson, W. M., Chen-Mayer, H. H., Mildner, D. F. R., Prask, H. J., Schultz, A. J., Youngman, R., Gnäupel-Herold, T., Miller, M. E., Vitt, R., "Polycapillary Optics Based Neutron Focusing for Small Sample Neutron Crystallography," in *Proceedings of the SPIE Optical Science and Technology* (San Diego, 2001), in press.

Giebultowicz, T. M., Kepa, H., Blinowski, J., Kacman, P., "Neutron Scattering Studies of Interlayer Correlations in Magnetic Semiconductor Superlattices," Physics E, in press.

Gilliam, D. M., "NIST Neutron Physics and Dosimetry," in *Proceedings Transactions of the American Nuclear Society/European Nuclear Society Winter Meeting*, November 12-16, 2000, (Washington, DC.), in press

Glinka, C. J., "Review of 'Methods of X-Ray and Neutron Scattering in Polymer Science,' by Ryong-Joon Roe," *Physics Today Magazine* **60**, 2001

Gnäupel-Herold, T., "Single Crystal Elastic Constants from Powder Measurements," in *Proceedings of Accuracy in Powder Diffraction III* (NIST Special Publication), in press.

Gnäupel-Herold, T., Haeffner, D. R., Prask, H. J., Matejicek, J., "Stress Determination by Whole Pattern Analysis-Application to Synchrotron HEXRD Measurements on Thermal Sprayed Coatings," in *Proceedings of the The Sixth International Conference on Residual Stresses*, (IOM, London, 2000), p. 751.

Gnäupel-Herold, T., Matejicek, J., Prask, H. J., "Mechanical Properties of Plasma Sprayed Coatings – Measured by Diffraction," in 9th International Metallurgical Conference Metal 2000, in press.

Gnäupel-Herold, T., Prask, H., Fisher, J., Cheng, X., "Residual Stress Modification by Means of Ultrasonic Impact Treatment," in *Proceedings of the Annual Conference of Society for Experimental Mechanics* (Portland, OR, June 2001), in press.

Gnäupel-Herold, T., Prask, H. J., Magiera, J., "Effect of Grinding Strategy on Accumulation of Damage in Rails: Neutron Diffraction Investigation of Residual Stresses in Transverse and Oblique Cut Rail Slices," in Proceedings of *The Sixth International Conference on Residual Stresses* (IOM, London, 2000), p. 879.

Green, M. A., Prassides, K., Stalick, J. K., Day, P., "The Crystal Structure of $SrSnO_3$," Inorg. Chem., in press

Green, M. A., Waldron, J. E. L., Neumann, D. A., "Charge and Spin Ordering in Monoclinic $Nb_{12}O_{29}$," J. Am. Chem. Soc. **123** (24), 5833 (2001).

Greenberg, C. C., Foster, M. D., Teale, D. M., Turner, C. M., Cloutet, E., Corona-Galvan, S., Quirk, R. P., Butler, P., Majkrzak, C. F., "Thermodynamics of Blends of Linear and Branched Polymers: Bulk and Surface Behavior," Bull. Am. Phys. Soc. **44** (1), 1909 (1999).

Greenberg, C. C., Teale, D. M., Foster, M. D., Turner, C. M., Corona-Galvan, S., Cloutet, E., Quirk, R. P., Majkrzak, C. F., Demaree, D., "Surface Segregation in Blends of Linear and Regularly Star Branched Polystyrene," Macromol., in press.

Grohn, F., Bauer, B. J., Akpalu, Y. A., Jackson, C. L., Amis, E. J., "Dendrimers as Templates for the Formation of Inorganic Nanoclusters," Macromol., in press.

Grohn, F., Bauer, B. J., Amis, E. J., "Organic-Inorganic Hybrid Particles by Dendrimer Nanotemplating," in *Proceedings of the Materials Research Society Meeting* (April 2000), in press.

Gruell, H., Sung, L., Karim, A., Douglas, J. F., Satija, S. K., Hayashi, M., Jinnai, H., Hashimoto, T., Han, C. C., "Surface Segregation of a Symmetrical Segregating Polymer Blend Film Above and Below the Critical Point of Phase Separation," Phys. Rev. Lett., in press.

Gulseren, O., Yildirim, T., Ciraci, S., "Tunable Adsorption on Carbon Nanotubes," Phys. Rev. Lett., in press.

Gulseren, O., Yildirim, T., Ciraci, S., Kilic, C., "First-Principles Study of the Electronic Structure of Carbon Nanotubes: Variable and Reversible Band Gap Engineering," Phys. Rev. B, in press.

Hagemann, I. S., Huang, Q., Gao, X. P. A., Ramirez, A. P., Cava, R. J., "Geometric Magnetic Frustration in $Ba_2Sn_2ZnGa_3Cr_6O_{22}$: A Two-Dimensional Spinel Based Kagome Lattice," Phys. Rev. Lett. **86** (5), 894 (2001).

Hammouda, B., "SANS From Polymers Under Pressure," Neutron News **12** 20 (2001)

Hawari, A. I., Adams, J. M., "A Method for the Minimization of the HPGe Detector Efficiency Bias in the Measurement of the Spectral Index," *REACTOR DOSIMETRY, Radiation Metrology and Assessment*, edited by J. Williams, D. Vehar, F. Ruddy, D. Gilliam. (ASTM, West Conshohocken, PA, Feb. 2001).

Hayashi, M., Hashimoto, T., Hasegawa, H., Takenaka, M., Gruell, H., Esker, A. R., Weber, M., Satija, S. K., Han, C. C., Nagao, M., "Interface Between a Polysulfone and Polyamide as Studied by Combined Neutron Reflectivity and Small-Angle Neutron Scattering Techniques," Macromol. **33** (22), 8375 (2000).

Hayashi, M., Hashimoto, T., Weber, M., Gruell, H., Esker, A., Han, C. C., Satija, S. K., "Transient Interface Instability in Bilayer Polymer Films as Observed by Neutron Reflectivity Studies," Macromol., in press.

He, T., Huang, Q., Cava, R. J., "Comparison of the Magnetic Properties of Isoelectronic $Sr_x(Na_{0.5}La_{0.5})_{1-x}RuO_3$ and $Sr_xCa_{1-x}RuO_3$," Phys. Rev. B **63**, 4402 (2001)

He, T., Huang, Q., Ramirez, A. P., Wang, Y., Regan, K. A., Rogado, N., Hayward, M. A., Haas, M. K., Slusky, J. S., Inumaru, K., Zandbergen, H. W., Ong, N. P., Cava, R. J., "Superconductivity in the Non-Oxide Perovskite $MgCNi_3$," Nature **411**, 54 (2001).

Heuser, B. J., Chen, W. C., "Comparison of Deutride (Hydride) Morphology During Precipitation and Decomposition in Single Crystal Pd: A Clue to the Pressure Hysteresis," Phys. Rev. B, in press.

Hiraka, H., Endoh, Y., Fujita, M., Lee, Y. S., Kulda, J., Ivanov, A., Birgeneau, R. J., "Spin Fluctuations in the Underdoped High-T_c Cuprate $La_{1.93}Sr_{0.07}CuO_4$," J. Phys. Soc. Japan **70** (3), 853 (2001).

Hjörvarsson, B., Andersson, G., Dura, J. A., Udovic, T. J., Isberg, P., Majkrzak, C. F., "Temperature Dependence of the Magnetic Interlayer Ordering in $Fe_3/V_{15}H_x$ (001) Superlattices," Phys. Rev. B, in press.

Ho, D. L., Briber, R. M., Glinka, C. J., "Studies on Organically Modified Clays Using Scattering Techniques," ACS Symposium of Polymer Nanocomposites **804**, (11) (2001).

Ho, D. L., Briber, R. M., Glinka, C. J., "Characterization of Organically Modified Clays Using Scattering and Microscopy Techniques," Chem. Mater. **13** (5), 1923 (2001).

Hone, J. H. E., Howe, A. M., Cosgrove, T., "A Small Angle Neutron Scattering Study of the Structure of Gelatin/Polyelectrolyte Complexes," Macromol. **33**, 1206 (2000).

Hone, J. H. E., Howe, A. M., Cosgrove, T., "A Rheological and Small Angle Neutron Scattering Study of the Structure of Gelatin/Polyelectrolyte Complexes Under Shear," Macromol. **33** (4), 1199, (2000).

Horkay, F., Basser, P. J., Hecht, A. M., Geissler, E., "Osmotic and SANS Observations on Sodium Polyacrylate Hydrogels in Physiological Salt Solutions," Macromol. **33**, 8329 (2000).

Horkay, F., Hecht, A. M., Geissler, E., "Neutron Scattering Investigations on Filled Polymer Gels," in *Proceedings of the 219th ACS National Meeting 41* (San Francisco, CA, March 26-30, 2000) **219**, 158 (2000).

Horkay, F., Hecht, A. M., Geissler, E., "Neutron Scattering Investigations on Bimodal Polymer Gels," J. Phys. Chem. B **105**, 5637 (2001)

Horkay, F., McKenna, G. B., Deschamps, P., Geissler, E., "Neutron Scattering Properties of Randomly Cross-Linked Polyisoprene Gels," Macromol. **33** (14), 5215 (2000).

Horkay, F., McKenna, G. B., Deschamps, P., Geissler, E., "Relationship Between Microscopic Structure and Osmotic and Mechanical Behavior of Polysoprene Gels," Macromol. **33**, 5215 (2000).

Horkay, F., McKenna, G. B., Geissler, E., "Nanostructures in Swollen Polymer Networks," in *Proceedings of the Polymer Networks 98, 14th Polymer Networks, Group Conference* (Trondheim, Norway, June 28-July 1, 1998), The Wiley Polymer Networks Group Review.

Huang, Q., He, T., Regan, K. A., Rogado, N., Hayward, M., Haas, M. K., Inumaru, K., Cava, R. J., "Temperature Dependence of the Structural Parameters of the Non-Oxide Perovskite Superconductor $MgCNi_3$," Physica C, in press.

Huffman, P. R., Brome, C. R., Butterworth, J. S., Dzhosyuk, S. N., Golub, R., Lamoreaux, S. K., Mattoni, C. E. H., McKinsey, D. N., Doyle, J. M., "Magnetically Stabilized Luminescent Excitations in Hexagonal Boron Nitride," Lumin. **92** (4), 291 (2001)

Huffman, P. R., Coakley, K. J., Thompson, A. K., Yang, G. L., Wietfeldt, F. E., Alvine, K. J., Brome, C. R., Dzhosyuk, S. N., Mattoni, C. E. H., Michniak, R. A., McKinsey, D. N., Yang, L., Doyle, J. M., Golub, R., Habicht, K., Koch, J., Lamoreaux, S. K., Leite, M. L., Maia, L., Rodrigues, A. C., Zanotto, E. D., "Magnetic Trapping of Ultracold Neutrons: Prospects for an Improved Measurement of the Neutron Lifetime," in *Proceedings of the The Workshop on Fundamental Physics with Pulsed Neutron Beams* (World Scientific Inc.), in press.

Hwang, S. R., Li, W. -H., Lee, K. C., Lynn, J. W., Luo, H. M., Ku, H. C., "Structural and Magnetic Properties of $Pr_{1+x}Ba_{2-x}Cu_3O_{7+x}$," Phys. Rev. B **6317** (17), 2401 (2001).

Hwang, S. -R., Li, W. -H., Lee, K. C., Lynn, J. W., Wu, C. -G., "Spiral Magnetic Structure of Fe in van der Waals Gaped FeOCl," Phys. Rev. B **62** (21), 14157 (2000).

Ilavsky, J., Stalick, J. K., Wallace, J., "Thermal-Spray Yttria-Stabilized Zirconia Phase Changes During Annealing," in *Proceedings of the International Thermal Spray Conference*, May 8-11, 2000, Montreal, Quebec, Canada) edited by Christopher C. Berndt (New York), p 1185-1189.

Ivkov, R., Butler, P. D., Satija, S. K., "Effect of Solvent Flow on a Polymer Brush: A Neutron Reflectivity Study of the Brush Height and Chain Density Profile," Langmuir **17** (10), 2999 (2001).

Ivkov, R., Gehring, P. M., Maliszewskyj, N. C., Krishnamoorti, R., "Structure and Dynamics of Polymers in Confined Geometries: Neutron Studies of Intercalated Clay-Polymer Nanocomposites," in *Proceedings of the SPE 57th Annual Technical Conference and Exhibits*, (Society of Plastics Engineers, Inc., Brookfield, 2000), p. 1783.

Jacobson, D. L., Arif, M., Bergmann, L., Ioffe, A., "Development of the Neutron Phase Contrast Imaging Technique and its Application in Materials Science Research," in *Proceedings, SPIE Conference*, (Denver, July 17-23, 1999), in press.

James, W. D., Zeisler, R., "Uptake of Oxygen in a Coal Standard Reference Material Determined by 14-MeV Neutron Activation Analysis," J. Radioanal. Nucl. Ch. **248** (1), 233 (2001).

Jones, R. L., Kumar, S. K., Ho, D. L., Briber, R. M., Russell, T. P., "Chain Conformation in Ultrathin Polymer Films Using Small Angle Neutron Scattering," Macromol. **34**, 559 (2001).

Kamitakahara, W. A., Trevino, S. F., Buga, S. G., Blank, V. D., "Destructive Annealing of a Superhard Carbon Derived From C_{60}," Phys. Rev. B, in press.

Keimer, B., Casa, D., Ivanov, A., Lynn, J. W., Zimmermann, M. V., Hill, J. P., Gibbs, D., Taguchi, Y., Tokura, Y., "Spin Dynamics and Orbital State in $LaTiO_3$," Phys. Rev. Lett. **85** (18), 3946 (2001).

Kent, M., "A Quantitative Study of Tethered Chains in Various Solution Conditions Using Langmuir Diblock Copolymer Monolayers," Macromol., in press.

Kepa, H., Kutner-Pielaszek, J., Twardowski, A., Sipatov, A. Y., Majkrzak, C. F., Story, T., Galazka, R. R., Giebultowicz, T. M., "Interlayer Correlations in Ferromagnetic Semiconductor Superlattices EuS/PbS," J. Magn. Magn. Mater., in press.

Khalifah, P., Huang, Q., Ho, D. M., Zandbergen, H. W., Cava, R. J., "$La_7Ru_3O_{18}$ and $La_{4.87}Ru_2O_{12}$: Geometric Frustration in Two Closely Related Structures With Isolated RuO_6 Octahedra," J. Solid State Chem. **155** (1), 189 (2000).

Khalifah, P., Jin, R., Liu, Y., Huang, Q., Gao, X. P. A., Ramirez, A. P., Cava, R. J., "Non-Fermi-Liquid Behavior in $La_3Ru_6O_{19}$: A Cubic, non-Perovskite Ruthenate With Metal-Metal Bonding," Nature **411** (6838), 669 (2001).

Kilic, C., Ciraci, S., Gulseren, O., Yildirim, T., "Variable and Reversible Quantum Structures on a Single Carbon Nanotube," Phys. Rev. B **62** (24), 16345 (2000).

Kim, S. D., Klein, A., Sperling, L. H., Boczar, E. M., Bauer, B. J., "SANS Study of Sulfite End Group Effect on Polystyrene Self-Diffusion," Macromol. **33** (22), 8334 (2000).

Kim, S. D., Klein, A., Sperling, L. H., Boczar E.M., Bauer, B. J., "A Direct Comparison of SANS and DET for Polymer Diffusion in Polystyrene Latex Film," Macromol., in press.

Kim, Y. J., Birgeneau, R. J., Chou, F. C., Erwin, R. W., Kastner, M. A., "Critical Spin Dynamics of the 2D Quantum Heisenberg Antiferromagnets $Sr_2CuO_2C_{12}$ and $Sr_2Cu_3O_4C_{12}$," Phys. Rev. Lett. **86** (14), 3144 (2001).

Kim, Y. J., Birgeneau, R. J., Chou, F. C., Greven, M., Kastner, M. A., Lee, Y. S., Wells, B. O., Aharony, A., Entin-Wohlman, O., Korenblit, I. V., Harris, A B., Erwin, R. W., Shirane, G., "Neutron Scattering Study of $Sr_2Cu_3O_4C_{12}$," Phys. Rev. B **6402** (2), 4435 (2001).

Kim, Y. J., Wakimoto, S., Shapiro, S. M., Gehring, P. M., Ramirez, A. P., "Neutron Scattering Study of Antiferromagnetic Order in $CaCu_3Ti_4O_{12}$," Phys. Rev. B, in press.

Kiryukhin, V., Kim, Y. J., Thomas, K. J., Chou, F. C., Erwin, R. W., Huang, Q., Kastner, M. A., Birgeneau, R. J., "Magnetic Properties of the S=½ Quasi-One-Dimensional Antiferromagnet $CaCu_2O_3$," Phys. Rev. B **6314** (14), 4418 (2001).

Kneller, L.R., Edwards, A. M., Nordgren, C. E., Blasie, J. K., Berk, N. F., Krueger, S., Majkrzak, C. F., "Hydration State of Single Cytochrome Monolayers on Soft Interfaces Via Neutron Interferometry," Biophys. J. **80** (5), 2248 (2001).

Koehler, R. D., Raghavan, S. R., Kaler, E. W., "Microstructure and Dynamics of Wormlike Micellar Solutions Formed by Mixing Cationic and Anionic Surfactants," J. Phys. Chem. B **104**, 11035 (2000).

Koga, T., Shin, K., Zhang, Y., Seo, Y.-S., Rafailovich, M. H., Sokolov, J., Chu, B., Satija, S. K., "Polymer Thin Films in Supercritical CO_2," in *Proceedings of the ASR-2000,* (Journal of Physical Society, Japan), in press.

Kolb, R., Lin, E. K., Wu, W. L., Satija, S. K., "Neutron Reflectivity Measurements of Polymer Melt Mobility Near Oxidized Silicon Surfaces Modified with Self-Assembled Monolayers," Langmuir, in press.

Koubi, L., Tarek, M., Bandyopadhyay, S., Klein, M. L., Scharf, D., "Distribution of Non-Immobilizers and Anesthetics in Model Membranes," Anesthesisology, in press

Krone, C. A., Robisch, P. A., Tilbury, K. L., Stein, J. E., Mackey, E. A., Becker, P. R., O'Hara, T. M., Philo, L. M., "Heavy Metals and Other Elements in Liver Tissues of Bowhead (Balaena Mysticetus) Whales," Mar. Mam. Sci., in press.

Krueger, J. K., Gallagher, S. C., Wang, C. L., Trewhella, J., "Calmodulin Remains Extended Upon Binding to Smooth Muscle Caldesmon. A Combined Scattering and Fourier Transform Infrared Spectroscopy Study," Biochem. **39** (14), 3979 (2000).

Krueger, J. K., Trewhella, J., "Neutron Scattering Studies of Muscle Protein Structures and Their Interactions" in *Proceedings of the Molecular Interactions of Actin. Actin Structure and Actin-Binding Proteins*, edited by C. G. do Remedios, D. D. Thomas, (Springer Verlag, 1999), in press.

Krueger, S., "Neutron Reflection From Interfaces With Biological and Biomimetic Materials," Curr. Opin. Sld. St. Mtls. Sci. **6** (2), 111 (2001).

Krueger, S., Meuse, C. W., Majkrzak, C. F., Dura, J. A., Berk, N. F., Tarek, M., Plant, A. L., "Investigation of Hybrid Bilayer Membranes With Neutron Reflectometry: Probing the Location of Interactions of Melittin," Langmuir **17** (2), 511 (2001).

Kuznicki, S. M., Bell, V. A., Hillhouse, H. W., Braunbarth, C. M., Jacubinas, R M., Nair, S., Toby, B. H., Tsapatsis, M., "A Titanosilicate Molecular Sieve with Adjustable Pores for Size-Selective Adsorption of Molecules," Nature **412**, 720 (2001).

Lamaze, G. P., Chen-Mayer, H. H., "Nitrogen Analysis in Thin Films Using Cold Neutron Depth Profiling," in *Proceedings of the 9th International Conference on Modern Materials and Technologies*, edited by P. Vincenzini, (TECHNA, Faenza, Italy), in press.

Lamaze, G. P., Chen-Mayer, H. H., Gerouki, A., and Goldner, R. B., "Analysis of Lithium Transport in Electrochromic Multilayer Films by Neutron Depth Profiling," Surf. Interface Anal. **29**, 638 (2000).

La-Orauttopong, D., Noheda, B., Ye, Z.-G., Gehrong, P. M., Toulouse, J., Cox, D., Shirane, G., "New Phase Diagram for the Relaxor $(1-x)Pb(Zn_{1/3}Nb_{2/3})O_3$-$xPbTiO_3$," in press.

Lee, S.-H., Cheong, S. -W., Yamada, K., Majkrzak, C. F., Aeppli, G., "Charge and Canted Spin Order in $La_{2-x}Sr_xNiO_4$," Phys. Rev. B, **63** (6), 0405 (2001).

Lee, S.-H., Broholm, C., Aeppli, G., Cheong, S.-W., "Short-Range Spin Correlations in a Geometrically Frustrated Magnet, $SrCr_{9p}Ga_{12-9p}O_{19}$," in *Proceedingsof the International Workshop on Cold Neutron Utilization, Korean Atomic Energy Institute*, (Taejon, South Korea, December 1997), in press.

Lee, S.-H., Qiu, Y., Broholm, C., Ueda, Y., Rush, J. J., "Spin Fluctuations in a Magnetically Frustrated Metal LiV_2O_4," Phys. Rev. Lett. **86** (24), 5554 (2001).

Lee, Y., Reisner, B. A., Hanson, J. C., Jones, G. A., Parise, J. B., Corbin, D. R., Toby, B. H., Freitag, A., Larese, J. Z., "New Insight Into Cation Relocations Within the Pores of Zeolite Rho: *In Situ* Synchrotron X-ray and Neutron Powder Diffraction Studies of Pb- and Cd-Exchanged Rho," J. Phys. Chem. B **105** (30), 7188 (2001).

Lefebvre, A. A., Lee, J. H. Balsara, N. P., Hammouda, B., "Neutron Scattering From Pressurized Polyolefin Blends Near the Limits of Metastability," Macromol. **33** (21), 7977 (2000).

Leighton, C., Fitzsimmons, M. R., Yashar, P., Hoffman, A., Nogues, J., Dura, J., Majkrzak, C. F., Schuller, I. K., "Two-Stage Magnetization Reversal in Exchange Biased Bilayers," Phys. Rev. Lett. **86** (19), 4394 (2001).

Levin, I., Chan, J. Y., Geyer, R. G., Maslar, J. E., Vanderah, T. A., "Cation Ordering Types and Dielectric Properties in the Complex Perovskite $Ca(Ca_{1/3}Nb_{2/3})O_3$," J. Solid State Chem. **156** (1), 122 (2001).

Levin, I., Chan, J. Y., Maslar, J. E., Vanderah, T. A., Bell, S. M., "Phase Transitions and Microwave Dielectric Properties in the Perovskite-Like $Ca(A_{1/3}Nb_{0.5})O_3$-$CaTiO_3$ System," J. Appl. Phys. **90** (2), 904 (2001).

Li, W.-H., Wu, S. Y., Lee, K. C., Lynn, J. W., Liu, R. S., Wu, J. B., Huang, C. Y., "Noncollinear Magnetic Structure and Spin Reorientation in $Nd_{1/4}MnO_3$," Phys. Rev. B., in press.

Licci, F., Gauzzi, A., Marezio, M., Huang, Q., Santoro, A., Masini, R., Bougerol-Chaillout, C., Bordet, P., "Effects of Re Substitute on the Structure and Superconductivity of $Cu_{1-x}RexBa_2Cu_2O_z$," Physica C **355** (3), 267 (2001).

Likos, C. N., Vaynberg, A., Lowen, H., Wagner, N. J., "Colloidal Stabilization by Adsorbed Gelatin," Langmuir **16** (9), 4100 (2000).

Lin, E. K., Lee, H. J., Wang, H., Wu, W. L., "Structure and Property Characterization of Low-k Dielectric Porous Thin Films Determined by X-ray Reflectivity and Small-Angle Neutron Scattering," in Proceedings of the *2000 International Conference on Characterization and Metrology for ULSI Technology* (July 2000), in press.

Lin, E. K., Pochan, D. J., Wu, W. L., Satija, S. K., "Neutron Reflectivity Measurements of Molecular Mass Effects on Polymer Mobility Near the Polymer/Solid Interface," in *Proceedings of the Materials Research Society Meeting* (April 2000), in press.

Lin, E. K., Wu, W. L., Jin, C., Wetzel, J. T., "Structure and Property Characterization of Porous Low-k Dielectric Constant Thin Films Using X-ray Reflectivity and Small-Angle Neutron Scattering," in *Proceedings* of the *Materials Research Society Meeting* (April 2000), in press.

Lindstrom, R. M., "Limits for Qualitative Detection and Quantitative Determination," edited by, D.R. Lide, A Century of Excellence in Measurements, Standards, and Technology (NIST SP 958), U.S. Govt Print. Off., Washington, 164-166, 2001.

Ling, X. S., Park, S. R., McClain, B. A., Choi, S. M., Dender, D. C., Lynn, J. W., "Superheating and Supercooling of Vortex Matter in a Nb Single Crystal: Direct Evidence for a Phase Transition at the Peak Effect from Neutron Diffraction," Phys. Rev. Lett. **86** (4), 712 (2001).

Liu, W. J., Jeng, U., Lin, T. L., Lai, S. H., Shih, M. C., Tsao, C. S., Chiang, L. Y., Sung, L. P., "Adsorption of Dodecahydroxylated-Fullerene Monolayers at the Air-Water Interface," Physica B **283**, 49 (2000).

Livingston, R., Neumann, D. A., Allen, A. J., FitzGerald, S. A., Berliner, R., "Application of Neutron Scattering to Portland Cement," Neutron News **11** (4), 18 (2000).

Loureiro, S. M., Felser, C., Huang, Q., Cava, R. J., "Refinement of the Crystal Structures of Strontium Cobalt Oxychlorides by Neutron Powder Diffraction," Chem. Mat. **12** (10), 3181 (2000).

Luchette, P. A., Vetman, T. N., Prosser, R. S., Hancock, R. E. W., Nieh, M., Glinka, C. J., Krueger, S. K., Katsara, J., "Morphology of Fast Tumbling Bicelles: A Small Angle Neutron Scattering and NMR Study," Bioch. Et Biophy. Acta **1513** (2), 83 (2001).

Lynch, M. L., Wireko, F., Tarek, M., Klein, M., "Intermolecular Interactions and the Structure of Fatty Acid-Soap Crystals," J. Phys. Chem. B **105**, 552 (2001).

Lynn, G. W., Dadmun, M. D., Wu, W. L., Lin, E. K., Wallace, W. E., "Neutron Reflectivity Studies of the Interface Between a Small Molecule Liquid Crystal, and a Polymer," Liquid Crystals, in press.

Lynn, J. W., "Neutron Studies of Exchange-Coupled Superconductors," in *Proceedings of the NATO Advanced Research Workshop* (June 13-18th), **14**, 121 (2001).

Lynn, J. W., "Progress in Borocarbide Research," in *Proceedings of the NATO Conference*, **14**, 431 (2001).

Lynn, J. W., "Spin Dynamics in the Ferromagnetic Phase of Colossal Magnetoresistive Oxides," J. Supercond. Novel Magn. **13** (2), 263 (2000).

Lynn, J. W., "Magnetic Neutron Scattering," in *Proceedings of Methods in Materials Research*, edited by Kaufman (John Wiley & Sons), in press.

Lynn, J. W., Adams, C. P., Mukovskii, Y. M., Arsenov, A. A., Shulyatev, D. A., "Charge Correlations in the Magnetoresistive Oxide $La_{0.7}Ca_{0.3}MnO_3$," J. Appl. Phys. **89** (11), 6846 (2001).

Lynn, J. W., Skanthakumar, S., "Neutron Scattering Studies of Lanthanide Magnetic Ordering," *Handbook on the Physics and Chemistry of Rare Earths* (edited by K. A. Gschneider, Jr., L. Eyring, and M. B. Maple) Elsevier Science **31**, 315 (2001).

Magid, L. J., Li, Z., Butler, P. D., "Flexibility of Elongated Sodium Dodecylsulfate Micelles in Aqueous Sodium Chloride: A Small-Angle Neutron Scattering Study," Langmuir **16** (26), 10028 (2000).

Majkrzak, C. F., "Neutron Applications in Materials Science and Engineering," J. Neutron Res., in press.

Majkrzak, C. F., Berk, N. F., "Advances in Specular Neutron Reflectometry," Appl. Phys. A, in press.

Majkrzak, C. F., Berk, N. F., Krueger, S., Dura, J. A., Tarek, M., Tobias, D., Silin, V., Meuse, C. W., Woodward, J., Plant, A. L., "First-Principles Determination of Hybrid Bilayer Membrane Structure by Phase-Sensitive Neutron Reflectometry," Biophysical J. **79** (6), 3330 (2000).

Majkrzak, C. F., Satija, S. K., Berk, N. F., Krueger, S. K., Borchers, J. A., Dura, J. A., Ivkov, R., O'Donovan, K., "Neutron Reflectometry at the NCNR," Neutron News **12**, 25 (2001).

Mallamace, F., Gambadauro, P., Micali, N., Tartaglia, P., Liao, C., Chen, S. H., "Kinetic Glass Transition in a Micellar System with Short-Range Attractive Interaction," Phys. Rev. Lett. **84**, 5431, (2000).

Manley, M. E., Fultz, B., McQueeny, R. J., Brown, C. M., Hults, W. L., Smith, J. L., Thomas, D. J., Osborn, R., Robertson, J. L., "Large Harmonic Softening of the Phonon Density of States of Uranium," Phys. Rev. Lett. **86** (14), 3076 (2001).

Manias, E., Chen, H., Krishnamoorti, R., Genzer, J., Kramer, E. J., Giannelis, E. P., "Intercalation Kinetics of Long Polymers in 2 nm Confinements," Macromol. **33** (21), 7955 (2000).

Mansky, P., Hawker, C. J., Mays, J., Cook, D. C., "Ordered Diblock Copolymers on Random Copolymer Brushes," Macromol., in press.

Manson, J. L., Huang, Q., Lynn, J. W., Koo, H., Whangbo, M., Bateman, R., Wada, N., Awaga, K., Argyriou, D. N., Miller, J. S., "Long-Range Magnetic Order in $Mn[N(CN)_2]_2(pyz)$ {pyz = pyrazine}. Susceptibility, Magnetization, Specific Heat and Neutron Diffraction Measurements and Electronic Structure Calculations," J. Am. Chem. Soc. **123** (1), 162 (2001).

Matejicek, J., Sampath, S., Gnäupel-Herold, T., Prask, H. J., "Processing Effects on Residual Stress in Ni+5%Al Coatings – Comparison of Different Spraying Methods," in *Proceedings of the International Thermal Spray Conference* 2000, in press.

Matejicek, J., Sampath, S., Gnäupel-Herold, T., Prask, H. J., "Residual Stress in Sprayed Ni+5%Al Coatings Determined by Neutron Diffraction," in *Proceedings of the International Conference on Neutron Scattering*, in press.

Maurer, R. H., Roth, D. R., Fainchtein, R., Goldsten, J. O., Kinnison, J. D., Thompson, A. K., "Portable Real Time Neutron Spectrometry," in *Proceedings* of *The Space Technology and Applications International Forum (STAIF-99), Conference on International Space Station Utilization*, in press.

Maxelon, M., Pundt, A., Pyckhout-Hintzen, W., Barker, J., Kirchheim, R., "Interaction of Hydrogen and Deuterium With Dislocations in Palladium as Observed by Small Angle Neutron Scattering," Acta Mater., in press

Maxelon, M., Pundt, A., Pyckhout-Hintzen, W., Kirchheim, R., "Small Angle Neutron Scattering of Hydrogen Segregation at Dislocations in Palladium," Scripta Materialia **44** (5), 817 (2001).

McKinley, J. P., Serne, R. J., Zachara, J. M., Schaef, H. T., Zeissler, C. J., Lindstrom, R. M., "The Distribution of Retention of ^{137}Cs in Sediments at the Hanford Site," Environmental Science and Technology, in press

McLaughlin, J. C., Neumann, D. A., Gress, D. L., Livingston, R. A., "Non-Destructive Measurement of Freeze/Thaw Cycles in Cement Paste Using Quasi-Elastic Neutron Scattering," in *Proceedings of the Third International Conference on Concrete Under Severe Conditions*, edited by N. Banthia, K. Sakai, O.E. Gjorv, (The University of British Columbia, Vancouver, Canada, 2001), p.1408.

Merfeld, G. D., Karim, A., Majumdar, B., Satija, S. K., Paul, D. R., "Interfacial Thickness Between Immiscible Bilayers of Poly (Phenylene Oxide) and Styrenic Copolymers," J. Poly. Sci. B, in press.

Michels, A., Weissmuller, J., Wiedenmann, A., Pedersen J. A., Barker, J. G., "Measuring the Exchange-Stiffness Constant of Nanocrystalline Solids by Elastic Small-Angle Neutron Scattering," Phil. Mag. Lett. **80** (12), 785 (2000).

Migler, K. B., Han, C. C., "Pressure Effects on Diblock Copolymers: Optical Birefringence and Neutron Scattering," Macromol., in press.

Mildner, D. F. R., "Time Focusing of Pulsed-Source Crystal Analyzer Spectrometers II. Practical Expressions," J. Nucl. Instrum. & Meth., in press.

Mildner, D. F. R., "X-ray and Neutron Optics," in *The Handbook of Optics*, edited by W. M. Gibson, C. A. MacDonald, Chapter 6 (Optical Society of America, McGraw-Hill Publishing, New York, NY), in press

Mildner, D. F. R., Carpenter, J. M., "Time Uncertainty for Guided Long Wavelength Neutrons on a Pulsed Source," J. Nucl. Instrum. & Meth. A, in press.

Mildner, D. F. R., Arif, M., Werner, S. A., "Neutron Transmission Through Pyrolytic Graphite Monochromators," J. Appl. Cryst. **34** (3), 258 (2001).

Mombru, A.W., Pardo, H., Suescum, L., Toby, B. H., Ortiz, W. A., Negreira, C. A., Araujo-Moreira, F. M., "Influence of Oxygen Disorder on the Magnetic Properties of $LaBaCuFeO_{5+d}$: an EXAFS and Neutron Diffraction Study," Physica C **356** (1), 149 (2001).

Nakatani, A. I., "Chain Dimensions in Polysilicate-Filled Poly (Dimethyl Siloxane)," in *Proceedings of the International Journal of Thermophysics, 14th Symposium on Thermophysical Properties*, (Boulder, CO), in press.

Nakatani, A. I., Chen, W., Schmidt, R. G., Gordon, G. V., Han, C. C., "Chain Dimensions in Polysilicate-Filled Poly(Dimethylsiloxane)," Polymer **42** (8), 3713 (2001)

Nakatani, A. I., Ivkov, R., Papanek, P., Jackson, C. L., Yang, H., Nikiel, L., Gerspacher, M., Krishnamoorti, R., "The Significance of Percolation in the Dynamics of Polymer Chains Bound to Carbon Black," in *Proceedings of the Filled and Nanocomposite Polymer Materials*, edited by A. Nakatani, Hjelm, L., Gerpacher, M., Krishnamoorti, R. P., (Materials Research Society, Pittsburgh, 2001), in press.

Nakatani, A. I., Ivkov, R., Papanek, P., Yang, H., Gerspacher, M., "Inelastic Neutron Scattering From Filled Elastomers," Rubber Chem. Technol. **73** (5), 847 (2000).

Nico, J. S., "Establishing International Collaborations. Examples of Mid-Size Collaborations," in *Proceedings Report of the American Association for the Advancement of Science and the AAAS Web Site*, in press

Nico, J. S., Abdurashitov, J. N., Gavrin, V. N., Girin, S. V., Gorbachev, V. V., Ibragimova, T. V., Kalikhov, A. V., Khairnasov, N. G., Knodel, V. N., Mirmov, I. N., Shikhin, A., Verentenkin, E. P., Vermul, V. M., Yants, V. E., Zatsepin, G. T., Bowles, T. J., Teasdale, W. A., Wark, D. L., Cherry, M. L., Cleveland, B. T., Davis, R., Lande, K., Wildenhain, P. S., Elliott, S. R., Wilkerson, J. F., "Solar Neutrino Results From SAGE," in *Proceedings of the 10th International Baksan School: Particles and Cosmology*, in press.

Nieh, M., Glinka, C. J., Krueger, S., Prosser, R. S., Katsaras, J., "SANS Study of the Structural Phases of Magnetically Alignable Phospholipid Mixtures," Langmuir **17** (9), 2629 (2001).

Norman, B. R., Iyengar, G. V., "Further Applications of Pre-Irradiation Combustion and Neutron Activation Analysis Technique for the Determination of Iodine in Food and Environmental Reference Materials. Merits and Demerits," Fresen. J. Anal. Chem., in press

O'Donovan, K. V., Borchers, J. A., Majkrzak, C. F., Hellwig, O., Fullerton, E. E., "Extracting Buried Twists With Polarized Neutron Reflectometry," Appl. Phys. Lett. A, in press.

O'Donovan, K. V., Borchers, J. A., Majkrzak, C. F., Hellwig, O., Fullerton, E. E., "Pinpointing Chical Polarized Using Front/Back Polarized Neutron Reflectivity," Phys. Rev. Lett., in press.

Ohwada, K., Hirota, K., Rehrig, P. W., Gehring, P. M., Noheda, B., Fujii, Y., EaglePark, S.-E., Shirane, G., "Neutron Diffraction Study of the Irreversible R-M_A-M_C Phase Transition in Single Crystal $Pb[(Zn_{1/3}Nb_{2/3})_{1-x}Ti_x]O_3$," J. Phys. Soc. Jpn. **70** (9), (2001)

Olson, D. H., Toby, B. H., Reisner, B. A., "Neutron Diffraction Study of Protons in Four Lanthanum Exchanged X and LSX Zeolites," in *Proceedings of the 13th International Zeolite Congress*, in press.

Orts, W. J., Glenn, G. M., "Reducing Soil Erosion Losses with Small Applications of Biopolymers," in *Proceedings of the Biopolymers: Utilizing Nature's Advanced Materials*, edited by R. V. Greene and S. H. Imam (ACS Symposium Series, Washington, DC, 1998), in press.

Oslanec, R., Composto, R. J., Vlcek, P., "Block Copolymer Adsorption at the Polymer Melt/Substrate Interface: Effect of Matrix Composition," Macromol. **33** (6), 2200 (2000).

Papanek, P., Fischer, J. E., Sauvajol, J. L., Dianoux, A. J., McNeillis, P. M., Mathis, C., Francois, B., "Low-Frequency Phonons in Pristine and Doped Phases of Polyacetylene: An Inelastic Neutron Scattering Study," J. Chem. Phys., in press.

Papanek, P., Kamitakahara, W. A., Zhou, P., Fischer, J.E., "Neutron Scattering Studies of Disordered Carbon Anode Materials," J. Phys. Condens. Mat. in press.

Paul, R. L., "Development of a Procedure for Measuring Nitrogen by Cold Neutron Prompt Gamma-ray Activation Analysis," Analyst **126** (2), 217 (2001).

Paul, R.L., "Determination of Nitrogen in Some Reference Materials by Cold Neutron Prompt Gamma-ray Activation Analysis," J. Radioanal. Nucl. Chem., in press.

Paul, R.L., "Determination of Phosphorus in Steels by Radiochemical Neutron Activation Analysis," J. Radioanal. Nucl. Chem., in press.

Paul, R.L., "Nitrogen in Some Reference Materials by Cold Neutron Prompt Gamma-ray Activation Analysis," Analyst, in press.

Paul R.L., "Nondestructive Measurement of Hydrogen and Other Elements by Cold Neutron Capture Prompt Gamma-ray Activation Analysis," Geostandards Newsletter, in press.

Paul, R. L., "Reference Minerals for Microanalysis of Light Elements," Geostandards Newsletter, in press.

Paul, R. L., Chen-Mayer, H. H., Lindstrom, R. M., "Characterization of Hydrogen in Concrete by Cold Neutron Prompt Gamma-ray Activation Analysis and Incoherent Scattering," in *Proceedings of the Materials Research Society Fall 1999 Conference on Nondestructive Methods and Materials Characterization*, edited by G.Y. Baaklini, N. Meyendorf, T. E. Matikas, R. S. Gilmore (Matls. Res. Soc., Warrendale, PA, 2000), p.175.

Paul, R. L., Simons, D. S., "Neutron Activation Analysis for Calibration of Phosphorus Implantation Dose," in *Proceedings of the 2000 International Conference on Characterization and Metrology for ULSI Technology*, edited by D. G. Seiler, A. C. Diebold, W. M. Bullies, T. J. Shaffner, R. McDonald, E. J. Walters (AIP Press, Woodbury, NY), in press.

Payne, A. C., Sprauve, A., Olmstead, M. M., Kauzlarich, S. M., Chan, J. Y., Reisner, B. A., Lynn, J. W., "Synthesis, Magnetic, and Electronic Properties of Single Crystals of $EuMn_2P_2$," J. Solid State Chem., in press.

Pearce, J. V., Azuah, R. T., Stirling, W. G., Dimeo, R. M., Sokol, P. E., Adams, M. A., "High-Resolution Measurements of the Temperature Dependence of the Roton Energy of Superfluid ^{4}He," J. Low Temp. Phys. **276**, 822 (2000).

Pelton, R., Richardson, R., Cosgrove, T., Ivkov, R., "The Effects of Temperature and Methanol Concentration on the Properties of Poly(N-Isopropylacrylamide) at the Air-Solution Interface," Langmuir **17** (16), 5118 (2001).

Pivovar, A. M., Ward, M. D., Yildirim, T., Neumann, D. A., "Vibrational Mode Analysis of Isomorphous Hydrogen-Bonded Guanidinium Sulfonates With Inelastic Neutron Scattering and Density Functional Theory," J. Chem. Phys. **115** (4), 1909 (2001).

Plazanet, M., Johnson, M. R., Gale, J. D., Yildirim, T., Kearley, G. J., Trommsdorff, H. P., Fernandez-Diaz, M. T., Sanchez-Portal, D., Artacho, E., Soler, J. M., Ordejon, P., Garcia, A., "The Structure and Dynamics of Crystalline Durene by Neutron Scattering and Numerical Modeling Using Density Functional Methods," Chem. Phys. **261** (1), 189 (2000).

Pochan, D. J., Lin, E. K., Wu, W. L., Satija, S. K., "Thermal Expansion of Supported Thin Polymer Films: A Direct Comparison of Free Surface vs. Total Confinement," Macromol. **34** (9), 3041 (2001).

Pochan, D. J., Lin, E. K., Wu, W. L., Satija, S. K., Cheng, S. Z. D., "Thermal Expansion and Glass Transition Behavior of Thin Polymer Films With and Without a Free Surface via Neutron Reflectometry," in *Proceedings of the Dynamics in Small Confining Systems IV*, edited by J. M. Drake, G. S. Grest, J. Klafter, R. Kopelman, MRS Symp. Series 543, (Materials Research Society, Warrendale, PA, 1999), in press.

Popovici, M., Stoica, A., Hubbard, C., Spooner, S., Prask, H., Gnäupel-Herold, T., Gehring, P., Erwin, R., "Multi-Wafer Focusing Neutron Monochromators and Applications," in *Proceedings of the SPIE Optical Science and Technology*, in press.

Prask, H. J., Brand, P. C., Gnäupel-Herold, T., Hicho, G. E., "Determination of Residual Stresses Using Neutron Diffraction: Tank-Car Welds and Rail Slices," in ASNT's Topics on Nondestructive Evaluation Series, in press.

Prask, H. J., Gnäupel-Herold, T., "Materials Science Using Neutron," Transactions of the American Nuclear Society, American Nuclear Society (Washington, D.C., November 12-16, 2000) **83**, 495 (2000).

Prask, H. J., Gnäupel-Herold, T., Fisher, J. W., Cheng, X., Stuart, J. T., "Residual Stress Modification by Means of Ultrasonic Impact Treatment," in *Proceedings of the 2001 SEM Annual Conference & Exposition on Experimental an Applied Mechanics*, in press.

Quijada, M. A., Simpson, J. R., Drew, H. D., Lynn, J. W., Vasiliu-Doloc, L., Mukovskii, Y. M., Karabashev, S. G., "Temperature Dependence of Low-Lying Electronic Excitations of $LaMnO_3$," Phys. Rev. B, in press.

Reidy, R. F., Allen, A. J., Krueger, S., "Small Angle Neutron Scattering Characterization of Colloidal and Fractal Aerogels," J. Non Cryst. Solids **285** (1-3), 181 (2001).

Reisner, B. A., Lee, Y., Hanson, J. C., Jones, G. A., Parise, J. B., Corbin, D. R., Toby, B. H., Freitag, A., Larese, J. Z., Kahlenberg, V., "Understanding Negative Thermal Expansion and Trap Door Cation Relocations in Zeolite Rho," Chem. Comm. **22**, 2221 (2000).

Reisner, B. A., Tripathi, A., Parise, J. B., "$Na_8[Zn_4Ge_8O_{18}(OH)_{12}]\cdot 2H_2O$: An Interrupted-Framework Zincogermanate Built From $[GeO_3(OH)]$ and $[Ge_2(OH)_2]$ Units," J. Mater. Chem. **11**, 887 (2001).

Rich, D. R., Fan, S., Gentile, T. R., Hussey, D., Jones, G. L., Neff, B., Snow, W. M., Thompson, A. K., "Polarized ^{3}He Neutron Spin Filter Development and Application at Indiana University and NIST," Physica B, in press.

Rizi, R. R., Roberts, D. A., Dimitrov, I. E., Lipson, D. A., Gentile, T. R., Jones, G., Thompson, A., Gefter, W. B., Schnall, M. D., Leigh, J. S., "Ventilation/Perfusion of Lung Parenchyma Using Hyperpolarized ^{3}He Gas and Arterial Spin-Tagging," J. Magnetic Resonance Imaging, in press.

Rols, S., Benes, Z., Anglaret, E., Sauvajol, J. L., Papanek, P., Fischer, J. E., Coddens, G., Schober, H., Dianoux, A. J., "Phonon Density of States of Single-Wall Carbon Nanotubes," Phys. Rev. Lett. **85** (24), 5222 (2000).

Rosenkranz, S., Osborn, R., Vasiliu-Doloc, L., Lynn, J. W., Sinha, S. K., Mitchell, J. F., "Observation of Kosterlitz-Thouless Spin Correlations in the Colossally Magnetoresistive Layered Manganite $La_{1.2}Sr_{1.8}Mn_2O_7$," Phys. Rev. Lett., in press.

Rosenkranz, S., Osborn, R., Vasiliu-Doloc, L., Lynn, J. W., Sinha, S. K., Mitchell, J. F., "Spin Correlations and Magnetoresistance in the Bilayer Manganite $La_{1.2}Sr_{1.8}Mn_2O_7$," Physica B, in press.

Rossbach, M., Zeisler, R., "Certified Reference Materials for Microanalytical Methods," in *Proceedings of the Reference Materials for Chemical Analysis Certification, Availability, and Proper Usage*, edited by M. Stoeppler, W. R. Wolf, P. Jenks, Chapter 4.3, (John Wiley and Sons, Inc., New York, NY), in press.

Sankar, S., Dender, D., Borchers, J. A., Smith, D. J., Erwin, R. W., Kline, S. R., Berkowitz, A. E., "Magnetic Correlations in Non-Percolated Co-SiO_2 Granular Films," J. Magn. Magn. Mater **221** (1), 1 (2000).

Santoro, A., "Neutron Crystallography at NBS/NIST," ACA Newsletter, in press.

Sayer, E. V., Yener, A. K., Joel, E. C., Blackman, M. J., Özbal, H., "Stable Lead Isotope Studies of Black Sea Anatolian Ore Sources and Related Bronze Age and Phrygian Artifacts From Nearby Archaeological Sites Appendix: New Central Taurus Ore Data," Archaeometry, in press.

Schirber, J. E., Morosin, B., Kwei, G. H., Yildirim, T. A., Fischer, J. E., Jorgensen, J. D., "Superconductivity in the Polymeric Phase of Na_2CsC_{60}," Physica C **353**, 207 (2001).

Schmidt, G., Nakatani, A. I., Butler, P. D., Karim, A., Han, C. C., "Shear Orientation of Viscoelastic Polymer-Clay Solutions Probed by Flow Birefringence and SANS," in *Proceedings of the XIIIth Congress of Rheology 2000*, Macromol. **33** (20), 7219 (2000).

Schober, H., Losert, C., Mezei, F., Cook, J. C., "Chopper Cascades: An Analytical Treatment of the Contamination Problem," J. Neutron Res., in press.

Schulz, J. C., Warr, G. G., Butler, P. D., Hamilton, W. A., "Adsorbed Layer Structure of Cationic Surfactants on Quartz," Phys. Rev. E **6304** (4), 1604 (2001).

Schwickert, B. E., Kline, S. R., Zimmermann, H., Lantzky, K. M., Yarger, J. L., "Early Stages of Glacial Clustering in Supercooled Triphenyl Phosphite," Phys. Rev. B **6404** (4), 5410 (2001).

Sharov, V. A., Xiao, Q. F., Ponomarev, I. Yu., Mildner, D. F. R., Chen-Mayer, H. H., "Cold Neutron Microprobe for Materials Analysis Using Tapered Capillary Optics," Rev. Sci. Instrum. **71**, 3247 (2000).

Sharpless, K. E., Colbert, J. C., Greenberg, R. G., Schantz, M. M., Welch, M. J., "Recent Developments in Good-Matrix Reference Materials at NIST," Fres. J. Anal. Chem. **370**, 275 (2001).

Shin, K., Ahang, Y., White, H., Rafailovich, M. H., Sokolov, J., Peiffer, D., "Organoclay Nanoplatelets at the Air/Water Interface," Mat. Res. Soc. Symp, KK8.4 (2001).

Shin, K., Hu, X., Zheng, X., Rafailovich, M. H., Sokolov, J., Zaitsev, V., Sewarz, S. A., "Silicon Oxide Surface as a Substrate for Polymer Thin Films," Macromol. **34** (14), 4993 (2001).

Shin, K., Pu, Y., Rafailovich, M., Sokolov, J., Seeck, O. H., Tolan, M., Sinha, S., "Corrected Surfaces of Free Standing Polystyrene Thin Films," Macromol. **34** (16), 5620 (2001).

Shin, K., Rafailovich, M. H., Sokolov, J., Change, D. M., Cox, J. K., Lennox, R. B., Eisenberg, A., Huang, J., Hsu, S. L., Satija, S, "Observation of Surface Ordering of Alkyl Side Chains in Polystyrene/Polyelectrolytes Diblock Copolymer Langmuir Films," Langmuir **17** (16), (2001).

Shin, K., Rafailovich, M., Sokolov, J., Nguyen, D., Yang, N.-L., Eisenburg, A., Satija, S. K., "Ionomer Thin Films in Mixed Solvent," Langmuir, in press.

Shirane, G., Gehring P. M., "Soft Phonon Anomalies in Relaxor Ferroelectrics," J. Phys. Soc. Jpn. **84** (22), 5216 (2000).

Sitepu, H., Prask, H. J., Vaudin, M. D., "Texture Characterization in X-ray and Neutron Powder Diffraction Data Using the Generalized Spherical-Harmonic," in *Proceedings of the Annual Conference on Applications of X-ray Analysis*, in press.

Sitepu, H., Schmahl, W. W., Stalick, J. K., "Use of Generalized Spherical-Harmonic Model for Describing Texture in NiTi Shape Memory Alloy by Neutron Diffraction," Appl. Phys. A in press.

Skripov, A. V., Cook, J. C., Udovic, T. J., Kozhanov, V. N., "Quasielastic Neutron Scattering Study of Hydrogen Motion in C15-Type $HfMo_2H_{0.26}$," Phys. Rev. B **62** (21), 14099 (2000).

Skripov, A. V., Cook, J. C., Udovic, T. J., Kozhanov, V. N., Hempelmann, R., "Quasiclastic Neutron Scattering Studies of H Motion in Laves-Phase Compounds," Appl. Phys. A. **62** (21), 14099 (2000).

Sitepu, H., Prask, H. J., "Use of Generalized

Spherical-Harmonic Method for Describing Preferred Orientation With Neutron Powder Diffraction Data," J. Mater. Sci., in press.

Skripov, A. V., Udovic, T. J., Huang, Q., Cook, J. C., Kozhanov, V. N., "Neutron Diffraction Study of the Location of Deuterium in the Seuterium-Stablized $ZrTi_2D_{3.83}$ Phase," J. Alloy Compd. **311** (2), 234 (2000).

Smee, S. A., Brand, P. C., Barry, D. D., Broholm, C. L., Anand, D. K., "An Elastic, Low-Background Vertical Focusing Element for a Doubly Focusing Neutron Monochromator," Nucl. Instrum. Methods A **466** (3), 513 (2001).

Smee, S. A., Orndorff, J. D., Scharfstein, G. A., Qiu, Y., Brand, P. C., Broholm, C. L., Anand, D. K., "MACS Low Background Doubly Focusing Neutron Monochromator," Appl. Phys. A, in press.

Sokolov, M. A., Spooner, S. E., Odette, G. R., Wirth, B. D., Lucas, G. E., "SANS Study of High-Copper RPV Welds in Irradiated and Annealed Conditions," in *Proceedings of the Effects of Radiation on Materials: 18th International Symposium*, ASTM 1325, edited by R. K. Nanstad, M. L. Hamilton, F. A. Garner, A. S. Kumar (ASTM, West Conshohocken, PA, 1999), p. 333.

Soles, C. L., Dimeo, R. M., Neumann, D. A., Kisliuk, A., Sokolov, A. P., Liu, J., Yee, A. F., Wu, W. L., "Correlations of the Boson Peak with Annihilation in Series of Polycarbonate Copolymers," Macromol. **34** (12), 4082 (2001).

Soles, C. L., Douglas, J. F., Wu, W.-L., Dimeo, R. M., "Incoherent Neutron Scattering and the Dynamics of Confined Polycarbonate Films," Phys. Rev. E, in press.

Steinle-Neumann, G., Stixrude, L., Cohen, R. E., Gulseren, O., "Elasticity of Iron at High Pressure and Temperature Implications for the Earth's Inner Core," Nature, in press.

Sung, L., Karim, A., Douglas, J. F., Han, C. C., "Modification of Thin Film Phase Separation by a Surfactant," Macromol., in press.

Tarek, M., Martyna, G. J., Tobias, D. J., "Amplitudes and Frequencies of Protein Dynamics: Analysis of Discrepancies Between Neutron Scattering and Molecular Dynamics Simulations," J. Am. Chem. Soc. **122** (42), 10450 (2000).

Tarek, M., Tobias, D. J., "The Dynamics of Protein Hydration Water: A Quantitative Comparison of Molecular Dynamics Simulations and Neutron Scattering Experiments," Biophys. J., **79** (6), 3244 (2000).

Tarek, M., Tobias, D. J., "Effects of Solvent Damping on Side Chain and Backbone Contributions to the Protein Boson Peak," J. Chem. Phys. **115** (3), 1607 (2001).

Thomas, J. J., Jennings, H. M., Allen, A. J., "The Surface Area of Hardened Cement Paste as Measured by Various Techniques," Con. Sci. Eng., in press.

Thomas, J. J., Neumann, D. A., Fitzgerald, S. A., Livingston, R. A., "The State of Water in Hydrating Tricalcium Silicate and Portland Cement Pastes as Measured by Quasi-Elastic Neutron Scattering," J. Am. Ceram. Soc. **84** (8), 1811 (2001).

Toby, B. H., "The Classification of Powder Diffraction Data," International Tables for Crystallography, in press.

Toby, B. H., "Diffraction Analysis and Crystallographic Structure Determination," *Handbook of Ceramic Engineering*, edited by M. N. Rahaman, in press.

Toby, B. H., "EXPGUI, a Graphical User Interface for GSAS," J. Appl. Crystallgr. **34**, 210 (2001).

Toby, B. H., "Structural Studies of Zeolitic Materials With the NIST BT-1 Neutron Powder Diffractometer," Neutron News, in press.

Travis, J. C., Smith, M. V., Mildner, D. F. R., Kramer, G. W., "Performance of the New Reference Spectrophotometer in the NIST Analytical Chemistry Division," Pittsburgh Conf., New Orleans, LA, March 2001.

Trewhella, J., Krueger, J. K., "Small-Angle Solution Scattering Reveals Information on Conformational Dynamics in Calcium-Binding Proteins and in Their Interactions With Regulatory Targets" in *Proceedings of the Calcium Binding Proteins Protocols*, edited by H. Vogel, J. M. Walker, (Humana Press, 1999), in press.

Truong, M. T., Walker, L. M., "Controlling the Shear-Induced Structural Transition of Rodlike Micelles Using Nonionic Polymer," Langumir **16**, 7991 (2000).

Tsai, A. M., Neumann, D. A., Bell, L. N., "Molecular Dynamics of Solid-State Lysozyme as Affected by Glycerol and Water: A Neutron Scattering Study," Biophys. J. **79** (5), 2728 (2000).

Tsai, A. M., Udovic, T. J., Neumann, D. A., "The Inverse Relationship Between Protein Dynamics and Thermal Stability," Biophys. J., in press.

Tung, C.-S., Wall, M. E., Gallagher, S. C., Trewhella, J., "A Molecular Model of the Troponin C/Troponin Interaction Using Constraints From X-Ray Crystallography, NMR, Small Angle Scattering, Cross-Linking and FRET," Protein Science **78** (1), 2158 (2001).

Udovic, T. J., Karmonik, C., Huang, Q., Rush, J. J., Vennstrom, M., Anderson, Y., Flanagan, T. B., "Comparison of the Dynamics of Hydrogen and Deuterium Dissolved in Crystalline Pd_9Si_2 and $Pd_3P_{0.8}$," J. Alloy Compnds., in press.

Vasiliu-Doloc, L., Osborn, R., Rosenkranz, S., Mesot, J., Mitchell, J. F., Sinha, S. K., Seeck, O. H., Lynn, J. W., Islam, Z., "Neutron and X-ray Evidence of Charge Melting in Layered Colossal Magnetoresistance Manganites," J. Appl. Phys. **89** (11), 6840 (2001).

Vasiliu-Doloc, L., Osborn, R., Rosenkranz, S., Mesot, J., Mitchell, J. F., Sinha, S. K., Seeck, O. H., Lynn, J. W., Islam, Z., "Neutron and X-ray Evidence of Charge Melting in Layered CMR Manganites," J. Solid State Chem. J. Appl. Phys. **89**, 6840 (2001).

Vasiliu-Doloc, L., Osborn, R., Rosenkranz, S., Mesot, J., Mitchell, J. F., Sinha, S. K., Seeck, O. H., Lynn, J. W., Islam, Z., "Polaron Ordering in Ferromagnetic Colossal Magnetoresistive Oxides," Int. J. Mod. Phys. B **14** (29), 3711 (2000).

Wada, N., Kamitakahara, W. A., "Quasielastic and Inelastic Neutron Scattering Studies on Intercalated Water Molecules in Zeolite LTA and FAU," Mol. Cryst. Liq. Cryst., in press.

Wagner, N. J., Butera, R., "Shear Distortion and Relaxation Dynamics of Colloidal Crystals Investigated by SANS Time Slicing" Phys. Rev. E, in press.

Wakimoto, S., Tranquada, J. M., Ono, T., Kojima, K. M., Uchida, S., Lee, S. H., Gehring, P. M., Birgeneau, R. J., "Diagonal Static Spin Correlations in the Low Temperature Orthorhombic Pccn Phase of $La_{1.55}Nd_{0.4}Sr_{0.05}CuO_4$," Phys. Rev. B, in press.

Walker, L. M., Truong, M. T., "Rheology and Structural Transitions in Wormlike Micellar Systems Controlled by Added Nonionic Polymer," in *Proceedings of the XIIIth International Congress on Rheology* (Cambridge, UK 2000), p.310.

Wall, M. E., Gallagher, S. C., Trewhella, J., "Large-Scale Shape Changes in Proteins and Macromolecular Complexes" Annual Rev. of Phys. Chem **51**, 335 (2000).

Wang, H. Y., Hwang, S. R., Li, W.-H., Lee, K. C., Lynn, J. W., Luo, H. M., Ku, H. C., "Variation in the Structural and Magnetic Properties Induced by La-doping in $Pr(Ba_{1-x}La_x)_2Cu_3O_{7+\delta}$," Phys. Rev. B **62**, (17), 11549 (2001).

Weissmüller, J., Michels, A., Barker, J. G., Wiedenmann, A., Pedersen, J. S., Erb, U., Shull, R. D., "Analysis of Small-Angle Neutron Scattering of Nanocrystalline Ferromagnets by a Micromagnetics Model," Phys. Rev. B **6321** (21), 4414 (2001).

Welp, K. A., Co, C., Wool, R. P., "Improved Reflectivity Fitting Using SERF: Spreadsheet Environment Reflectivity Fitting," J. Neutron Res., in press.

Wesley, R., Armes, S. P., Thompson, L. J., "Block Copolymer Interactions With Surfactants," Langmuir, in press.

White, D. C. C., Wu, W. L., Pu, Y., Rafailovich, M., Sokolov, J., "Probe Segregation Within an Ultra-Thin Polystyrene Film Studied by X-ray, Neutron Reflectivity and SIMS and Tg Determination of Polystyrene on a Quartz Substrate by X-ray Reflectivity," Macromol., in press.

Williams, R. E., "Recent Advances in Cold Neutron Utilization at the NIST Research Reactor," Trans. Am. Nucl. Soc. **84**, 124 (2001).

Williams, R. E., Rowe, J. M., "Developments in Neutron Beam Devices and an Advanced Cold Source for the NIST Research Reactor," Physica B, in press.

Wirth, B. D., Odette, G. R., Pavinich, W. A., Lucas, G. E., Spooner, S. E., "Small Angle Neutron Scattering Study of Linde 80 RPV Welds," in *Proceedings of the Effects of Radiation on Materials: 18th International Symposium*, ASTM STP 1325, edited by R. K. Nanstad, M. L. Hamilton, F. A. Garner, and A. S. Kumar (West Conshohocken, PA, 1999).

Wong-Ng, W., Huang, Q., Lavin, I., Kaduk, J. A., Dillingham, J., Huagan, T., Suh, J., Cook, L. P., "Crystal Chemistry and Phase Equilibria of Selected SrO-R_2O_3-CuO_x and Related Systems, R=Lanthanides and Yttrium," J. Solid State Chem., in press.

Wong-Ng, W., Kaduk, J. A., Huang, Q., Roth, R. S., "Crystal Structure of the Monoclinic Perovskite $Sr_{3.94}Ca_{1.31}Bi_{2.70}O_{12}$," Powder Diff. **15** (4), 227 (2000).

Wu, W., Lin, E. K., Jin, C., Wetzel, J. T. A., "Three-Phase Model for the Structure of Porous Thin Films Determined by X-ray Reflectivity and Small Angle Neutron Scattering," in *Proceedings of the Materials Research Society Meeting* (April 2000), in press.

Wu, W. L., Lin, E. K., Lin, Q., Angelopolous, M., "Small-Angle Neutron Scattering Measurements for the Characterization of Lithographically Prepared Structures," in *Proceedings of the 2000 International Conference on Characterization and Metrology for ULSI Technology*, in press.

Wu, W. L., Lin, E. K., Lin, Q., Angelopolous, M., "Small Angle Neutron Scattering Measurements of Nanoscale Lithographic Features," J. Appl. Phys. **88** (12), 7298 (2000).

Xu, G., Broholm, C., Reich, D. H., Adams, M. A., "Triplet Waves in Quantum Spin Liquid," Phys. Rev. Lett., in press.

Yamaura, K., Huang, Q., Takayama-Muromachi, E., "Crystal Structure and Magnetism of the Linear-Chain Copper Oxides $Sr_3Pb_{3-x}Bi_xCuO_{12}$," Phys. Rev. B, in press.

Yang, H., Al-Brithen, H., Smith, A. R., Borchers, J. A., Cappelletti, R. L., Vaudin, M. D., "Structural and Magnetic Properties of δphase Manganese Nitride Films Grown by Molecular Beam Epitaxy," App Phys. Lett. **78** (24), 3860 (2001).

Yang, L., Slawecki, T. M., Alexandridis, P., "Shear Induced Orientation and Structural Transitions in Micellar Cubic Crystals Formed by Solvated Block Copolymers: A SANS Investigation," Macromol., in press

Yildirim, T., "Structure and Dynamics From Combined Neutron Scattering and First-Principles Studies," Chem. Phys. **261** (1), 205 (2000)

Yildirim, T., Gehring, P. M., Neumann, D. A., "The Dynamics of Solid Cubane," Neutron News **12** (2), 18 (2001).

Yildirim, T., Gulseren, O., "A Simple Theory of 40K Superconductivity in MgB_2: First Principles Calculations of T_c, its Dependence in Boron Mass and Pressure," J. Phys. Chem. Solids, in press.

Yildirim, T., Gulseren, O., "First-Principles Zone-Center Theory of Superconductivity in MgB_2," Physica A, in press

Yildirim, T., Gulseren, O., Ciraci, S., "Exohydrogenated Single-Wall Carbon Nanotubes," Phys. Rev. B **64**, 75404 (2001).

Yildirim, T., Gulseren, O., Ciraci, S., Kilic, C., "Pressure-Induced Interlinking of Carbon Nanotubes," Phys. Rev. B **62** (19), 12648 (2000).

Yildirim, T., Gulseren, O., Lynn, J. W., Brown, C. M., Udovic, T. J., Huang, Q. Z., Rogado, N., Regan, K. A., Sluksy, J. S., He, T., Haas, M. K., Khalifah, P., Inumaru, K., Cava, R. J., "Giant Anharmonicity and Non-Linear Electron-Phonon Coupling in MgB_2: Combined First-Principles Calculations and Neutron Scattering Study," Phys. Rev. Lett. **8703** (3), 7001 (2001).

Yildirim, T., Reisner, B., Udovic, T. J., Neumann, D. A., "The Combined Neutron Scattering and First-Principles Study of Solid State Protonic Conductors," Solid State Ionics, in press.

Yong, G., Toulouse, J., Erwin R., Shapiro, S. M., Hennion, B., "Pretransitional Diffuse Neutron Scattering in the Mixed Perovskite Relaxor $K_{1-x}Li_xTaO_3$," Phys. Rev. B **62** (22), 14736 (2000).

Young, S. K., Trevino, S. F., Beck Tan, N. C., Paul, R. L., "Utilization of Prompt Gamma Neutron Activation Analysis in the Evaluation of Various Counterion Nafion Membranes," J. Polym. Sci., in press.

Zaliznyak, I., Broholm, C., Kibune, M., Takagi, H., "Spin Freezing in the Cuprate S = ½ Antiferromagnetic Chain Compound $SrCuO_2$," Phys. Rev Lett., in press.

Zaliznyak, I. A., Hill, J. P., Tranquada, J. M., Erwin, R., Moritomo, Y., "Independent Freezing of Charge and Spin Dynamics in $La_{1.5}Sr_{0.5}CoO_4$," Phys. Rev. Lett. **85** (20), 4353 (2000)

Zaliznyak, I. A., Lee, S. –H., Petrov, S. V., "Continuum in the Spin Excitation Spectrum of a Haldane Chain, Observed by Neutron Scattering in $CsNiCl_3$," Phys. Rev. Lett. **87** (1), 7202 (2001).

Zamlynny, V., Burgess, I., Szymanski, G., Lipkowski, J., Majewski, J., Smith, G., Satija, S., Ivkov, R., "Electrochemical and Neutron Reflectivity Studies of Spontaneously Formed Amphiphilic Surfactant Bilayers at the Gold-Solution Interface," Langmuir **16** (25), 9861 (2000).

Zeisler, R., Jenks, P., "Chapter 7-Proper Usage of Reference Materials," in *Proceedings Reference Materials for Chemical Analysis – Certification, Availability, and Proper Usage*, edited by M. Stoeppler, W. R. Wolf, P. Jenks (John Wiley and Sons, Inc., New York, NY), in press.

Zeisler, R., Lamaze, G. P., Chen-Mayer, H. H., "Coincidence and Anti-Coincidence Measurements in Prompt Gamma Neutron Activation Analysis With Pulsed Cold Neutron Beams," J. Radioanal. Nucl. Ch. **248** (1), 35 (2001).

Zeissler, C. J., Lindstrom, R. M., and McKinley, J. P., "Radioactive Particle Analysis by Digital Autoradiography," J. Radioanal. Nucl. Chem. **248**, 407 (2001).

Zhang, Y., Douglas, J. F., Ermi, B. D., Amis, E. J., "Influence of Counterion Valency on the Scattering Properties of Highly Charged Polyelectrolyte Solutions," J. Chem. Phys. **114** (7), 3299 (2001).

Zhang, Y., Ge, S., Tang, B., Rafailovich, M. H., Sokolov, J., Peiffer, D., Li, Z., Lin, M., Dias, J. A., McElrath, K. O., Nguyen, D., Satija, S., Schwarz, S. A., "Interfacial Properties of Brominated Isobutylene-co-p-Methylstyrene and Butadiene Polymers" in *Proceedings of the American Chemical Society 154th Rubber Conference*, in press.

Zhang, Y. M., Ge, S., Tang, B., Rafailovich, M. H., Sokolov, J. C., Peiffer, D. G., Li, Z., Dias, A. J., McElrath, K. O., Satija, S. K., Lin, M. Y., Nguyen, D., "Reduced Mobility of Elastomers Near A Solid Surface as Measured by Neutron Reflectometry," Langmuir **17** (14), 4437 (2001).

Zheludev, A., Chen, Y., Broholm, C. L., Honda, Z., Katsumata, K., "Haldane-Gap Excitations in the Low-H-c One-Dimensional Quantum Antiferromagnet Ni(C5D14N2)(2)N-3(PF6)," Phys. Rev. B **6310** (10), 4410 (2001).

Zheludev, A., Maslov, S., Zaliznyak, I., Regnault, L. P., Masuda, T., Uchinokura, K., Erwin, R., Shirane, G., "Experimental Evidence for Shekhtman-Entin-Wohlman-Aharony (SEA) Interactions in $Ba_2CuGe_2O_7$," Phys. Rev. B Cond. Matt., in press.

Zheludev, A., Masuda, T., Tsukada, I., Uchiyanna, Y., Uchinokura, K., Bonl, P., Lee, S.-H., "Magnetic Excitations in Coupled Haldane Spin Chains Near the Quantum Critical Point," Phys. Rev. B **62** (13), 8921 (2000)

Zhokhov, A. A., Fmelchenko, G. A., Naumenko, I. G., Barilo, S. N., Khasanov, S. S., Zverkov, S. A., Lynn, J. W., "Growth of Large $PrBa_2Cu_3O_7$-Delta Single Crystals by Modified TSSG Method Using Zirconium Dioxide Crucibles," J. Cryst. Growth **219** (4), 385 (2000).

Zhou, C., Hobbie, E. K., Bauer, B. J., Han, C. C., "Equilibrium Structure of Hydrogen-Bonded Polymer Blends," J. Polym. Sci. Pol. Phys., in press.

Instruments and Contacts

High resolution powder diffractometer (BT-1)
J. K. Stalick, (301) 975-6223, judy.stalick@nist.gov
B. H. Toby, (301) 975-4297, brian.toby@nist.gov

DARTS, Residual stress and texture diffractometer (BT-8)
H. J. Prask, (301) 975-6226, hank@nist.gov
T. Gnaeupel-Herold, (301) 975-5380, thomas.gnaeupel-herold@nist.gov

30-m SANS instrument (NG-7)
J. C. Schulz, (301) 975-6469, jamie.schulz@nist.gov
C. J. Glinka, (301) 975-6242, cglinka@nist.gov
J. G. Barker, (301) 975-6732, john.barker@nist.gov

30-m SANS instrument (NG-3) (NIST/NSF-CHRNS)
B. Hammouda, (301) 975-3961, hammouda@nist.gov
S. R. Kline, (301) 975-6243, steven.kline@nist.gov
D. Ho, (301) 975-6422, derek.ho@nist.gov

8-m SANS instrument (NG-1)
D. Ho, (301) 975-6422, derek.ho@nist.gov
C. J. Glinka, (301) 975-6242, cglinka@nist.gov
J. G. Barker, (301) 975-6732, john.barker@nist.gov

USANS, Perfect crystal SANS (BT-5) (NIST/NSF-CHRNS)
J. G. Barker, (301) 975-6732, john.barker@nist.gov
C. J. Glinka, (301) 975-6242, cglinka@nist.gov

Cold neutron reflectometer-vertical sample-polarized beam option (NG-1)
C. F. Majkrzak, (301) 975-5251, cmajkrzak@nist.gov
J. A. Dura, (301) 975-6251, jdura@nist.gov

Cold neutron reflectometer-horizontal sample (NG-7)
S. K. Satija, (301) 975-5250, satija@nist.gov
K. W. Shin, (301) 975-8829, kwshin@nist.gov

Triple-axis polarized-beam spectrometer (BT-2)
J. W. Lynn, (301) 975-6246, jeff.lynn@nist.gov
R.W. Erwin, (301)975-6245, rerwin@nist.gov

Triple-axis fixed incident energy spectrometer (BT-7)
J. W. Lynn, (301) 975-6246, jeff.lynn@nist.gov
R.W. Erwin, (301)975-6245, rerwin@nist.gov

Triple-axis spectrometer (BT-9)
R. W. Erwin, (301) 975-6245, rerwin@nist.gov
P. M. Gehring, (301) 975-3946, pgehring@nist.gov

SPINS, Spin-polarized triple-axis spectrometer (NG-5) (NIST/NSF-CHRNS)
S. Park, (301) 975-8369, sungil.park@nist.gov
P. M. Gehring, (301) 975-3946, pgehring@nist.gov
S.-H. Lee, (301) 975-4257, seung-hun.lee@nist.gov

FANS, Filter-analyzer neutron spectrometer (BT-4)
T. J. Udovic, (301) 975-6241, udovic@nist.gov
C. M. Brown, (301) 975-5134, craig.brown@nist.gov
D. A. Neumann, (301) 975-5252, dan@nist.gov

FCS, Fermi-chopper time-of-flight spectrometer (NG-6)
C. M. Brown, (301) 975-5134, craig.brown@nist.gov
T. J. Udovic, (301) 975-6241, udovic@nist.gov

DCS, Disk-chopper time-of-flight spectrometer (NG-4) (NIST/NSF-CHRNS)
J. R. D. Copley, (301) 975-5133, jcopley@nist.gov
J. C. Cook, (301) 975-6403, jeremy.cook@nist.gov

HFBS, High-flux backscattering spectrometer (NG-2) (NIST/NSF-CHRNS)
R. M. Dimeo, (301) 975-8135, robert.dimeo@nist.gov
Z. Chowdhuri, (301) 975-4404, zema.chowdhuri@nist.gov
D. A. Neumann, (301) 975-5252, dan@nist.gov

NSE, Neutron spin echo spectrometer (NG-5) (NIST/NSF-CHRNS)
N. S. Rosov, (301) 975-5254, nrosov@nist.gov

Prompt-gamma neutron activation analysis (NG-7)
R. M. Lindstrom, (301) 975-6281, dick.lindstrom@nist.gov
R. L. Paul, (301) 975-6287, rpaul@nist.gov

Other activation analysis facilities
R. R. Greenberg, (301) 975-6285, rgreenberg@nist.gov

Cold neutron depth profiling (NG-0)
G. Lamaze, (301) 975-6202, lamaze@nist.gov

Instrument development station (NG-0)
D. F. R. Mildner, (301) 975-6366, mildner@nist.gov
H. H. Chen, (301) 975-3782, chenmayer@nist.gov

Neutron interferometer (NG-7)
M. Arif, (301) 975-6303, muhammad.arif@nist.gov

Fundamental neutron physics station (NG-6)
M. S. Dewey, (301) 975-4843, mdewey@nist.gov

Theory and modeling
N. F. Berk, (301) 975-6224, nfb@nist.gov
T. Yildirim, (301) 975-6228, taner@nist.gov

Sample environment
D. C. Dender, (301) 975-6225, dender@nist.gov

NIST IR 6798 — NIST CENTER FOR NEUTRON RESEARCH: FY 2001 PROGRAMS AND ACCOMPLISHMENTS